Microscopic studies of neutron star crust

E. Vigezzi

INFN Milano

Nuclear Physics School “Raimondo Anni” , 5th Course

Otranto May 30 –June 4

Schematic cross section of a Neutron Star

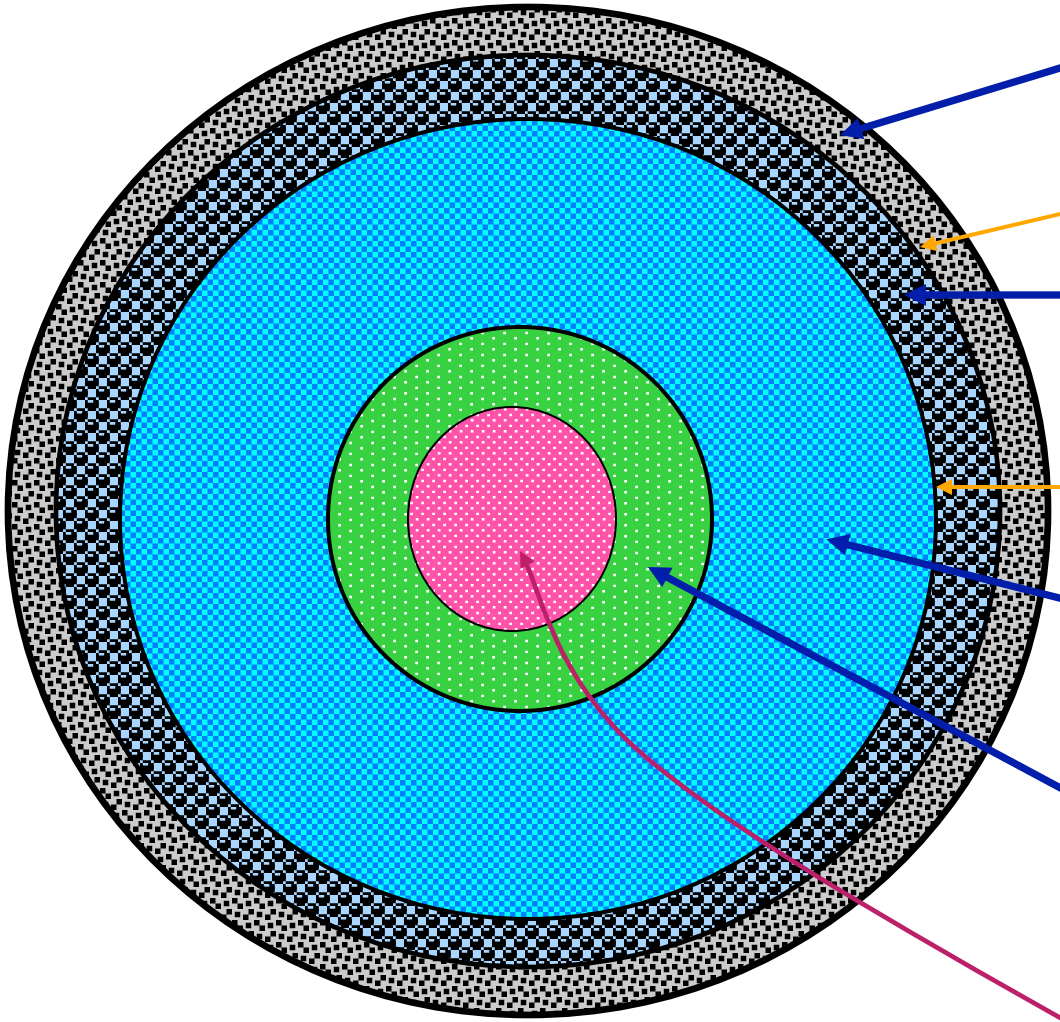

outer crust
nuclei, e^-

$\rho_{drip} = 4.3 \times 10^{11}$ g/cm^3

inner crust
nuclei, n, e^-

$\sim 1.5 \times 10^{14}$ g/cm^3

Nuclear matter layer
n, p, e^-, μ^-

exotic core
(*a*) **hyperonic matter**
(*b*) **kaon condensate**
(c) **quark matter**

M ~ 1.4 $M_\odot$

R ~ 10 km

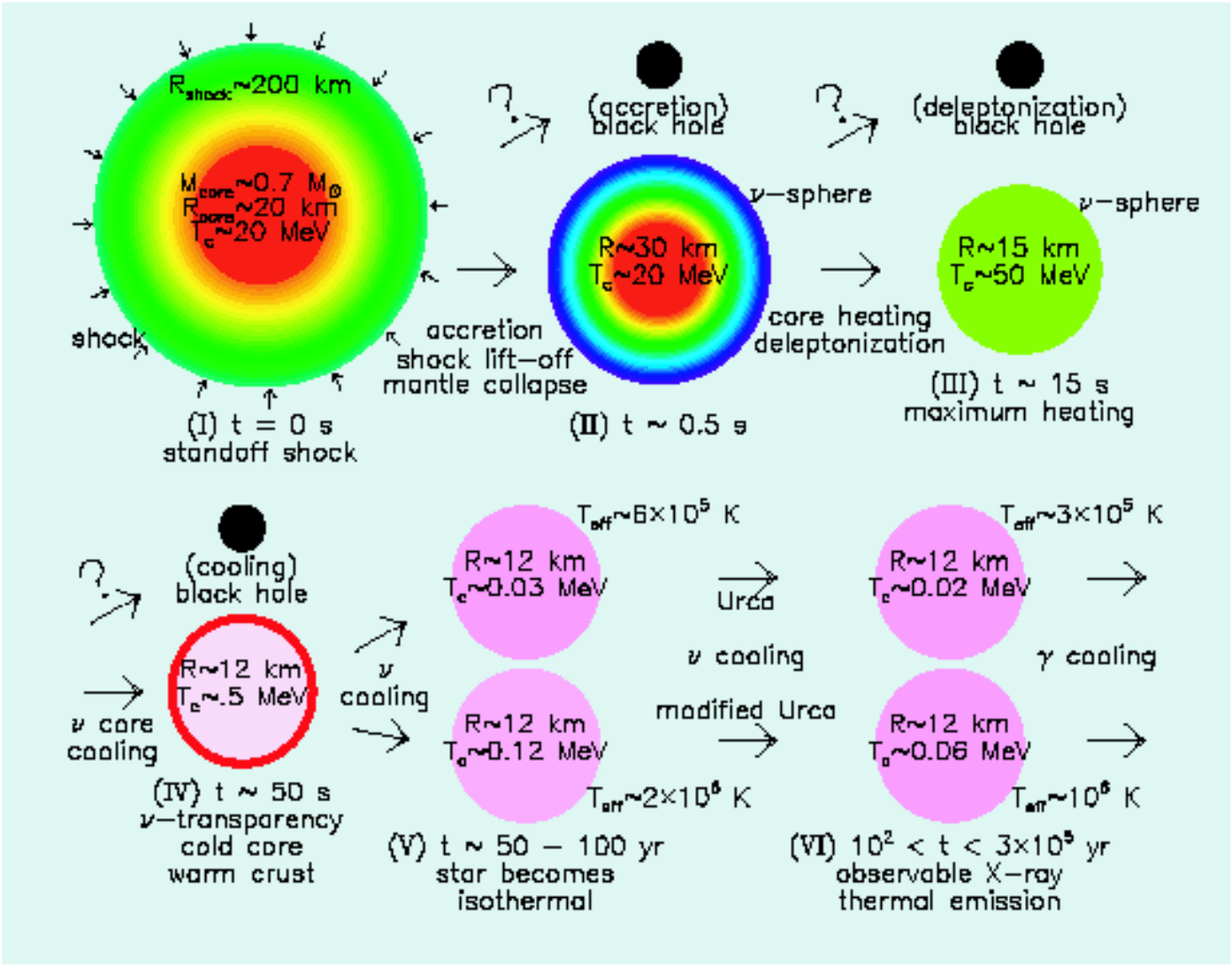

Fig. 1. The main stages of evolution of a neutron star. Roman numerals indicate various stages described in the text. The radius R and central temperatures T_c for the neutron star are indicated as it evolves in time t.

J.M. Lattimer , M. Prakash, Science 304(2004)

$\rho = 0.16\ \mathrm{fm}^{-3} = 2.8 \times 10^{14}\ \mathrm{g\ cm}^{-3}$

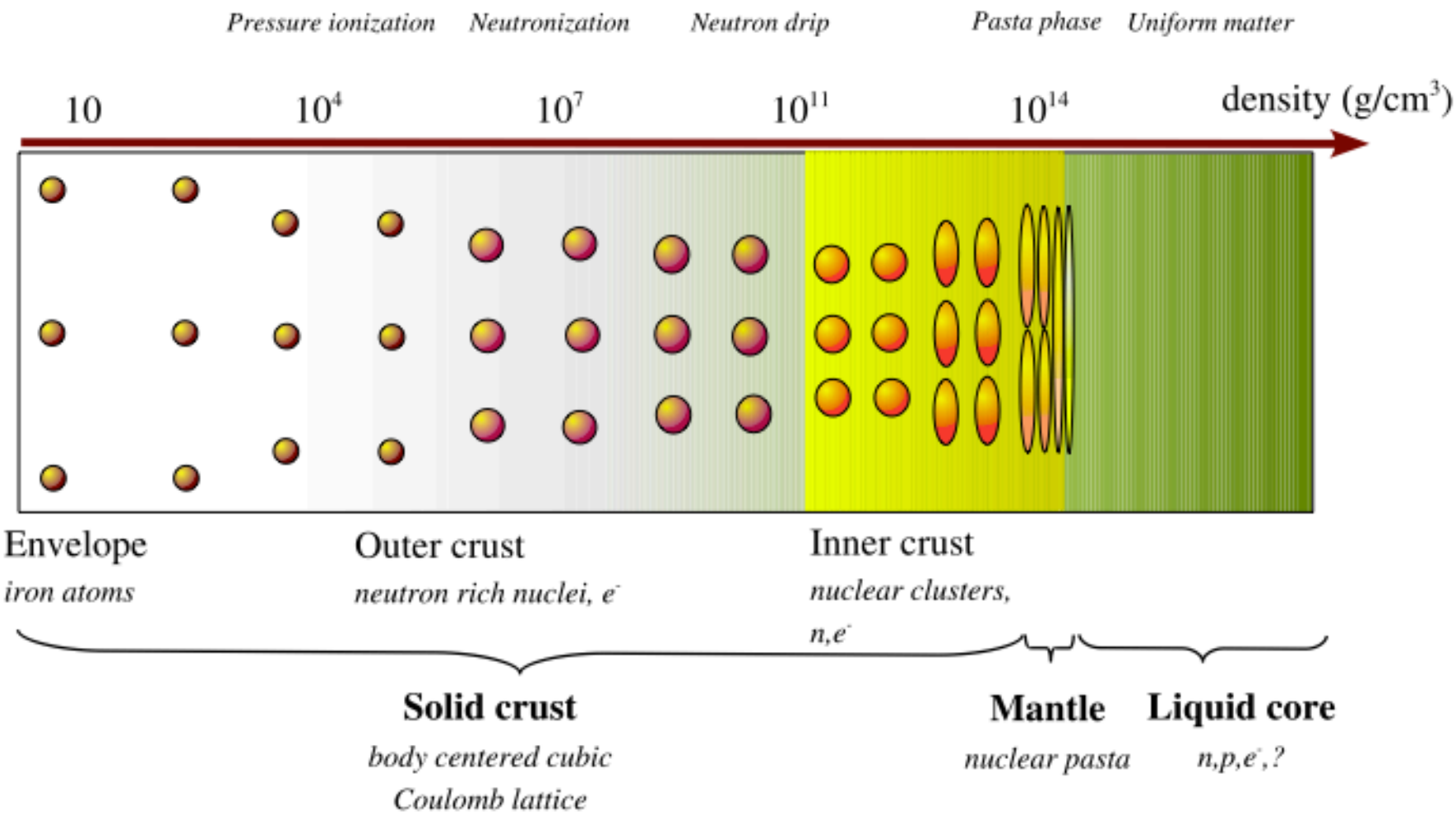

N. Chamel and P. Haensel, Living Rev. Relativity 11

1.C

Nuclear Physics **A175** (1971) 225—271; © *North-Holland Publishing Co., Amsterdam*

NEUTRON STAR MATTER

GORDON BAYM †, HANS A. BETHE †† and CHRISTOPHER J. PETHICK †††

Nordita, Copenhagen, Denmark

The identification of pulsars as rotating neutron stars [1]) has renewed interest in the properties of matter at very high densities. The density of matter in a neutron star increases with depth from low values near the surface to central densities on the order of the density of matter in nuclei (≈ 0.2 nucleons/fm^3 or 3×10^{14} g/cm^3) or greater. Except in the outermost layer of a neutron star, the matter is relatively very cold in the sense that characteristic energies required for microscopic excitations are very much greater than the characteristic thermal energy, $k_B T$. If the matter has had sufficient time in the earlier hot stages of the star to reach nuclear equilibrium, one may consider it to be in its absolute ground state. This requires that nuclear equilibration rates be fast compared with cooling rates.

Up to a mass density $\rho \sim 10^7$ g/cm^3, the ground state of matter consists of ^{56}Fe nuclei arranged in a lattice, most likely body-centered cubic (bcc), together with a

sea of electrons [2, 3, 4]). Beyond $\rho \sim 10^3$ g/cm^3 the electrons are fully ionized, and above $\sim 10^6$ g/cm^3 they are relativistic and virtually free. As the density of matter rises, with increasing depth in the star, the equilibrium nucleus present becomes more and more neutron rich, as a result of electron capture. The binding energy of the last neutron in the equilibrium nucleus becomes smaller, and eventually, at a density [4]) $\rho_d = 4.3 \times 10^{11}$ g/cm^3, it becomes favorable for neutrons to begin to "drip" out of the nuclei. At densities between ρ_d and $\rho \sim 2.4 \times 10^{14}$ g/cm^3, the matter is still solid, and consists of a lattice of nuclei immersed in a pure neutron gas, in addition to the electron gas; we shall refer to this regime as the *free neutron regime*. The nuclei dissolve at about nuclear matter density and at higher densities the matter consists of a uniform liquid of neutrons with a small fraction of protons and electrons. As we shall see, muons also appear at about this point. Finally, at densities a few times higher, various hyperons, Σ^-, Λ°, etc., make their appearance.

β-stable nuclear matter

$$p + e^- \leftrightarrow n + \nu_e$$
$$n \leftrightarrow p + e^- + \bar{\nu}_e$$

if $\mu_e \geq m_\mu = 105.6 MeV$

$$e^- \leftrightarrow \mu^- + \nu_e + \bar{\nu}_\mu$$
$$p + \mu^- \leftrightarrow n + \nu_\mu$$

$$\mu_\nu = \mu_{\bar{\nu}} = 0$$

neutrino-free matter

- **Equilibrium with respect to the weak interaction processes**

$$\mu_n - \mu_p = \mu_e$$

- **Charge neutrality**

$$n_p = n_e + n_\mu$$

To be solved for any given value of the total baryon number density n_B

Symmetry energy determines the proton fraction in uniform neutron star matter …

Defining

$$\beta = \frac{\rho_n - \rho_p}{\rho} = 1 - 2x, \tag{1}$$

with

$$x = \frac{\rho_p}{\rho} \tag{2}$$

write schematically the energy per nucleon in neutron star matter as

$$E(\rho, x) = E(\rho, 1/2) + S(\rho)(1-2x)^2 + \frac{3\hbar c}{4}\rho_e(3\pi^2\rho_e)^{1/3} \tag{3}$$

Minimum condition:

$$\left(\frac{\partial E}{\partial x}\right)_\rho = 0 \tag{4}$$

Using charge neutrality, $\rho_e = \rho_p = \rho x$, one finds

$$\hbar c(3\pi^2\rho x)^{1/3} = 4S(\rho)(1-2x) \tag{5}$$

Using $S(\rho_0) \approx 30$ MeV one finds $x \approx 0.04$ at $\rho = \rho_0$

.. and influences the neutron drip line

Write very schematically the energy of a nucleus with Z protons and $A-Z$ neutrons as

$$E(A,Z) \approx A[E_{vol} + S(\rho_0)(1-2x)^2] \tag{6}$$

Fixing Z, the chemical potential for neutrons is given by

$$\mu_n = \left(\frac{\partial E}{\partial N}\right)_Z \tag{7}$$

and one finds that the condition for $\mu_n = 0$ is

$$E_{vol} + 2S(\rho_0)(1-2x) - E_{sym}(1-2x)^2 = 0 \tag{8}$$

$x = 0.35$. Using Eq. (5), and the values $S_{\rho_0} = 30$ MeV, $E_{vol} = -16$ MeV, this determines the average electron and proton density ρ_{ND} at neutron drip, $\rho_{ND} \approx 2 \times 10^{11}$ g cm^{-3}, that is about half the value resulting from accurate models.

A proper calculation of the composition of the outer crust must minimize the energy density of a Coulomb lattice of nuclei in an uniform background of electrons for a given baryon density n:

$$\epsilon = n\frac{M(A,Z)}{A} + \epsilon_e(n_e) + \epsilon_L$$

where the lattice energy is given by (bcc lattice):

$$\epsilon_L = -1.44 Z^{2/3} e^2 n_e^{4/3}$$

Detailed calculation using experimental masses as much as possible

ρ_{max} [g cm^{-3}]	Element	Z	N	R_{cell} [fm]
8.02×10^{6}	^{56}Fe	26	30	1404.05
2.71×10^{8}	^{62}Ni	28	34	449.48
1.33×10^{9}	^{64}Ni	28	36	266.97
1.50×10^{9}	^{66}Ni	28	38	259.26
3.09×10^{9}	^{86}Kr	36	50	222.66
1.06×10^{10}	^{84}Se	34	50	146.56
2.79×10^{10}	^{82}Ge	32	50	105.23
6.07×10^{10}	^{80}Zn	30	50	80.58
8.46×10^{10}	^{82}Zn	30	52	72.77
9.67×10^{10}	^{128}Pd	46	82	80.77
1.47×10^{11}	^{126}Ru	44	82	69.81
2.11×10^{11}	^{124}Mo	42	82	61.71
2.89×10^{11}	^{122}Zr	40	82	55.22
3.97×10^{11}	^{120}Sr	38	82	49.37
4.27×10^{11}	^{118}Kr	36	82	47.92

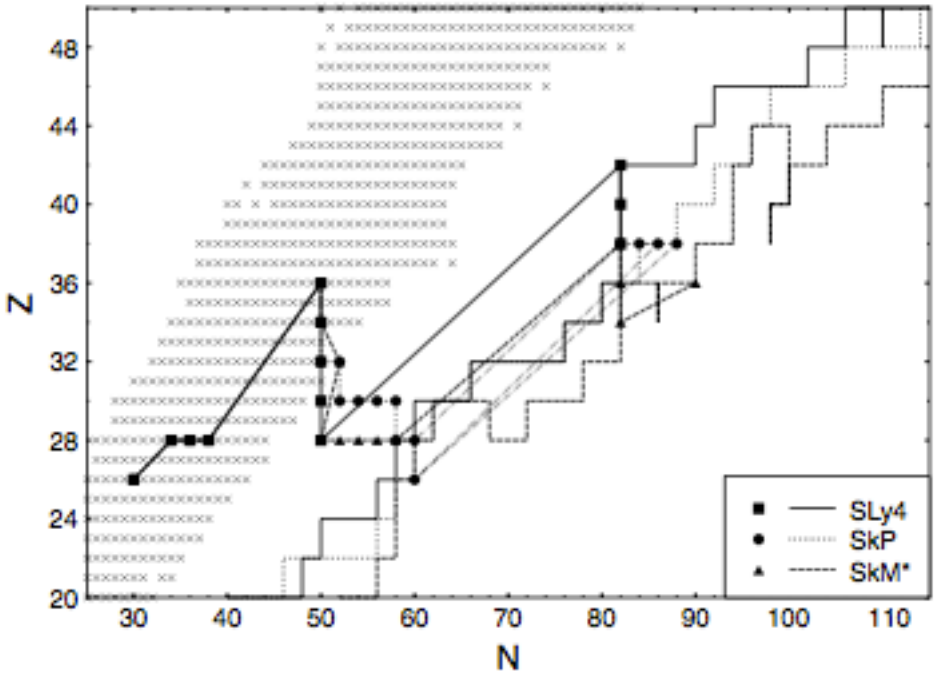

S.B. Rüster et al., Phys. Rev. C73 035804 (2006)

neutron and proton drip lines

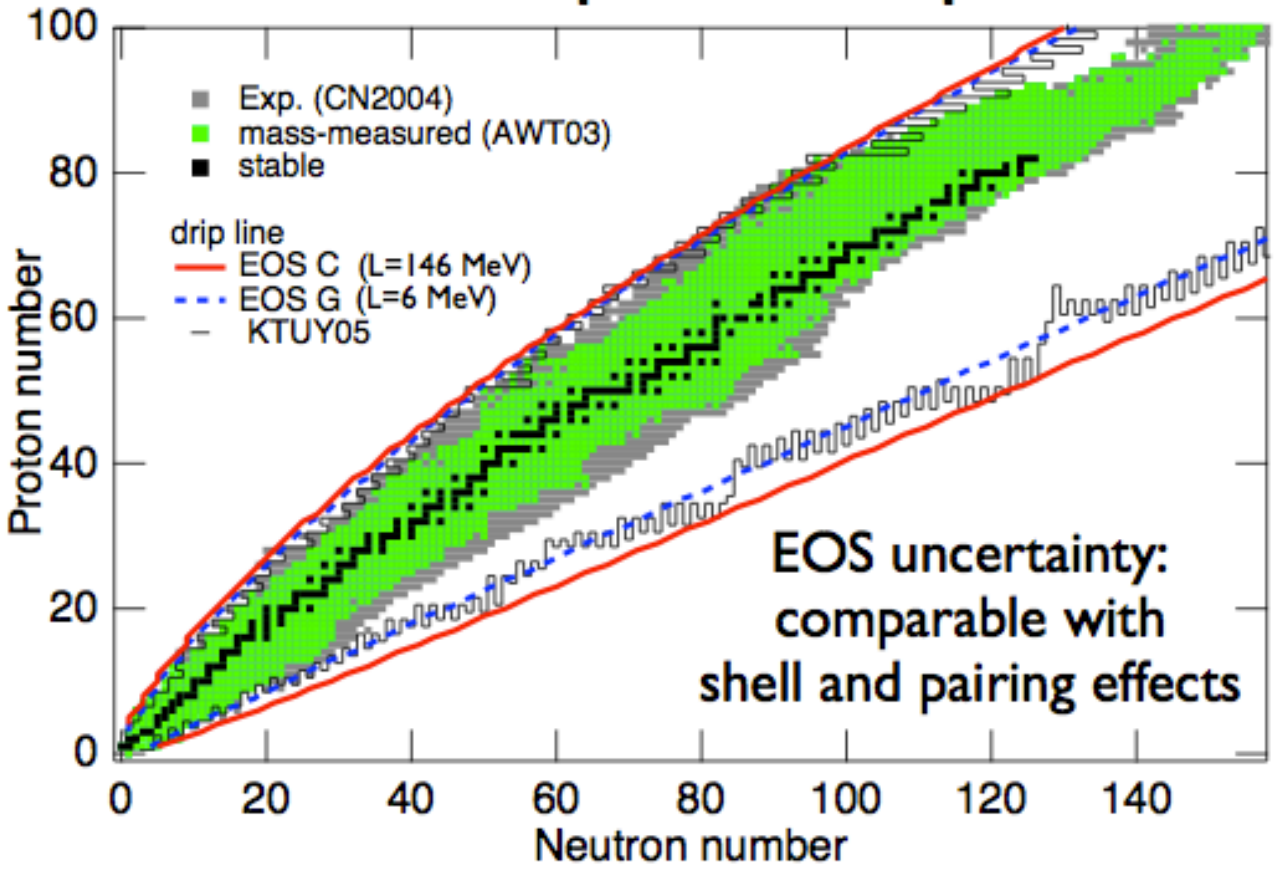

Oyamatsu, Iida, Koura, arXiv:1005.3183 (PRC (2010), to be published)

Many works have studied the coexistence of nuclei and neutron gas in the inner crust. This is an inhomogeneous system, difficult to attack with ab initio techniques.
Different methods have been applied:

- Macroscopic (Liquid drop)

- Semiclassical analysis (Thomas-Fermi)

- Molecular dynamics

- Quantum calculations (HF,HFB)

Wigner-Seitz approximation to crystal structure

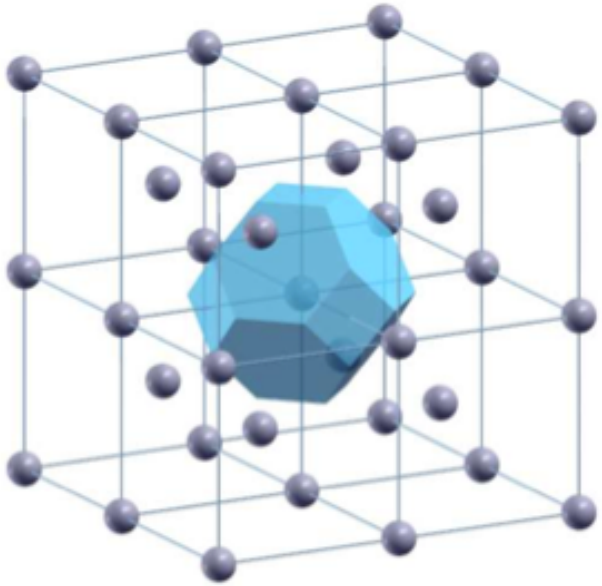

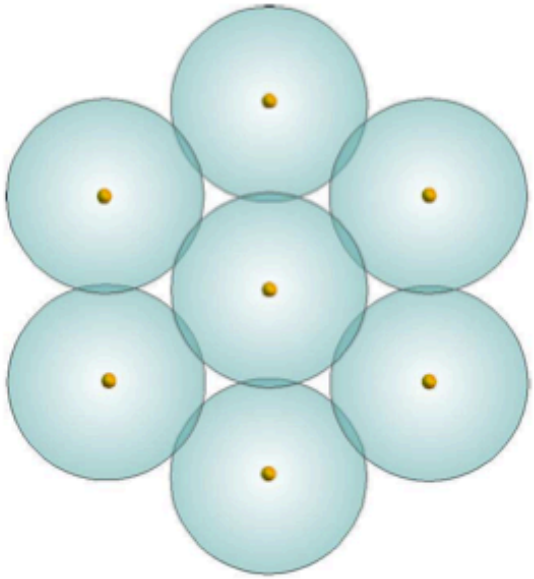

Figure 5: In the Wigner–Seitz approximation the crystal (represented here as a two-dimensional hexagonal lattice) is decomposed into independent identical spheres, centered around each site of the lattice. The radius of the sphere is chosen so that the volume of the sphere is equal to $1/n_{\mathrm{N}}$, where n_{N} is the density of lattice sites (ions).

N. Chamel and P. Haensel, Living Rev. Relativity 11

THE FIRST STUDY OF THE CRUST INCLUDING A MICROSCOPIC DESCRIPTION (HARTREE-FOCK) OF THE CLUSTERS:

J. Negele, D. Vautherin, Nucl. Phys. A207 (1973) 298

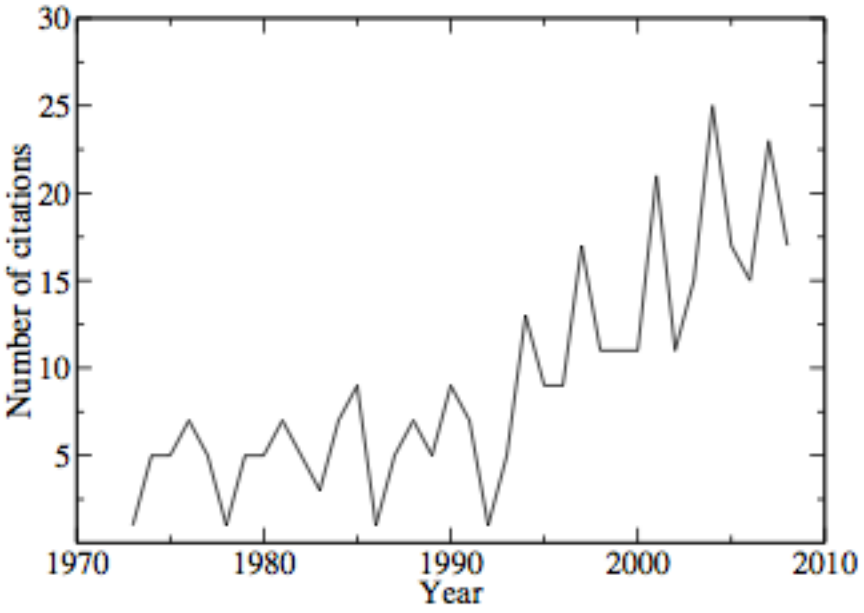

Figure 1. Citations of reference [1] per year. Source : ISI

Effective interactions like Skyrme force SLy4 have been fitted to properties of finite nuclei and to ab initio calculations in uniform matter.

If one gives too much weight to the fits in uniform matter, agreement with experimental data in nuclei deteriorates.

One can attempt at describing the crust with a given effective forces or matching a functional describing finite nuclei with one describing uniform matter

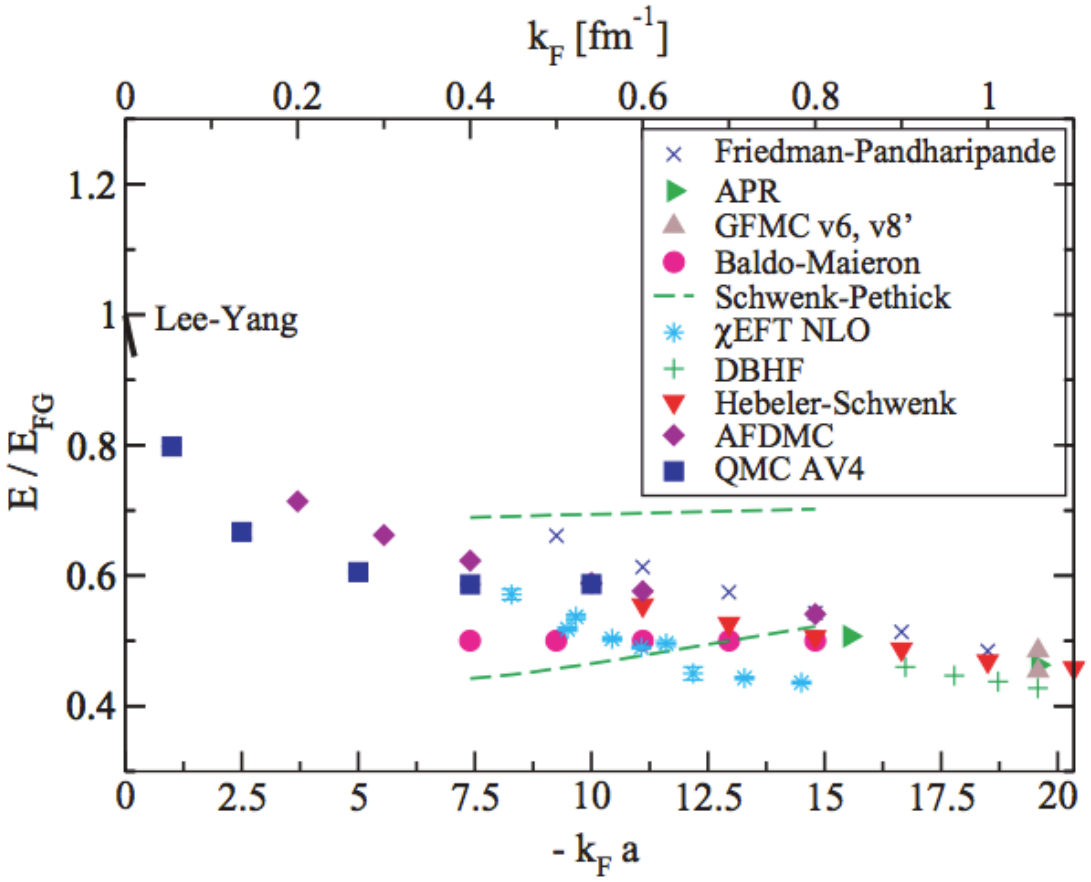

A. Gezerlis, J. Carlson
PRC 81 (2010) 025803

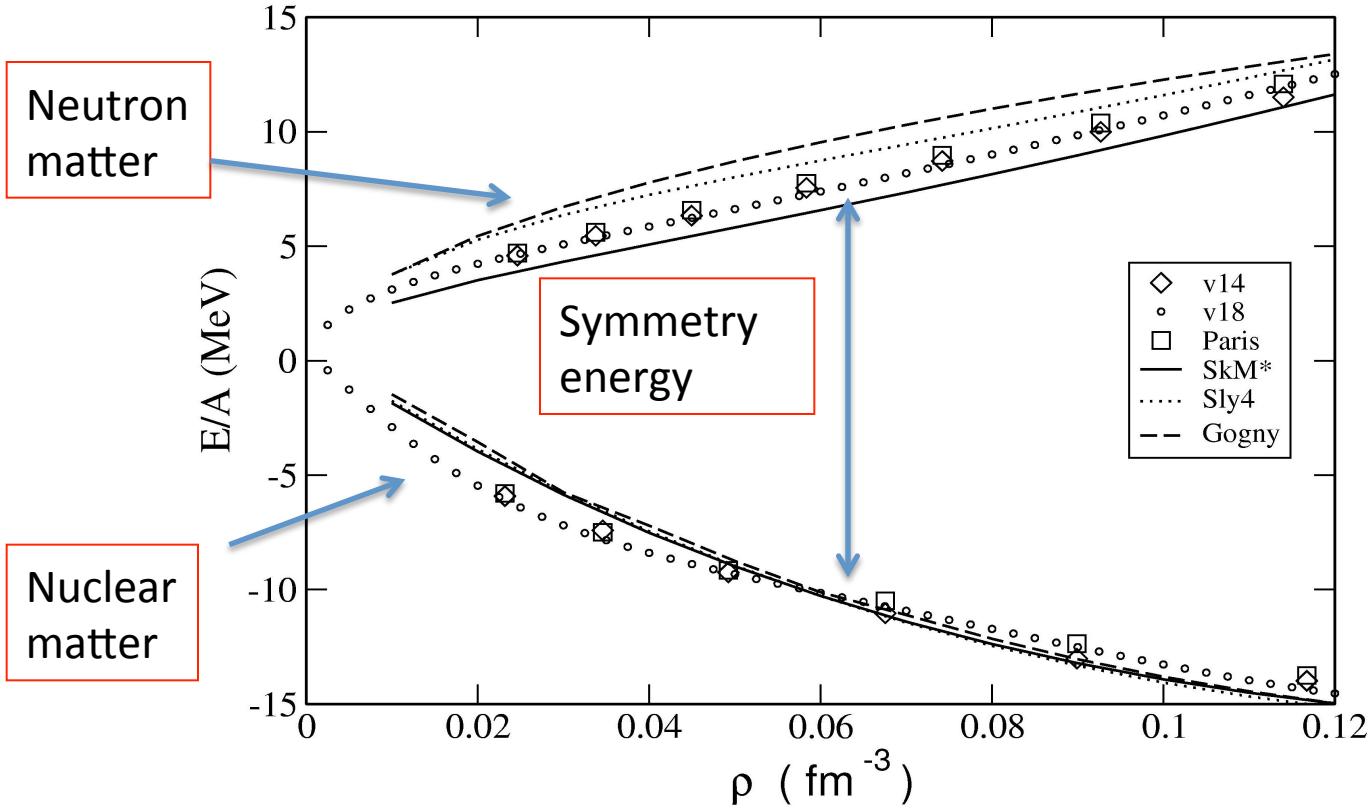

Comparison between phenomenological forces and microscopic calculations (BBG) at sub-saturation densities in uniform neutron and nuclear matter.

M. Baldo, C. Maieron, P.Schuck, X. Vinas, Nucl. Phys. A736(2004)241

I. Vidaña et al. ,
Phys. Rev. C80 (2009) 045806

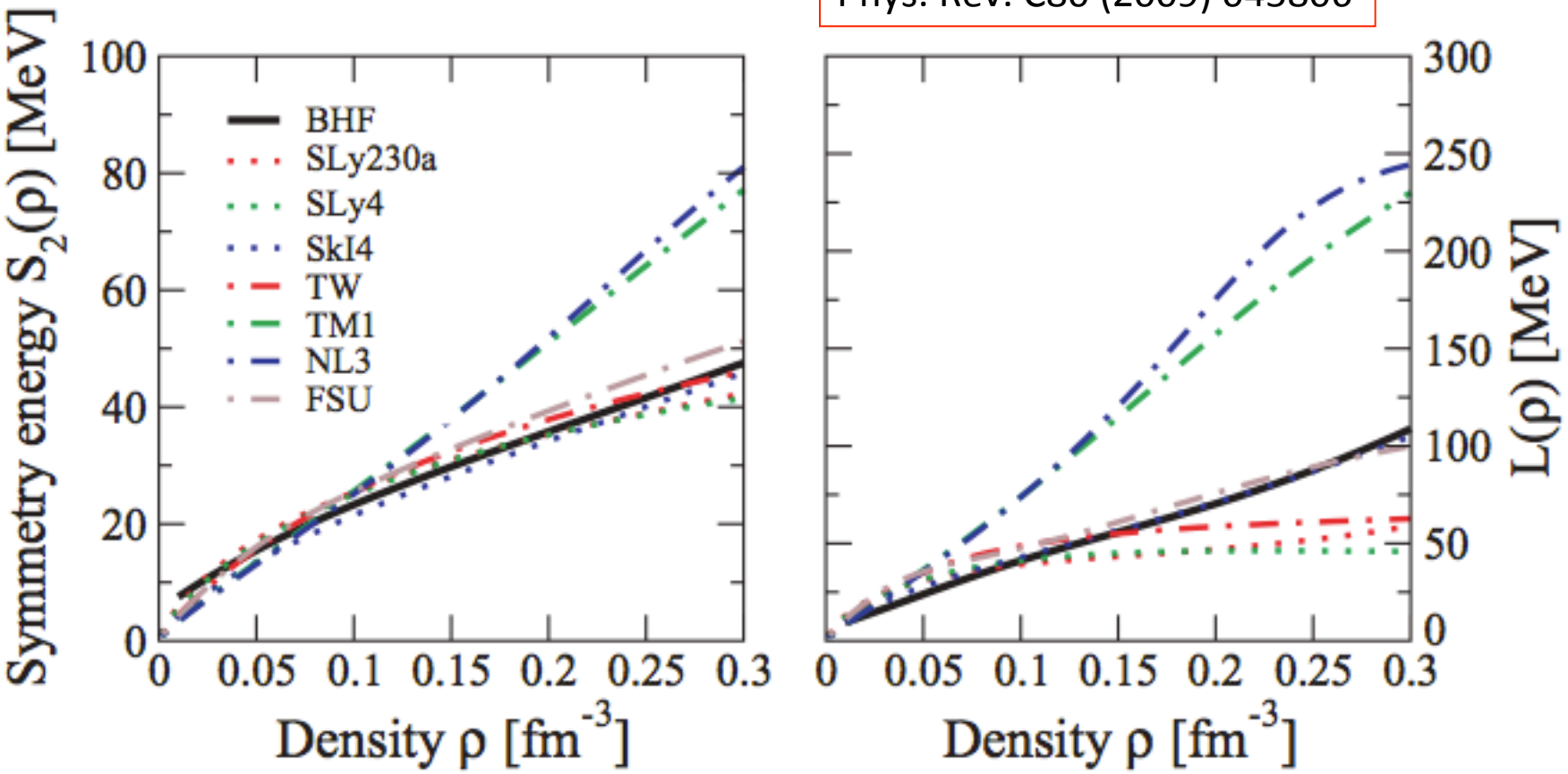

$$\frac{E}{A}(\rho,\beta) = E_{\mathrm{SNM}}(\rho) + S_2(\rho)\beta^2 \,.$$

$$S_2(\rho) = E_{\mathrm{sym}} + L\left(\frac{\rho-\rho_0}{3\rho_0}\right) + \frac{K_{\mathrm{sym}}}{2}\left(\frac{\rho-\rho_0}{3\rho_0}\right)^2$$

H.S. Than et al, PRC 80 (2009) 064312

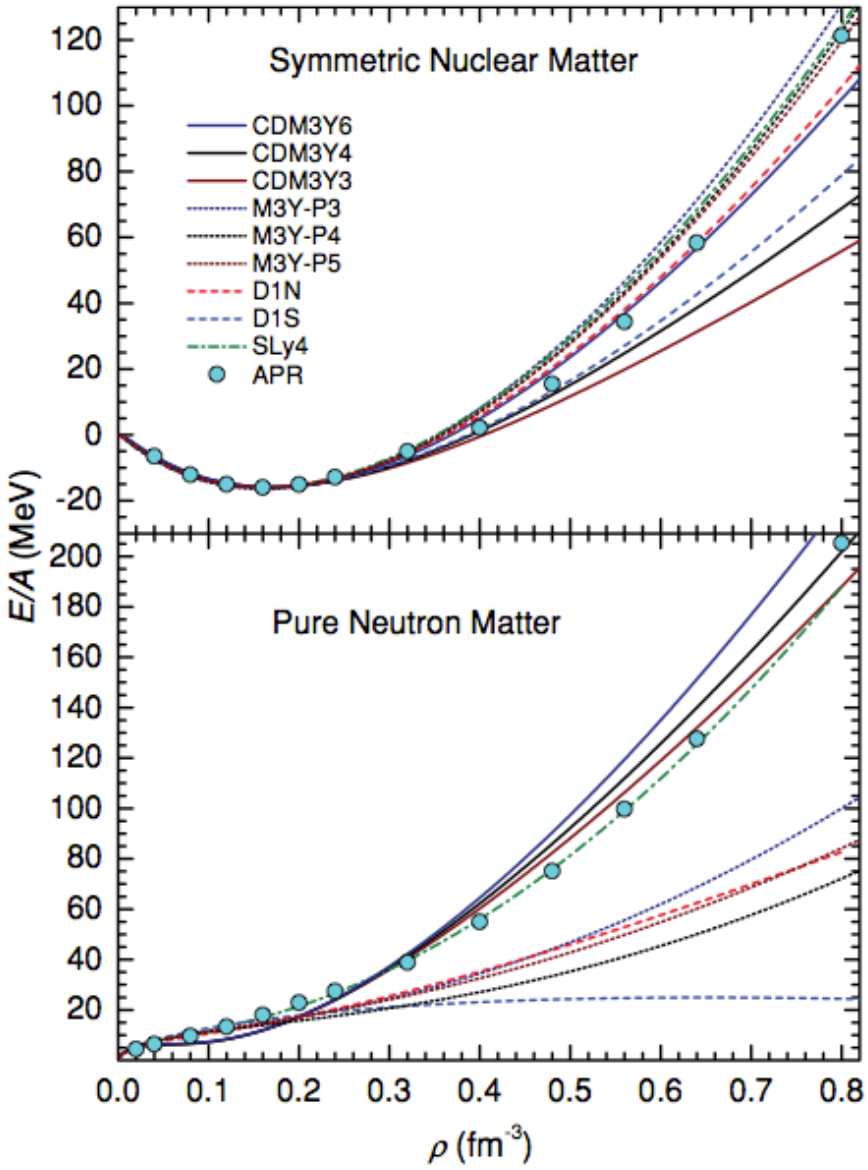

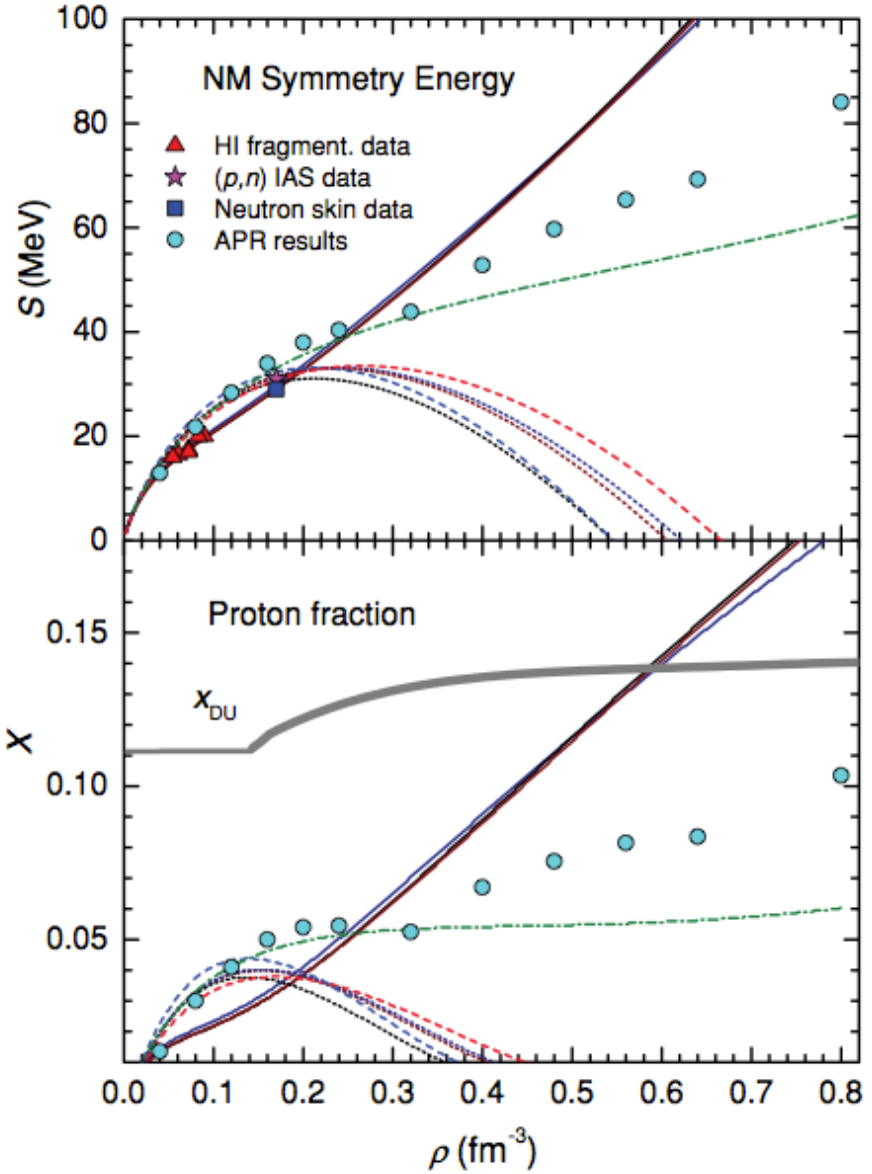

Finite nuclei : correlation between symmetry energy and energy of the GDR

$$f(\rho) \equiv \sqrt{S(\rho)(1+\kappa)}$$

$$23.3 \text{ MeV} < S(0.1) < 24.9 \text{ MeV}.$$

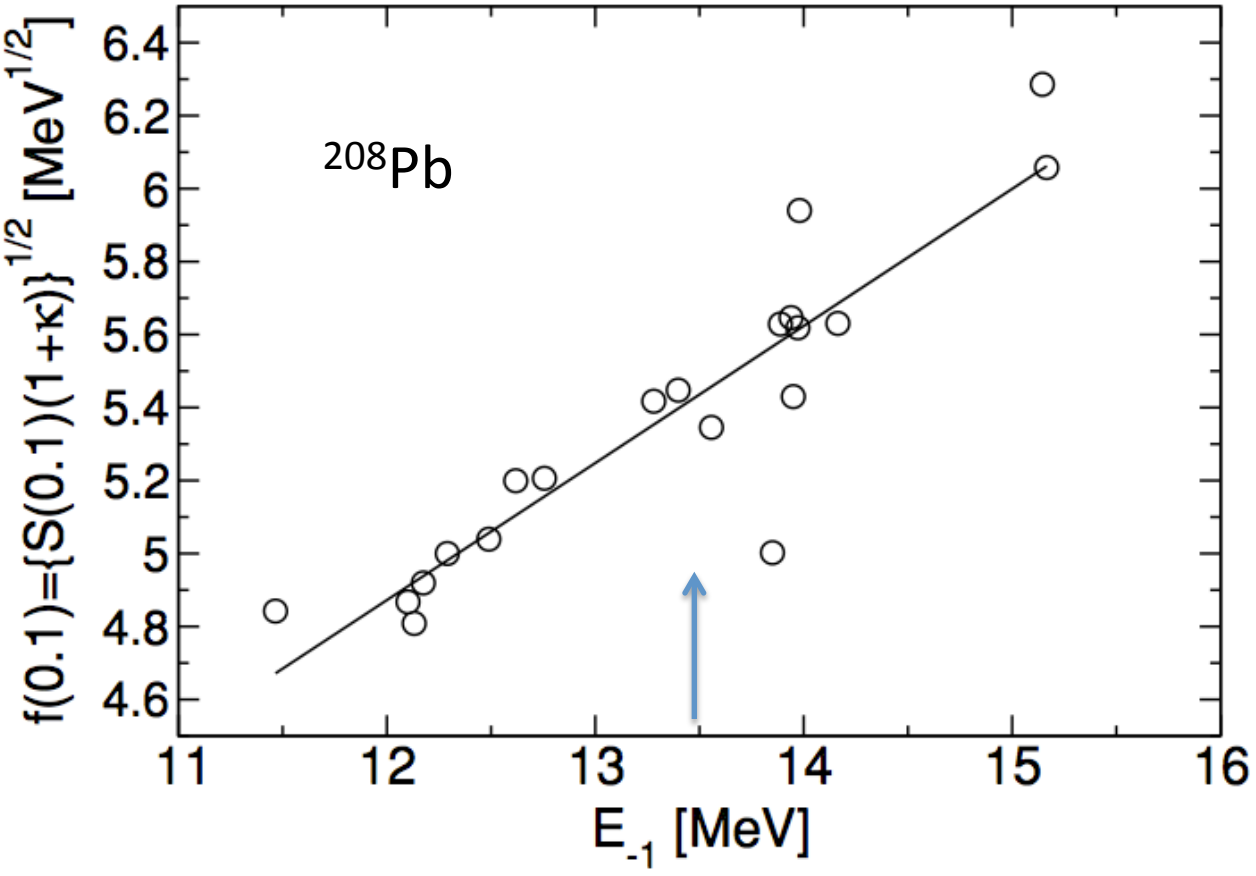

Hartree-Fock equations for Skyrme interaction in spherical systems

$$U_q(\vec{\mathbf{r}}) = t_0\left[\left(1+\tfrac{1}{2}x_0\right)\rho - \left(x_0+\tfrac{1}{2}\right)\rho_q\right] + \tfrac{1}{4}t_3(\rho^2-\rho_q{}^2)$$
$$-\tfrac{1}{8}(3t_1-t_2)\nabla^2\rho + \tfrac{1}{16}(3t_1+t_2)\nabla^2\rho_q + \tfrac{1}{4}(t_1+t_2)\tau$$
$$+\tfrac{1}{8}(t_2-t_1)\tau_q - \tfrac{1}{2}W_0(\vec{\nabla}\cdot\vec{\mathbf{J}} + \vec{\nabla}\cdot\vec{\mathbf{J}}_q) + \delta_{q,+\frac{1}{2}}\,V_C(\vec{\mathbf{r}})\,.$$

Mean field potential

$$\frac{\hbar^2}{2m_q^*}\left[-R_\alpha{}''(r) + \frac{l_\alpha(l_\alpha+1)}{r^2}R_\alpha(r)\right] - \frac{d}{dr}\left(\frac{\hbar^2}{2m_q^*}\right)R_\alpha{}'(r)$$
$$+\left\{U_q(r) + \frac{1}{r}\,\frac{d}{dr}\left(\frac{\hbar^2}{2m_q^*}\right) + \left[j_\alpha(j_\alpha+1) - l_\alpha(l_\alpha+1) - \tfrac{3}{4}\right]\right.$$
$$\left.\times\frac{1}{r}W_q(r)\right\}R_\alpha(r) = e_\alpha R_\alpha(r)\,.$$

Schrödinger equation

$$\frac{\hbar^2}{2m_q^*(\vec{\mathbf{r}})} = \frac{\hbar^2}{2m} + \tfrac{1}{4}(t_1+t_2)\rho + \tfrac{1}{8}(t_2-t_1)\rho_q\,;$$

Effective mass

Looking for the energy minimum at a fixed baryon density considering the system as a whole (no distinction between the nucleus and the neutron gas)

Density = 1/30 saturation density

Wigner-Seitz approximation

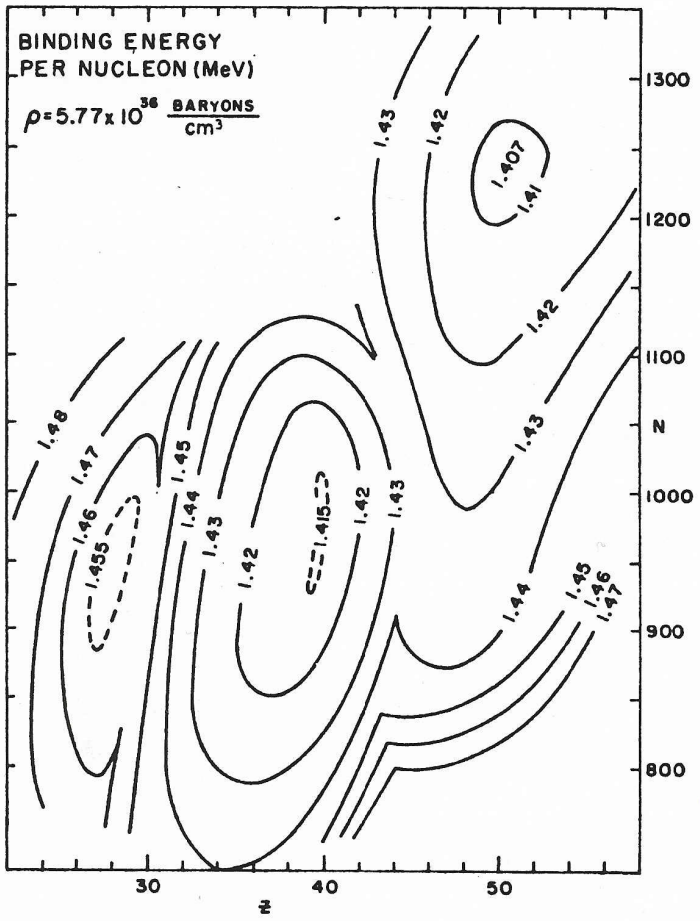

The structure of nuclei and Z/N ratio are dictated by beta equilibrium $\mu_n = \mu_p + \mu_e$

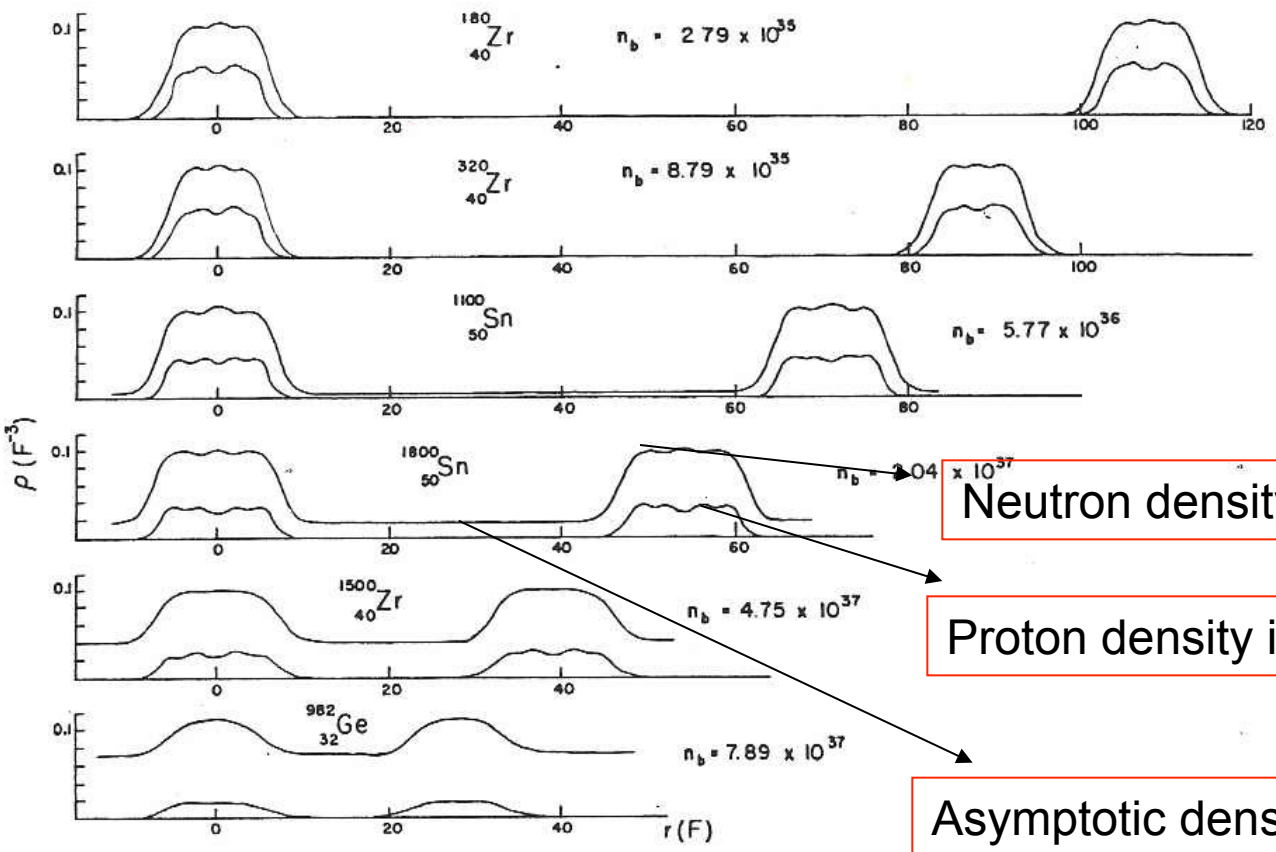

Neutron density in the nuclear cluster

Proton density in the nuclear cluster

Asymptotic density:
Uniform superfluid neutron matter

The inner crust: coexistence of finite nuclei with a sea of free neutrons

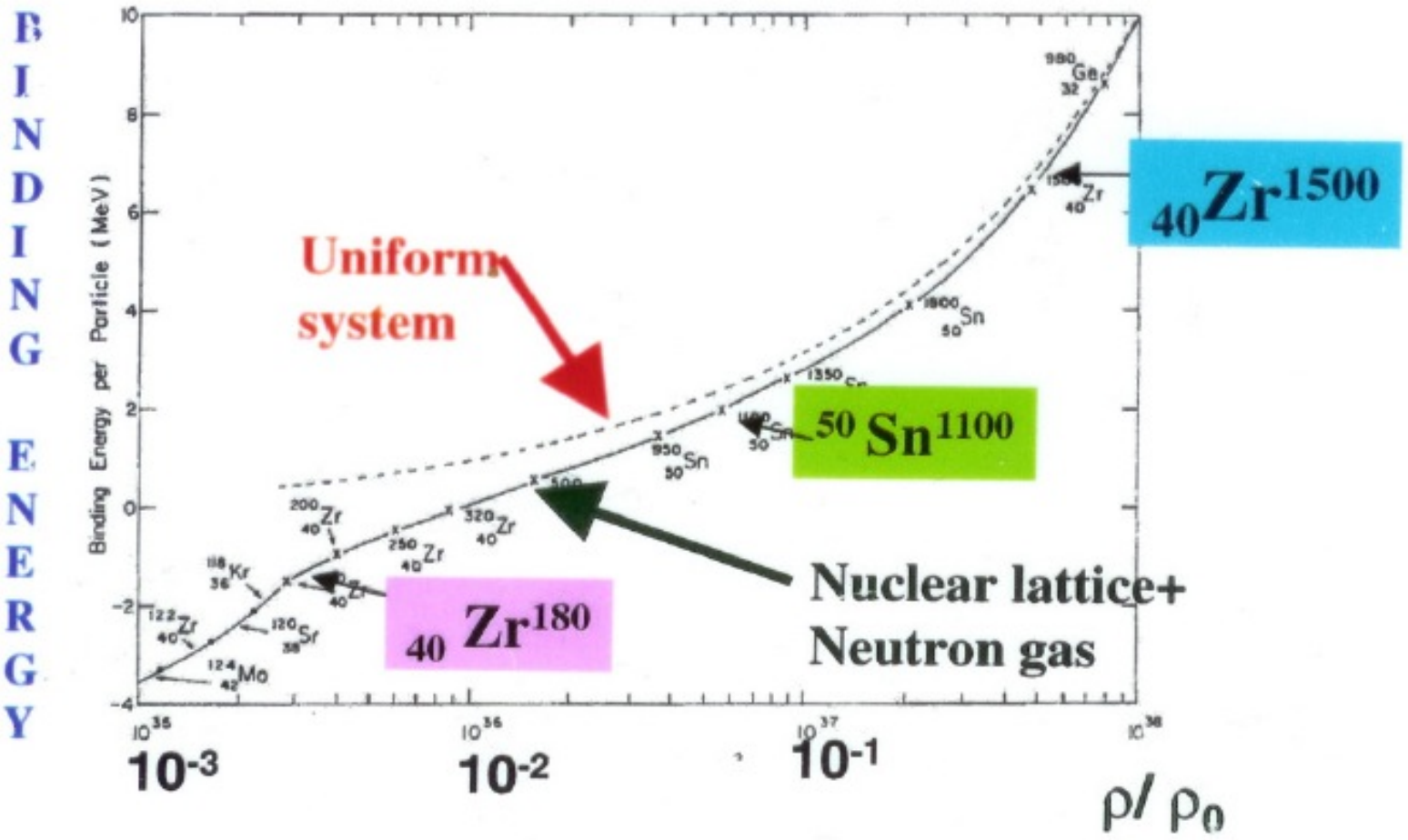

J. Negele, D. Vautherin
Nucl. Phys. A207 (1974) 298

TABLE 1

PROPERTIES OF WIGNER-SEITZ CELLS ALONG THE INNER CRUST

N_{zone}	ρ (g cm^{-3})	R_{WS} (fm)	N	N_{bound}	E_F (MeV)	E_F(unif) (MeV)	V_0 (MeV)	R_N (fm)	a_0 (fm)
10.....	4.7×10^{11}	54	140	110	0.2	0.7	...	...	...
9.....	6.7×10^{11}	49	160	110	0.4	0.9	...	...	...
8.....	1.0×10^{12}	46	210	110	0.8	1.2	...	...	...
7.....	1.5×10^{12}	44	280	110	1.3	1.7	...	...	...
6.....	2.7×10^{12}	42	460	110	2.2	2.6	...	...	...
5.....	6.2×10^{12}	39	900	110	4.1	4.6	...	...	...
4.....	9.7×10^{12}	36	1050	110	4.8	5.3	40	7	0.8
3.....	3.3×10^{13}	28	1750	110	13.5	14.4	31	7.5	0.9
2.....	7.8×10^{13}	20	1460	70	24	25.2	19	7	1.1
1.....	1.3×10^{14}	14	950	40	32	33	13.5	5.3	1.25

NOTE.—The physical parameters of the 10 zones in the inner crust analyzed in this paper are reported as derived from the results of Negele & Vautherin 1973. For each zone, we list the neutron density ρ, the radius of the cell R_{WS}, the total number of neutrons in the cell N, the number of neutrons bound in the nucleus N_{bound}, the Fermi energy E_F, and the Fermi energy E_F(unif) obtained if there was no nucleus at center of the cells so that no neutron was bound. For the zones 1–4, we also give the parameters of the Saxon-Woods potential used to simulate the density profile obtained by Negele and Vautherin: the depth of the potential is denoted by V_0, its radius by R_N, and its diffusivity by a_0.

Permanence of shell structure

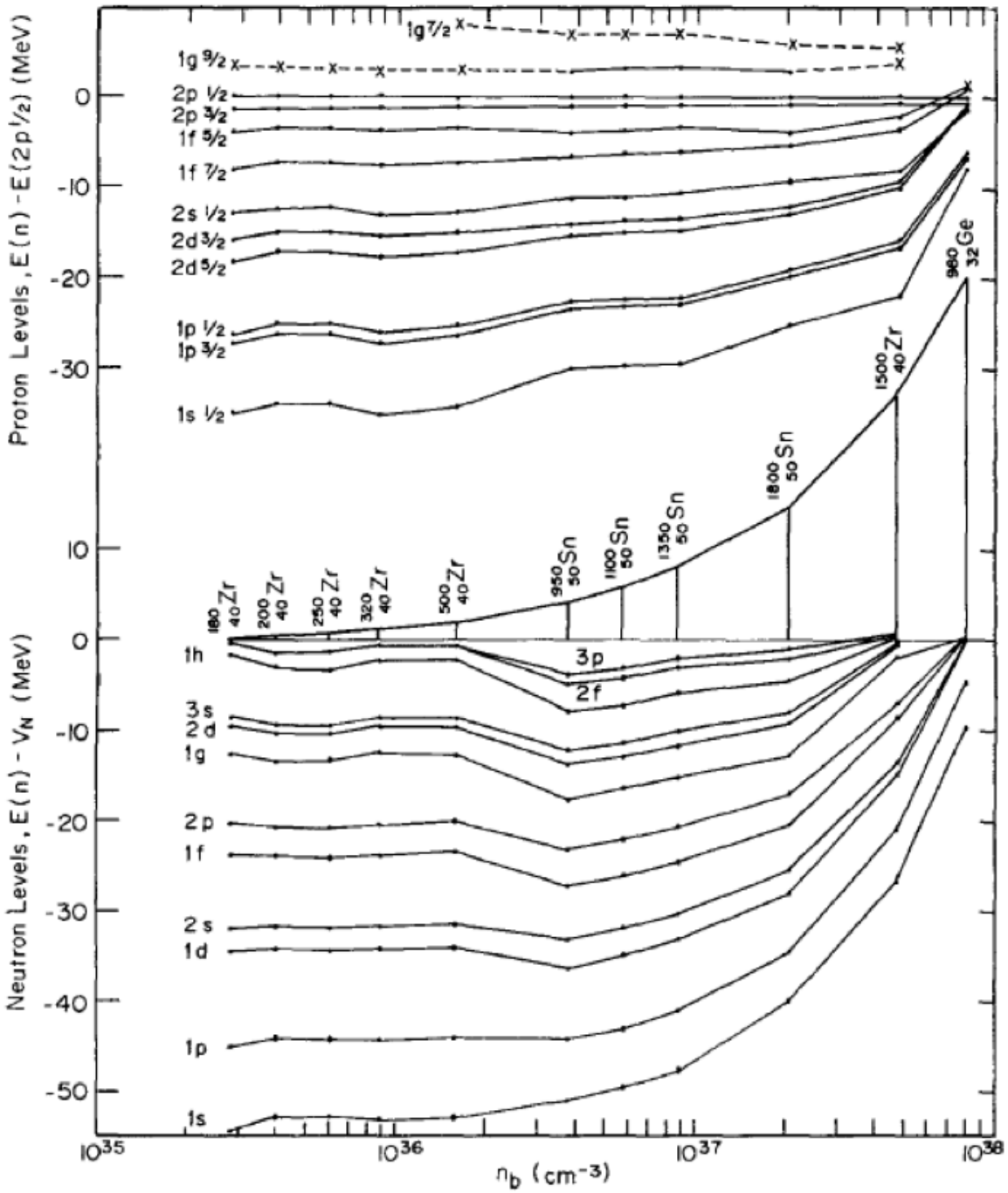

Fig 5. Single-particle spectrum of protons and neutrons

Resonant states studied through phase shift analysis

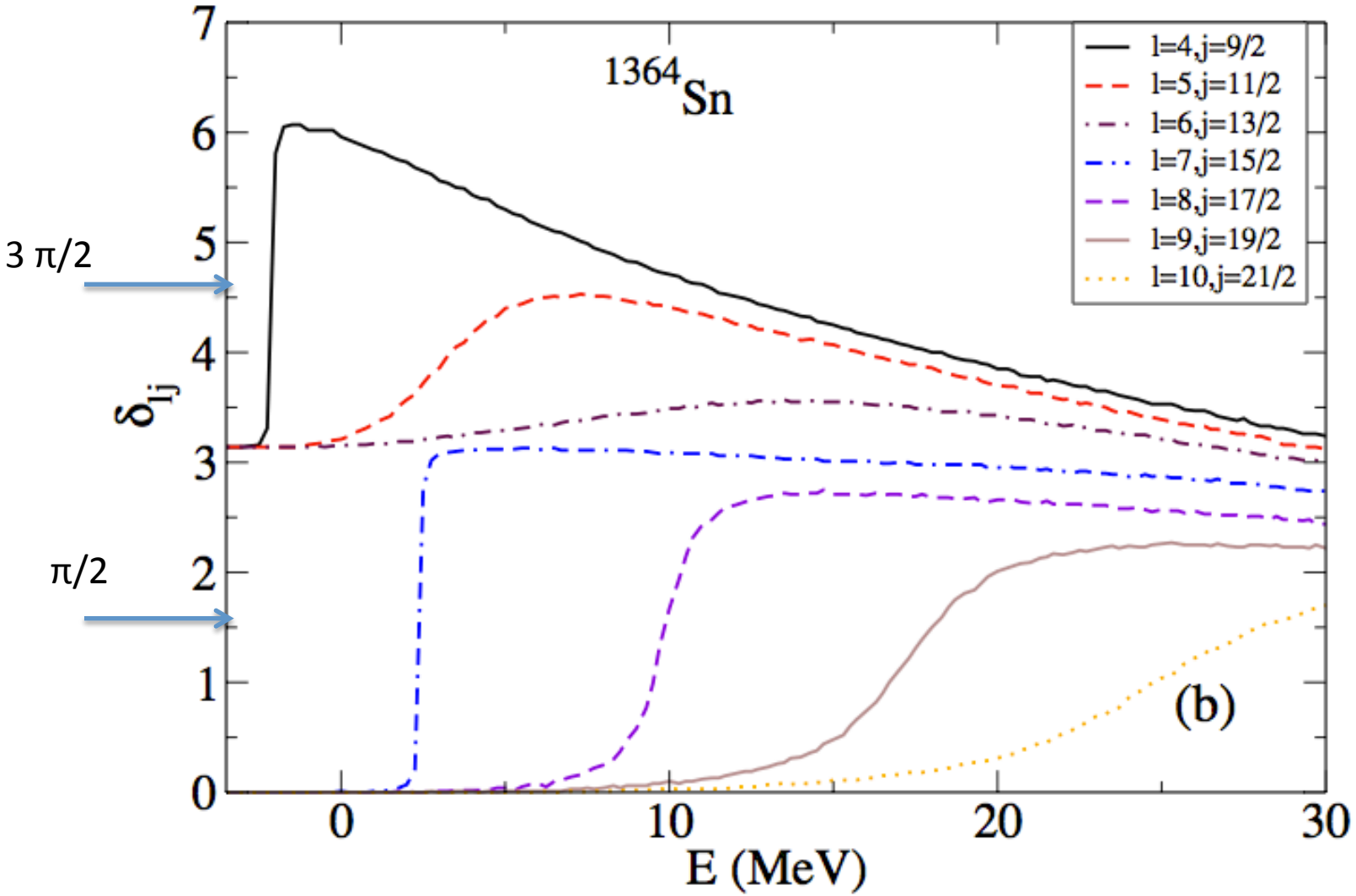

The strongest transitions involve resonant states

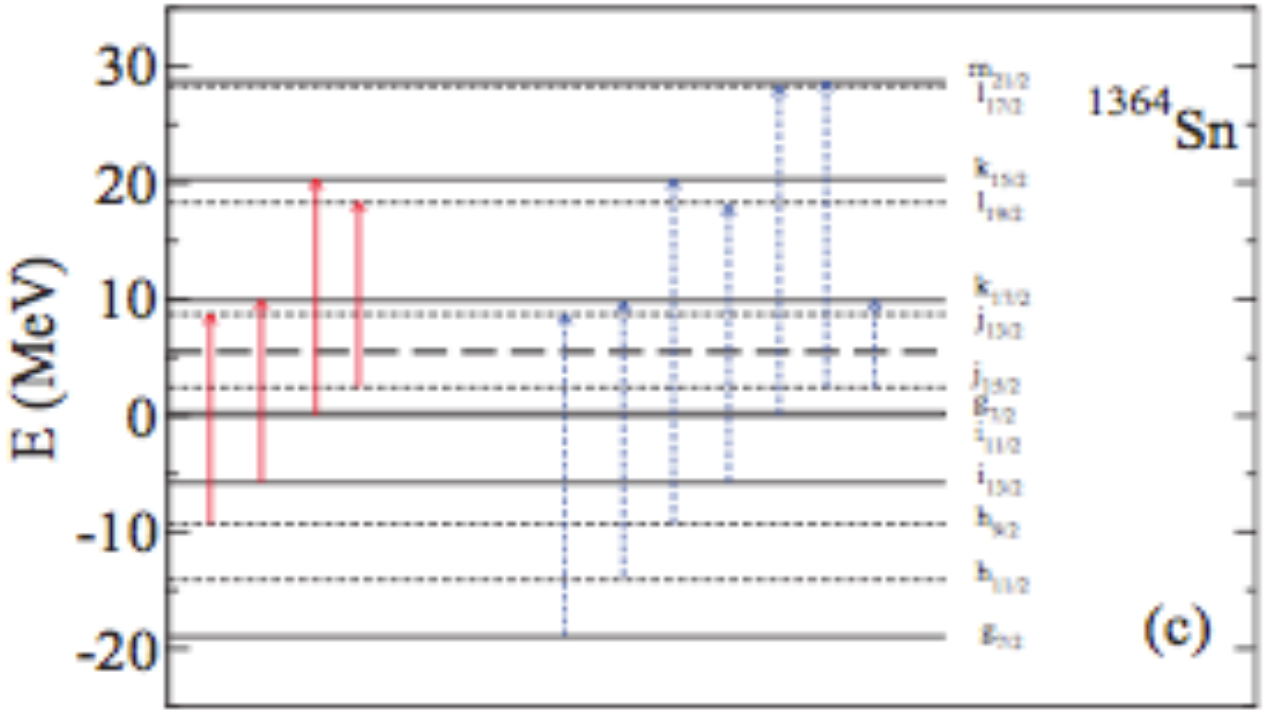

FIG. 10. (Color online) Strongest neutron particle-hole transitions in ^{132}Sn (a), in ^{498}Zr (b) and in ^{1364}Sn (c); see text for details. Single-particle levels of even and odd parity are drawn by solid and dashed lines. Solid (red) and dashed (blue) arrows refer to 2^+ and to 3^- transitions. The Fermi energy is represented by the thick dashed line.

The WS cell without protons should be like a piece of neutron matter.

Check the linear response to the operator

$$e^{i\vec{q}\cdot\vec{r}} = 4\pi \sum_{L=0}^{+\infty} \sum_{M=-L}^{+L} i^L j_L(qr) Y^*_{LM}(\Omega_q) Y_{LM}(\Omega_r)$$

$$S^{(0)}_{\mathrm{WS},L}(q, E) = 4\pi(2L+1) \sum_{\nu=0} \Bigg| \sum_{j_p j_h} \left[X^{\nu}_{ph}(L) + (-)^L Y^{\nu}_{ph}(L)\right] \times \langle j_p || i^L Y_L || j_h \rangle \langle R_p || j_L(qr) || R_h \rangle \Bigg|^2 L(E, E_\nu).$$

Response in the cell for the various multipolarities L (q= 0.51 fm^{-1})

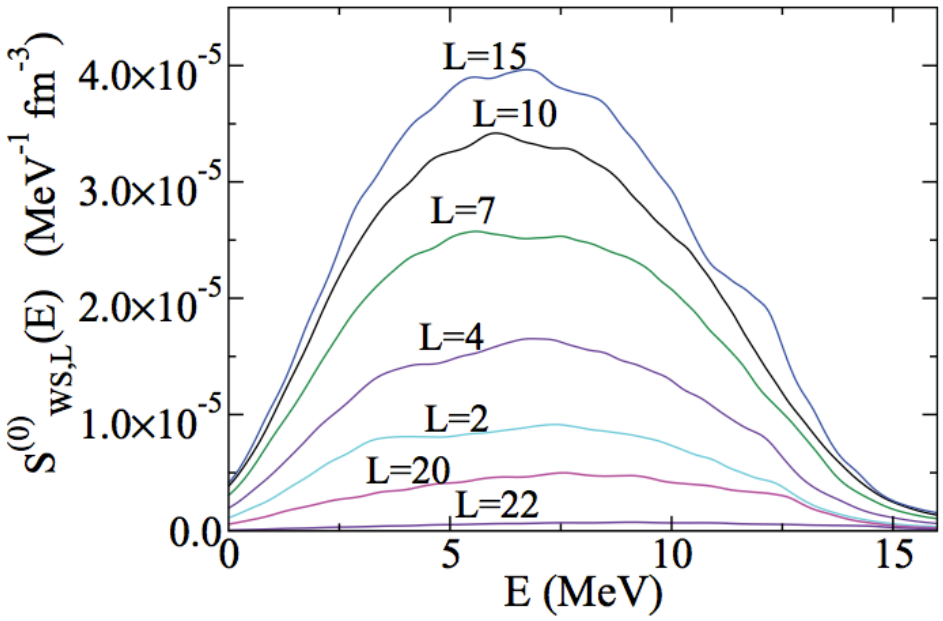

Summing over L, we recover the analytic result in neutron matter for S(q,E)

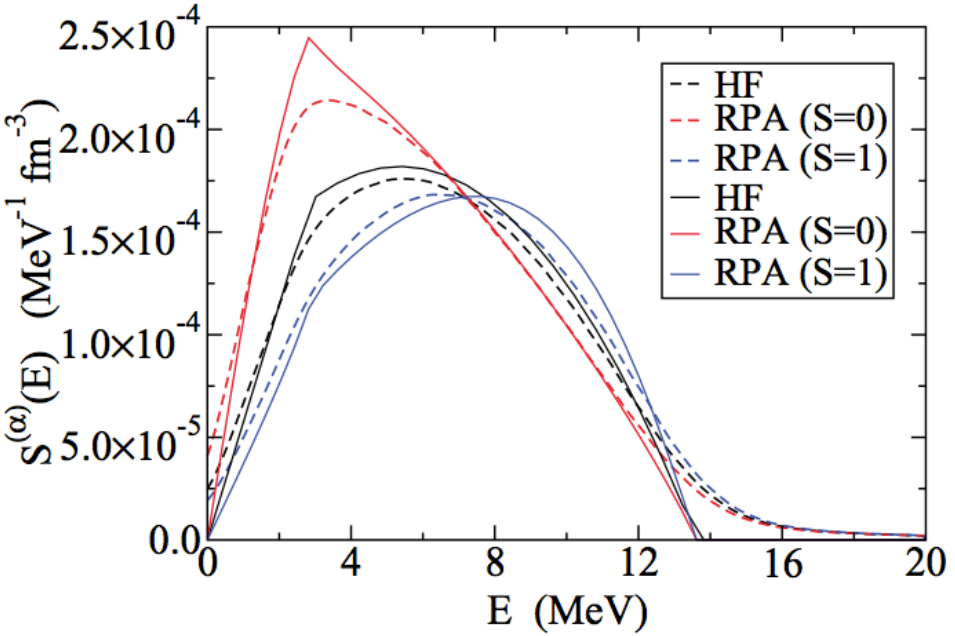

Response to the operator $dU/dr\ Y_{2M}$

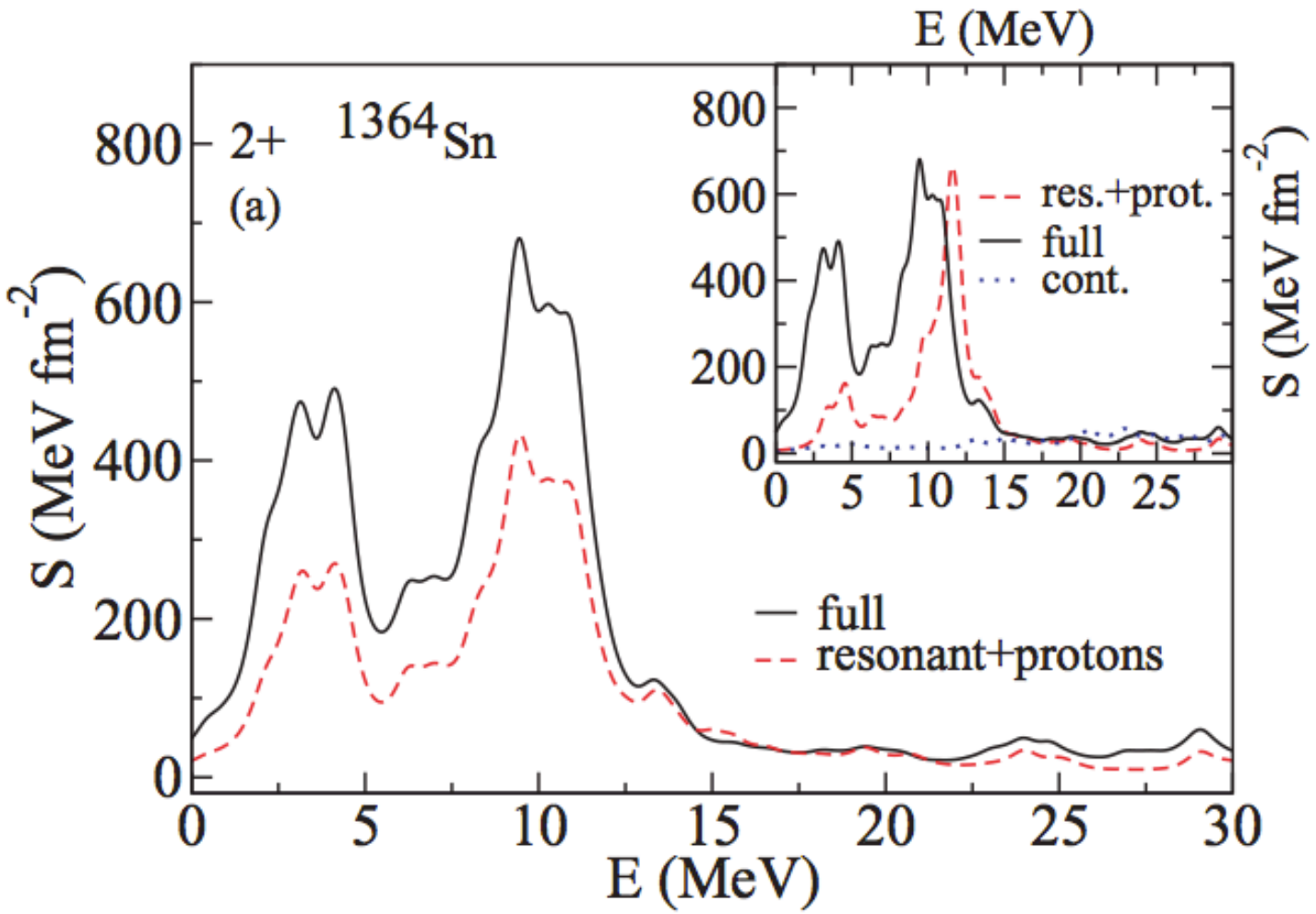

Evolution of the RPA response: from exotic nuclei to the crust

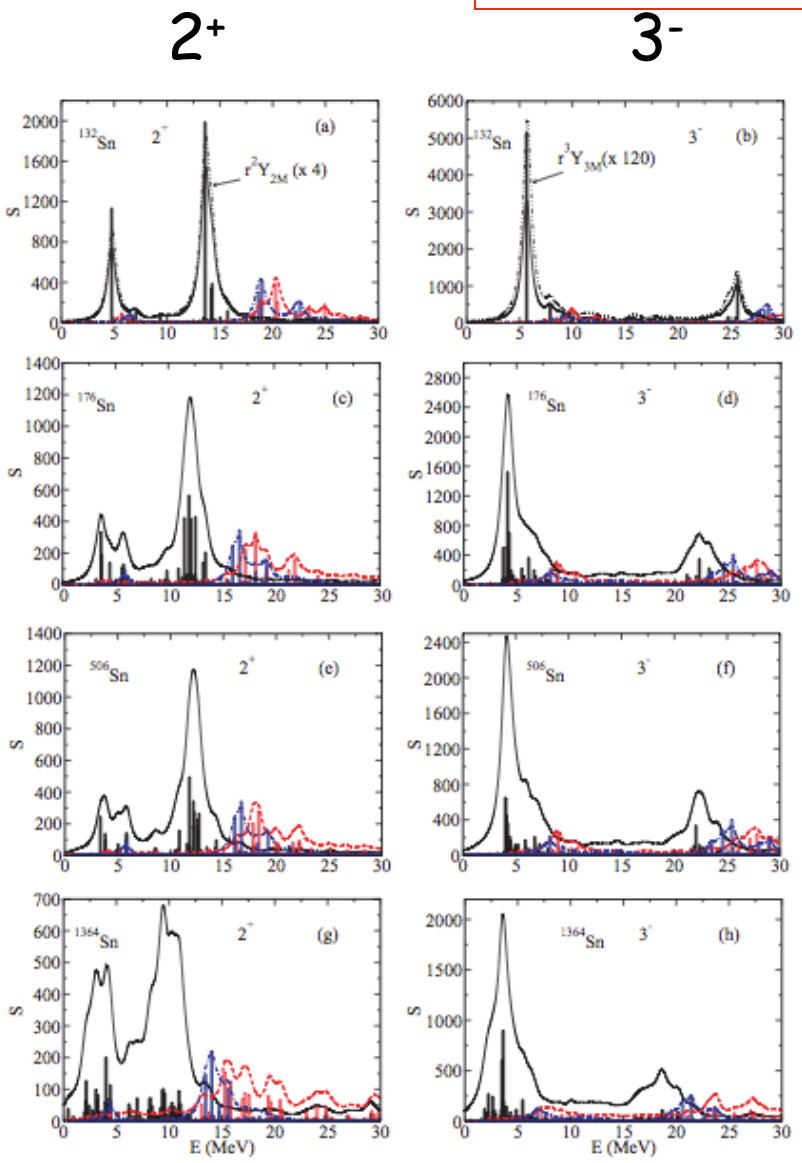

S. Baroni et al., Phys. Rev. C 82(2010)015807

First calculation of band structure beyond the WS approximation

The band theory is explained in standard solid-state physics textbooks, for instance in the book by Kittel [241]. Single particle wave functions of nucleon species $q = n, p$ in the crust are characterized by a wave vector $\boldsymbol{k}$ and obey the Floquet–Bloch theorem

$$\varphi_{\boldsymbol{k}}^{(q)}(\boldsymbol{r}+\boldsymbol{T}) = e^{\mathrm{i}\boldsymbol{k}\cdot\boldsymbol{T}}\varphi_{\boldsymbol{k}}^{(q)}(\boldsymbol{r})\,, \tag{61}$$

where $\boldsymbol{T}$ is any lattice translation vector (which transforms the lattice into itself). This theorem implies that the wave functions are modulated plane waves, called simply Bloch waves

$$\varphi_{\boldsymbol{k}}^{(q)}(\boldsymbol{r}) = e^{\mathrm{i}\boldsymbol{k}\cdot\boldsymbol{r}}u_{\boldsymbol{k}}^{(q)}(\boldsymbol{r})\,, \tag{62}$$

with $u_{\boldsymbol{k}}^{(q)}(\boldsymbol{r})$ having the full periodicity of the lattice, $u_{\boldsymbol{k}}^{(q)}(\boldsymbol{r}+\boldsymbol{T}) = u_{\boldsymbol{k}}^{(q)}(\boldsymbol{r})$.

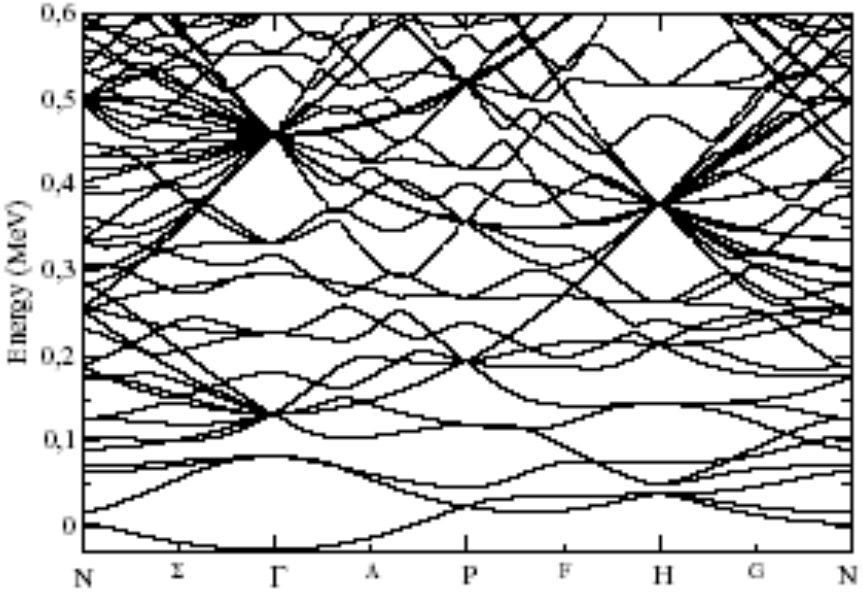

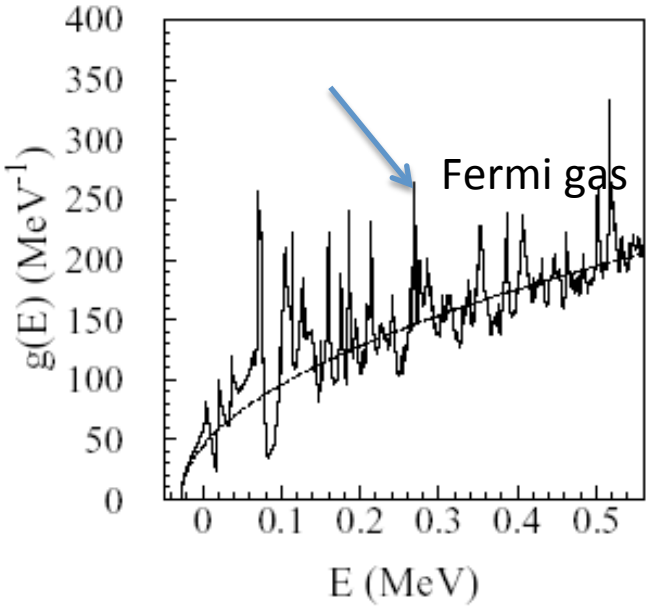

N. Chamel, S. Naimi, E. Khan, J. Margueron, Phys. Rev. C75 (2007) 055806

Integrated number of levels

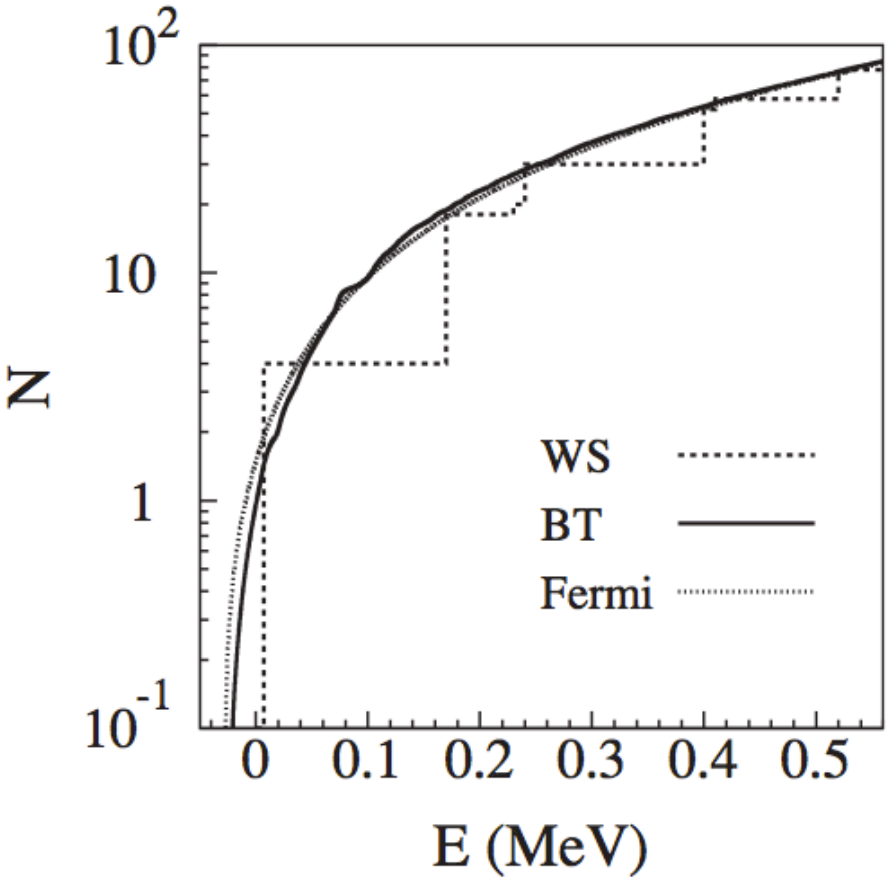

Wigner-Seitz approximation deteriorates at the bottom layers of the crust, when the distance between clusters becomes too small and the results depend on the specific boundary conditions.

Spherical nuclei may become unstable when they occupy a large fraction of the cell

One possibility: fission instability [Pethick & Ravenhall (1995)]

The Coulomb energy of lattice (within Wigner-Seitz approx.)

$$E_{\rm Coul} \simeq E^{(0)}_{\rm Coul}\left(1-\frac{3}{2}u^{1/3}\right)$$

u: volume frac. of nuclei

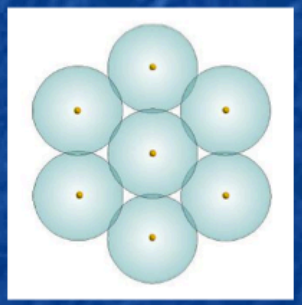

Chamel & Haensel (2008)

$$\left.\begin{array}{l} E_{\rm surf}/A \propto A^{-1/3} \\ E_{\rm Coul}/A \propto A^{2/3} \end{array}\right\} \Rightarrow \quad E_{\rm surf} = 2E_{\rm Coul}$$

(minimizing with respect to *A*)

Bohr-Wheeler's cond.

$$E^{(0)}_{\rm Coul} \geq 2E_{\rm surf}$$

$$u \geq 1/8$$

High density → volume frac. u↑ → fission inst. → pasta phases?

G. Watanabe

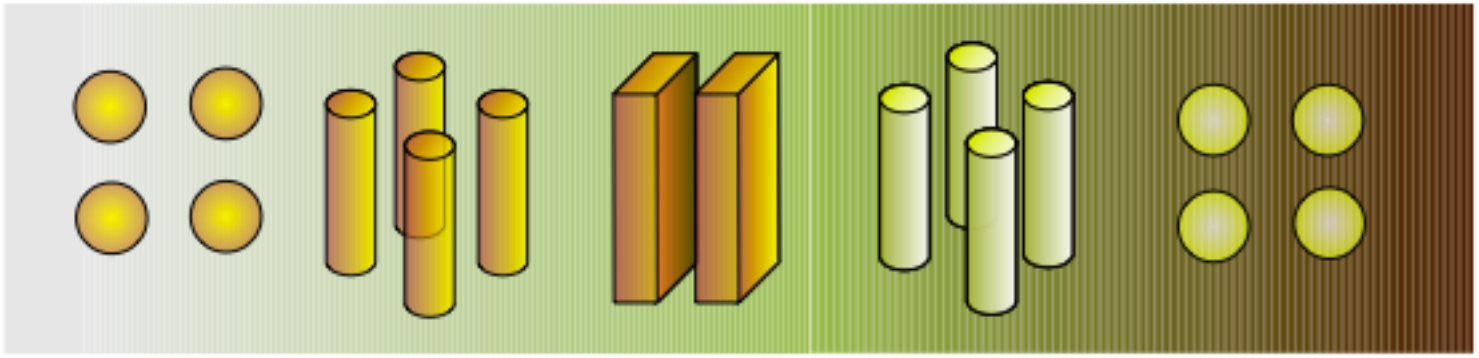

w (%)

Fraction of space occupied by nuclear clusters

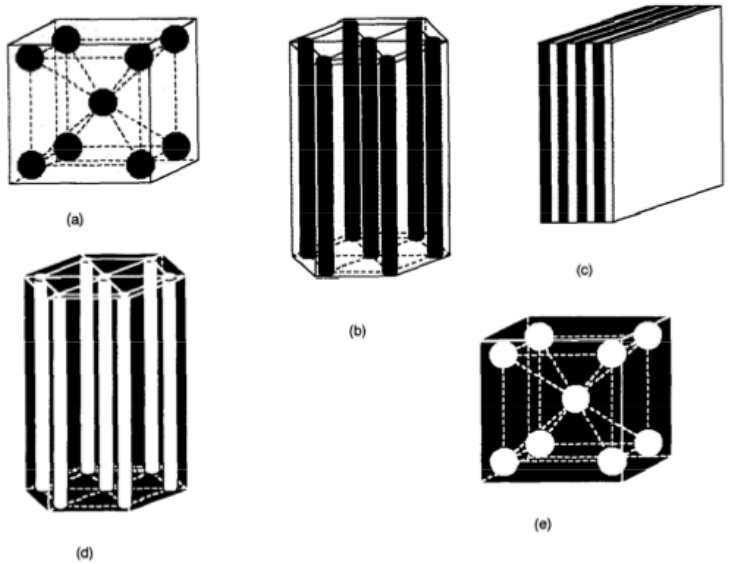

Fig. 1. Candidates for the nuclear shapes and lattice types. Spherical, cylindrical, slab, cylindrical hole and spherical hole nuclei are shown as (a)–(e). Both protons and neutrons occupy the darker parts, while only neutrons occupy the lighter parts.

Black: proton and neutrons
White: neutron gas

K. Oyamatsu

Pasta phases by QMD

$x = 0.3$, T=0

$0.1\rho_0$ sphere

$0.175\rho_0$ cylinder

$0.35\rho_0$ slab

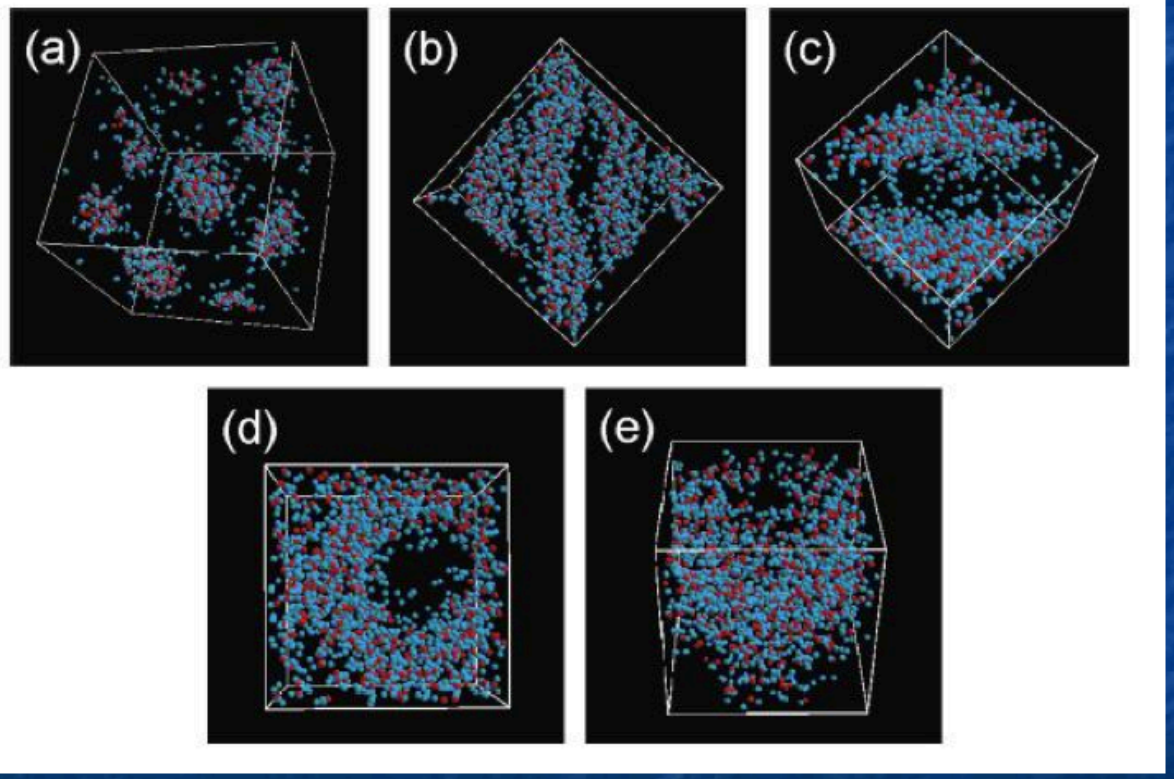

$0.5\rho_0$ cylindrical hole

$0.55\rho_0$ spherical hole

GW et al. (2003)

$x = 0.2$, $\rho = 0.3\ \rho_0$
T=1MeV

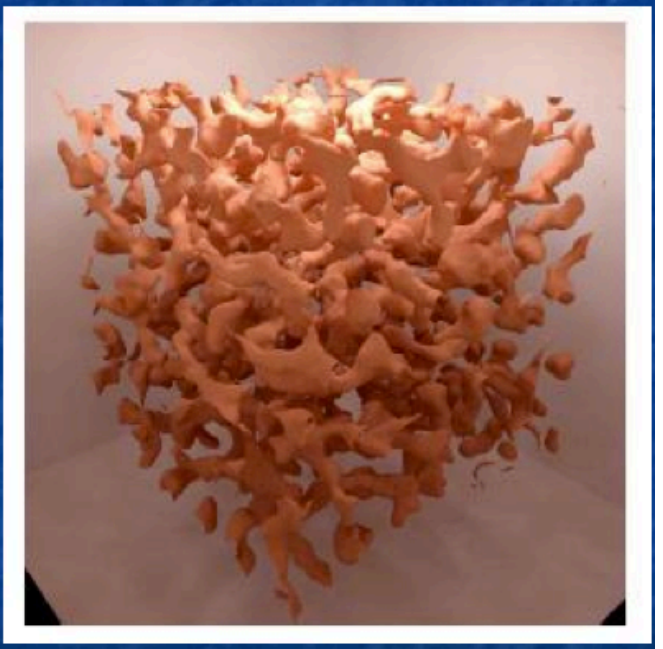

Horowitz et al. (2004)

Self-consistent Modeling: QMD

- **Quantum Molecular Dynamics (QMD): semi-classical dynamical simulations with nucleonic degrees of freedom (Watanabe and Sonoda, nucl-th/0512020).**
- **Pasta shapes emerge without pre-conditioning.**
- **Pasta formation from compression and cooling demonstrated.**

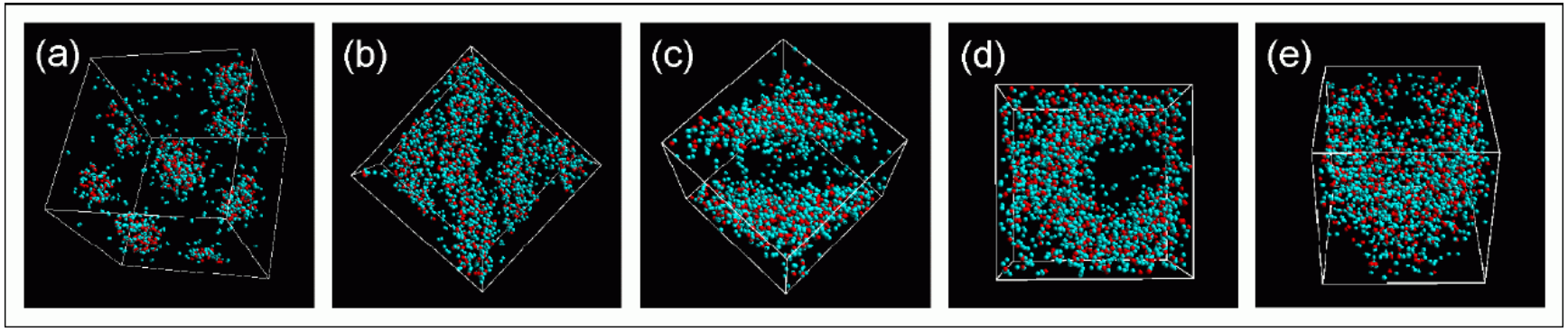

$0.1\rho_0$ $0.175\rho_0$ $0.35\rho_0$ $0.5\rho_0$ $0.55\rho_0$

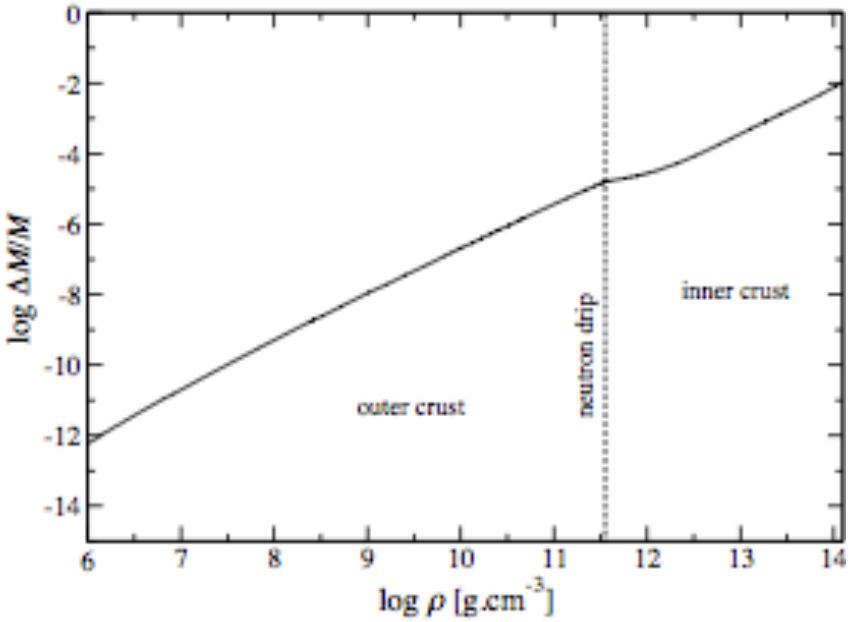

SLy4: transition to uniform matter

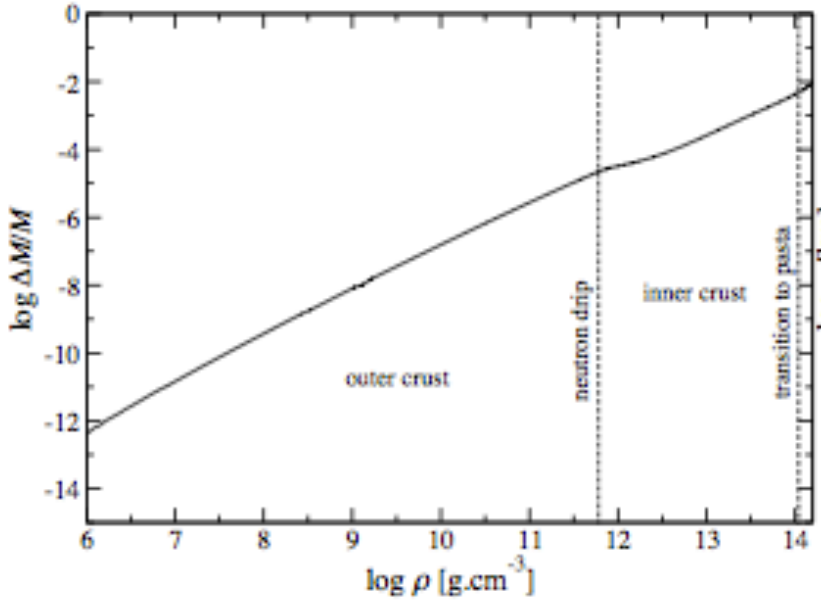

FPS: transition to pasta phase

SLy4

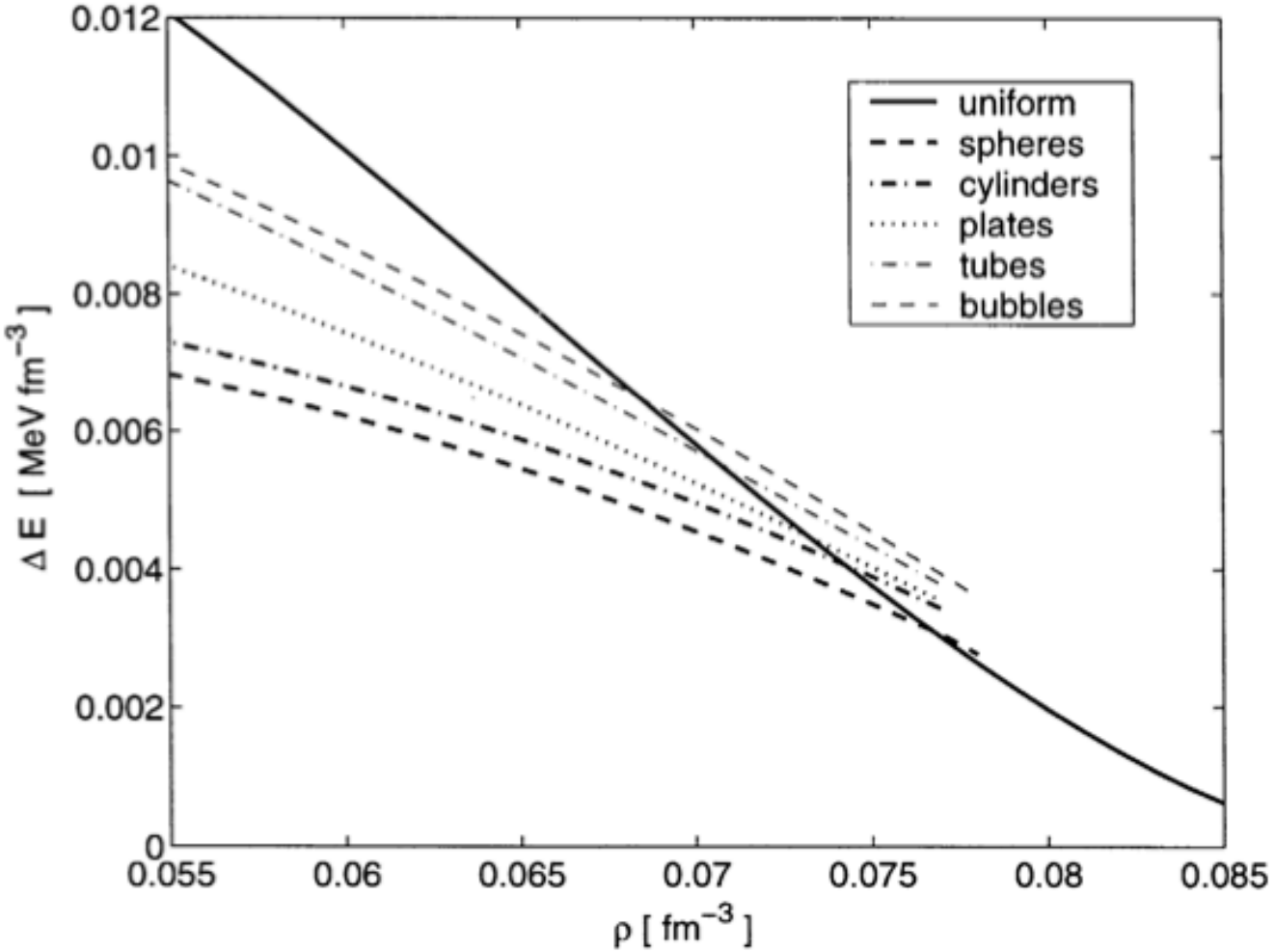

F. Douchin, P. Haensel, PLB 485 (2000) 107

The bulk energy per nucleon is an essential ingredient of the macroscopic nuclear model. We set this energy as

$$w = \frac{3\hbar^2(3\pi^2)^{2/3}}{10m_n n}\left(n_n^{5/3} + n_p^{5/3}\right) + (1-\alpha^2)v_s(n)/n + \alpha^2 v_n(n)/n, \quad (1)$$

where

$$v_s = a_1 n^2 + \frac{a_2 n^3}{1 + a_3 n} \quad (2)$$

and

$$v_n = b_1 n^2 + \frac{b_2 n^3}{1 + b_3 n} \quad (3)$$

are the potential energy densities for symmetric nuclear matter and pure neutron matter, n_n and n_p are the neutron and proton number densities, $n = n_n + n_p$, $\alpha = (n_n - n_p)/n$ is the neutron excess, and m_n is the neutron mass.

A set of expressions (1)–(3) is one of the simplest that reduces to the usual form (4) in the limit of $n \to n_0$ and $\alpha \to 0$,

$$w = w_0 + \frac{K_0}{18n_0^2}(n - n_0)^2 + \left[S_0 + \frac{L}{3n_0}(n - n_0)\right]\alpha^2. \quad (4)$$

Here w_0, n_0, and K_0 are the saturation energy, saturation density, and incompressibility of symmetric nuclear matter. The parameters L and S_0 are associated with the density-dependent symmetry energy coefficient $S(n)$: S_0 is the symmetry energy coefficient at $n = n_0$ and $L = 3n_0(dS/dn)_{n=n_0}$ is the symmetry energy density derivative coefficient (hereafter

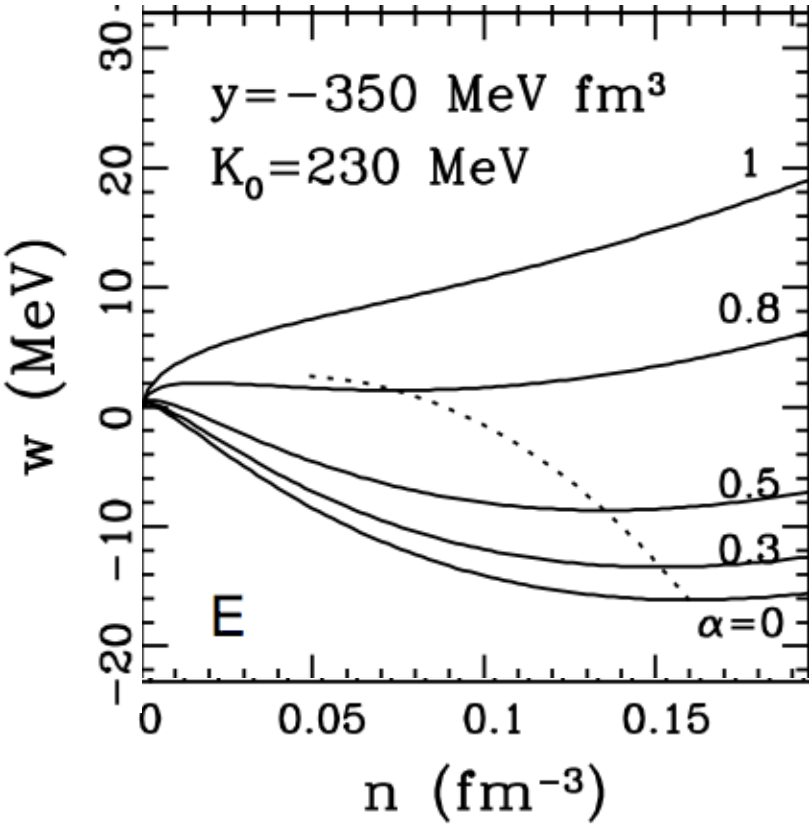

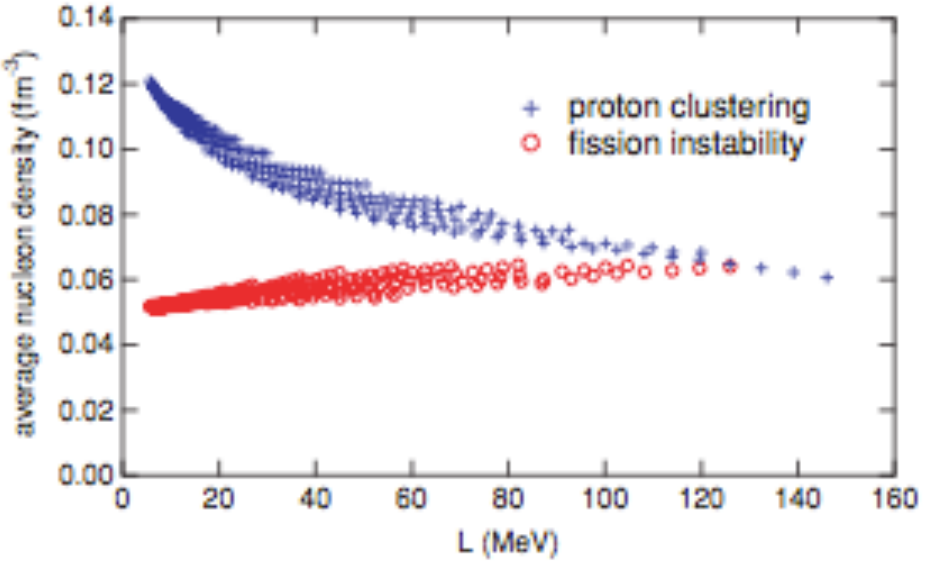

FIG. 8. (Color online) The onset density of proton clustering in uniform nuclear matter as a function of L. For comparison, we plot the density corresponding to $u = 1/8$ in the phase with spherical nuclei, which is taken from Fig. 6(a).

K. Oyamatsu and K. Iida, PRC 75 (2007) 015801

Active lines of development in microscopic studies of the inner crust (spherical nuclei, $^1S_0$ pairing)

Study the inhomogeneous structure of the Wigner-Seitz cell:
- Isotopic composition
- Mean field
- Collective excitations
- Superfluidity within BCS theory and beyond
- Specific heat, cooling
- Vortices

Study the influence of the Coulomb lattice:
- Band structure, Level density
- Entrainment, effective mass
- Transport properties
- Ion vibrations
- Specific heat

A few basic questions about pairing correlations

1. **Does superfluidity affect the results found by Negele and Vautherin?**

2. **What is the spatial dependence of the pairing gap?**

   How important are the nuclear clusters?

3. **How much are the gaps affected by many-body processes ?**

4. **Can we prove experimentally that the crust is really superfluid?**

Commonly used approach:
just use the value of the pairing gap at the Fermi energy calculated in neutron/neutron star matter

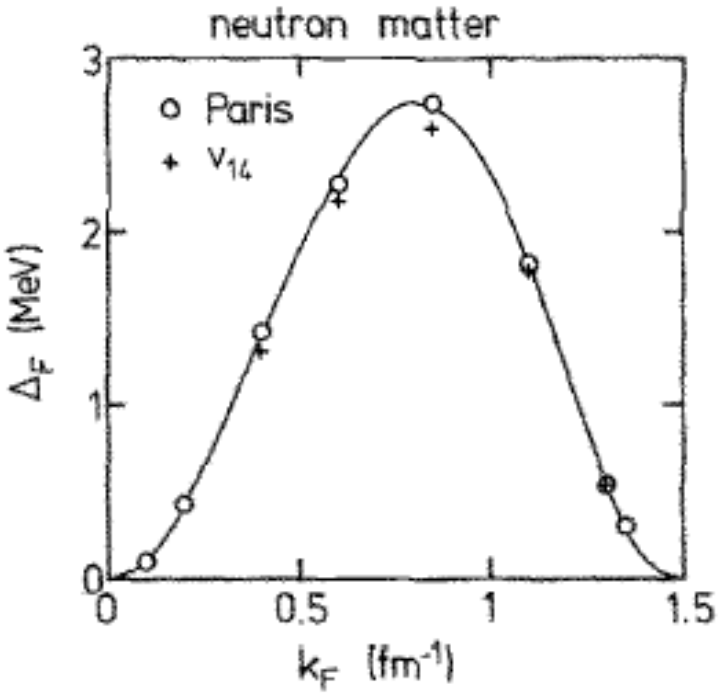

Independence of the BCS pairing gap from the specific bare potential

PHYSICAL REVIEW VOLUME 110, NUMBER 4 MAY 15, 1958

Possible Analogy between the Excitation Spectra of Nuclei and Those of the Superconducting Metallic State

A. Bohr, B. R. Mottelson, and D. Pines*
Institute for Theoretical Physics, University of Copenhagen, Copenhagen, Denmark, and Nordisk Institut for Teoretisk Atomfysik, Copenhagen, Denmark

(Received January 7, 1958)

The evidence for an energy gap in the intrinsic excitation spectrum of nuclei is reviewed. A possible analogy between this effect and the energy gap observed in the electronic excitation of a superconducting metal is suggested.

THE nuclear structure exhibits many similarities with the electron structure of metals. In both cases, we are dealing with systems of fermions which may be characterized in first approximation in terms of independent particle motion. For instance, the statistical level density, at not too low excitation energies, is expected to resemble that of a Fermi gas. Still, in both systems, important correlations in the particle motion arise from the action of the forces between the particles and, in the metallic case, from the interaction with the lattice vibrations. These correlations decisively influence various specific properties of the system. We here wish to suggest a possible analogy between the correlation effects responsible for the energy gaps found in the excitation spectra of certain types of nuclei and those responsible for the observed energy gaps in superconducting metals.

proximately[1]

$$\delta \approx 50 A^{-1} \text{ Mev}, \tag{1}$$

where A is the number of particles in the nucleus.

If the intrinsic structure could be adequately described in terms of independent particle motion, we would expect, for even-even nuclei, the first intrinsic excitation to have on the average an energy $\frac{1}{2}\delta$, when we take into account the possibility of exciting neutrons as well as protons. Empirically, however, the first intrinsic excitation in heavy nuclei of the even-even type is usually observed at an energy of about 1 Mev (see Fig. 1). The only known examples of intrinsic excitations with appreciably smaller energy are the $K=0-$ bands which occur in special regions of nuclei, and which may possibly represent collective octupole vibrations.[2]

Energies of first excited states: even-even vs. odd A nuclei

FIG. 1. Energies of first excited intrinsic states in deformed nuclei, as a function of the mass number. The experimental data may be found in *Nuclear Data Cards* [National Research Council, Washington, D. C.] and detailed references will be contained in reference 1 above. The solid line gives the energy $\delta/2$ given by Eq. (1), and represents the average distance between intrinsic levels in the odd-A nuclei (see reference 1).

The figure contains all the available data for nuclei with $150<A<190$ and $228<A$. In these regions the nuclei are known to possess nonspherical equilibrium shapes, as evidenced especially by the occurrence of rotational spectra (see, e.g., reference 2). One other such region has also been identified around $A=25$; in this latter region the available data on odd-A nuclei is still represented by Eq. (1), while the intrinsic excitations in the even-even nuclei in this region do not occur below 4 Mev.

We have not included in the figure the low lying $K=0$ states found in even-even nuclei around Ra and Th. These states appear to represent a collective odd-parity oscillation.

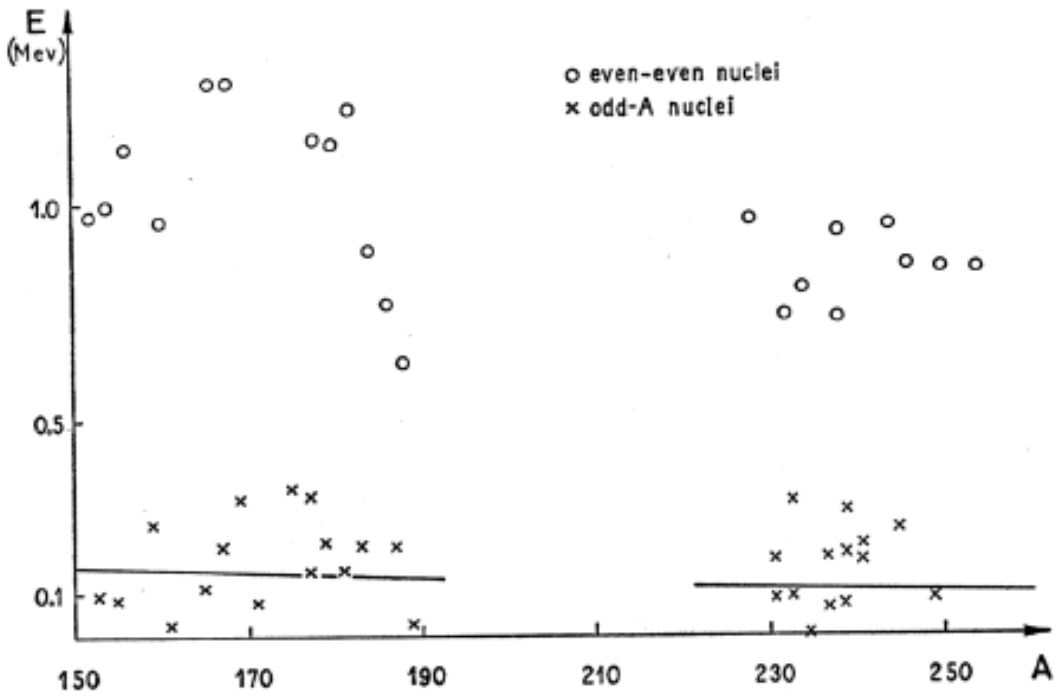

Reminder: the BCS equations

$$|BCS> = \prod_{k>0} u_k + v_k a_k^{+} a_{\bar{k}}^{+} \,|0> =$$

$$\sum_{k>0} \frac{v_k}{u_k} a_k^{+} a_{\bar{k}}^{+} \,|0> + \frac{1}{2} \sum_{kk'>0} \frac{v_k v_{k'}}{u_k u_{k'}} a_k^{+} a_{\bar{k}}^{+} a_{k'}^{+} a_{\bar{k}'}^{+} + ...$$

Gap equation

$$\Delta_k = -\sum_{k'>0} g_{k\bar{k}k'\bar{k}} u_{k'} v_{k'}$$

Number equation

$$2\sum_{k>0} v_k^{2} = N$$

Probability to be occupied

$$v_k^{2} = \frac{1}{2}\left(1 - \frac{\varepsilon_k - \lambda}{\sqrt{(\varepsilon_k - \lambda)^2 + \Delta_k^{2}}}\right)$$

Probability to be empty

$$u_k^{2} = \frac{1}{2}\left(1 + \frac{\varepsilon_k - \lambda}{\sqrt{(\varepsilon_k - \lambda)^2 + \Delta_k^{2}}}\right)$$

The simplest case: constant G

$$\hat{H} = \sum_{k>0} \varepsilon_k (a_k^+ a_k + a_{\bar{k}}^+ a_{\bar{k}}) - G \sum_{kk'>0} a_k^+ a_{\bar{k}}^+ a_{\bar{k}'} a_{k'}$$

$$v_k^{\,2} = \frac{1}{2}\left(1 - \frac{\varepsilon_k - \lambda}{\sqrt{(\varepsilon_k - \lambda)^2 + \Delta_k^{\,2}}}\right) \qquad u_k^{\,2} = \frac{1}{2}\left(1 + \frac{\varepsilon_k - \lambda}{\sqrt{(\varepsilon_k - \lambda)^2 + \Delta_k^{\,2}}}\right)$$

$$< BCS \mid \hat{H} - \lambda \hat{N} \mid BCS >= 2\sum_{k>0}\left((\varepsilon_k - \lambda - G v_k^{\,2}) v_k^{\,2} + \frac{1}{2} G v_k^{\,4}\right) - \frac{\Delta^2}{G}$$

$$\approx 2\sum_{k>0}\left((\varepsilon_k - \lambda) v_k^{\,2}\right) - \frac{\Delta^2}{G}$$

$$< BCS \mid + \sum_{k>0} a_k^+ a_{\bar{k}}^+ \mid BCS >= \frac{\Delta}{G} = \sum_{k>0} u_k v_k \rightarrow \textit{anomalous density}$$

Gap equation in uniform matter

Plane waves in time reversal

Matrix elements of the pairing Interaction in the $^1S_0$ channel

$$V_{kk'} = < k \uparrow -k \downarrow | V(^1S_0) | k' \uparrow -k' \downarrow >$$

Thermal factor

The equation for the (state-dependent) gap

$$\Delta_k = -\int \frac{d^3k'}{(2\pi)^3} V_{kk'} \frac{\Delta_{k'}}{2E_{k'}} \tanh\left(\frac{1}{2}\beta E_{k'}\right)$$

The quasi-particle energies

$$E_k = \left[(e_k - \varepsilon_F)^2 + \Delta_k\right]^{1/2}$$

Fermi energy

$$V_{kk'} = < k \uparrow -k \downarrow | V(^1S_0) | k' \uparrow -k' \downarrow >$$

$$\approx \frac{1}{4\pi} \int d\Omega_{k'} \int d^3 r \, e^{-i\vec{k}\cdot\vec{r}} \, V(r) e^{i\vec{k}'\cdot\vec{r}}$$

$$\approx \int dr \, r^2 \, V(r) \, j_0(kr) j_0(k'r)$$

The weak-coupling approximation:

$$\Delta_k = -\frac{1}{2\pi^2}\int_0^\infty dk' \quad k'^2 \frac{V(k,k')}{2E_{k'}}\Delta_{k'}$$

Let us make two approximations for $k \approx k_F$:

$$E_k \approx \sqrt{\left(\frac{\hbar^2 k^2}{2m^*} - \epsilon_F\right)^2 + {\Delta_{k_F}}^2}$$

$$\frac{1}{\sqrt{(x^2-1)^2+\alpha^2}} \quad \approx \ln\left(\frac{8}{\alpha}\right)\delta(x-1)$$

Then

$$\Delta_{k_F} \approx -\frac{m^* k_F}{2\pi^2\hbar^2}\ln\left(\frac{8}{\bar{\Delta}_{k_F}}\right) V(k,k_F)\Delta_{k_F}$$

$$\bar{\Delta}_{k_F} = 8\exp\left(\frac{2\pi^2\hbar^2}{m^* k_F V(k_F,k_F)}\right) = 8\exp\left(\frac{1}{N(0)V(k_F,k_F)}\right)$$

with

$$\bar{\Delta}_{k_F} \equiv \Delta_{k_F}/\epsilon_F$$

The choice of the pairing interaction

- Bare force (Argonne v18, Paris, CD Bonn…)
- $V_{low\text{-}k}$
- Effective finite range force (Gogny)
- Effective zero-range, density-dependent forces

Bare vs. effective forces

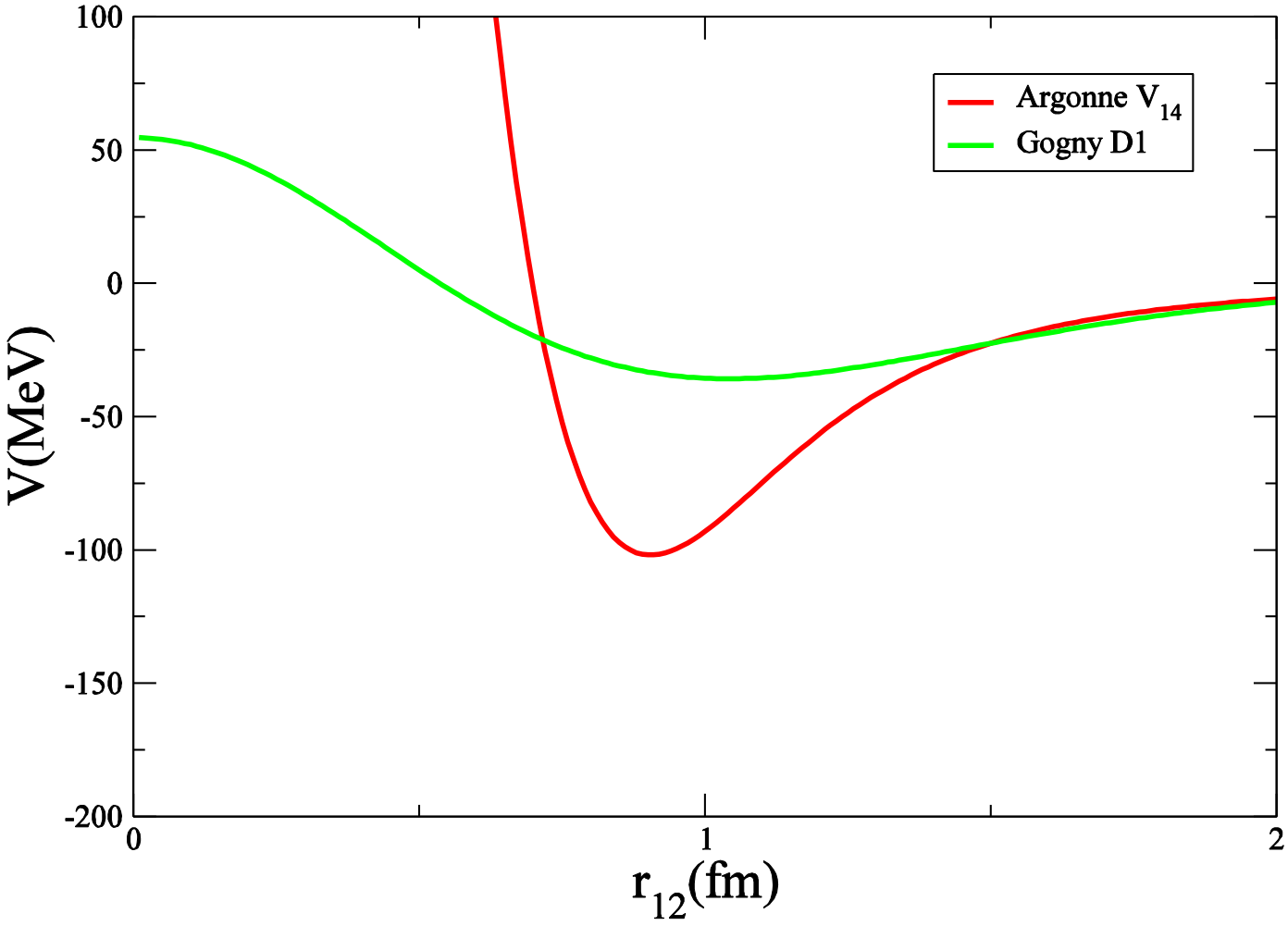

Bare vs. effective forces

Gogny D1

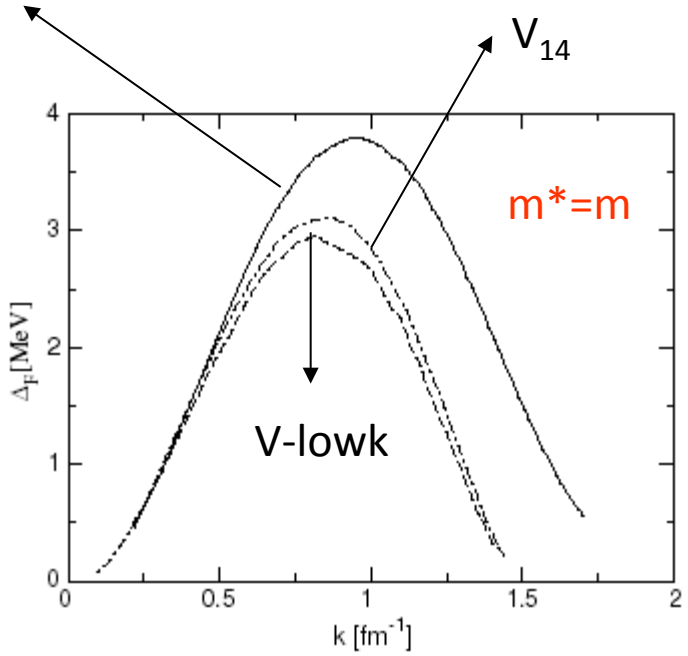

FIG. 7. Pairing gaps calculated in neutron matter as a function of the Fermi momentum, obtained with the Gogny interaction (solid line), the Argonne v_{14} potential (dash-dotted line), and the $v_{low\text{-}k}$ potential (dashed line). The bare effective mass has been used in the calculation.

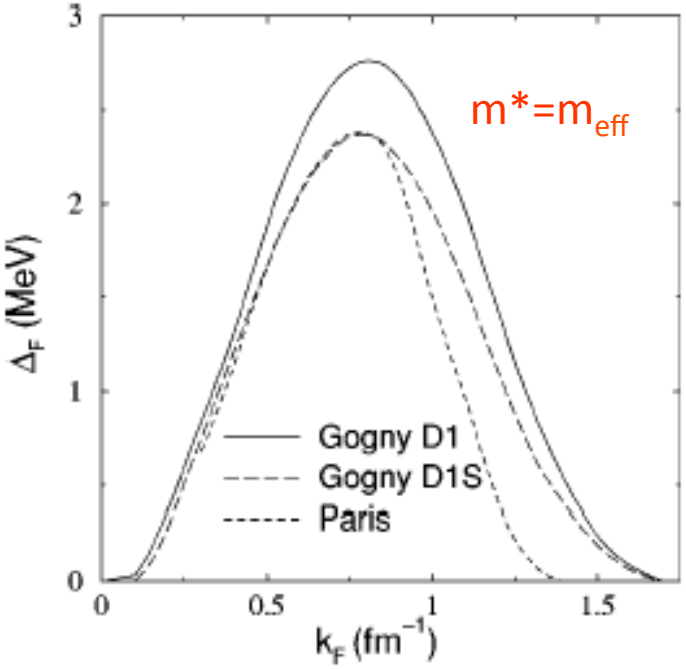

Density dependent, zero-range forces

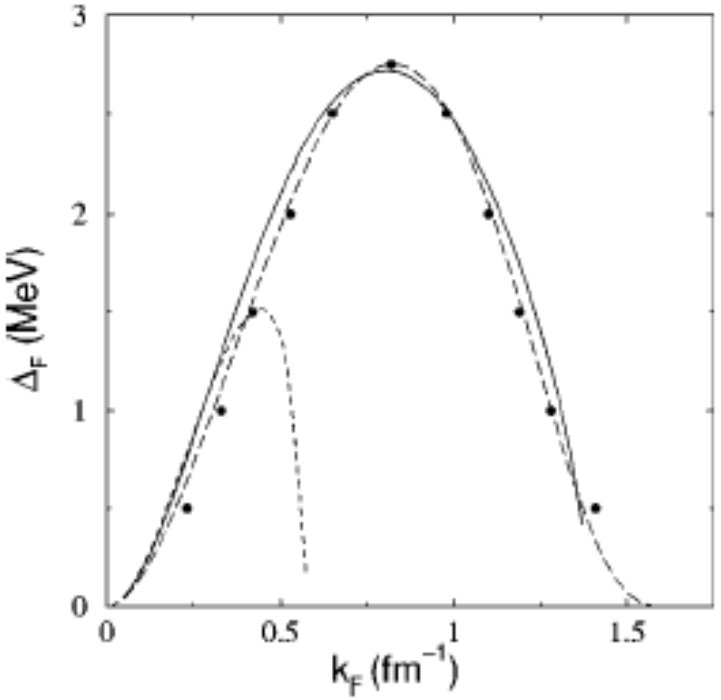

In Fig. 6 we show the fit to $\Delta(k_F)$ in the isovector channel obtained from Eq. (5) with $\epsilon_C = 60$ MeV, $\eta = 0.45$, $\alpha = 0.47$. Also shown is the fit corresponding to the bare mass (i.e., $m^*/m = 1$) with $\epsilon_C = 60$ MeV, $\eta = 0.70$, $\alpha = 0.45$, as in Ref. [4]. In both cases, the corresponding v_0 value is $v_0 = 481$ MeV fm^3. We see that the fits are good for values of

E. Garrido, E. Moya de Guerra, P. Sarriguren, P. Schuck, PRC60 (1999)64312

UNIFORM MATTER

Coherence length of nuclear systems is much larger than interparticle spacing

Pairing gaps have a strong dependence on the effective mass

Bare potentials with hard cores yield similar pairing gaps;
Vlowk reproduce them for a free single-particle spectrum

The Gogny force (its parameters are fitted in finite nuclei)
reproduce the pairing gaps at low density, while they give larger gaps close to saturation

The density dependence of zero range forces is partly due to simulate the momentum dependence of the matrix elements of realistic forces

Pairing in finite nuclei

Most often, pairing correlations in finite nuclei are calculated with effective forces which in some cases (Gogny,SkP), have some parameters determined by the comparison with experimental data about pairing correlations (quasiparticle energies, odd-even mass differences)

PHYSICAL REVIEW C VOLUME 21, NUMBER 4 APRIL 1980

Hartree-Fock-Bogolyubov calculations with the $D1$ effective interaction on spherical nuclei

J. Dechargé and D. Gogny

Service de Physique Neutronique et Nucléaire, Centre d'Etudes de Bruyères-le-Châtel, Boîte Postale No. 561, 92542 Montrouge Cedex, France

(Received 3 August 1979)

A self-consistent approach allowing the introduction of pairing into a comprehensive study of the bulk as well as the structure properties of nuclei is presented. It is emphasized that the density-dependent effective force used in the calculations reported here does permit the extraction of the mean field and the pairing field in the framework of the Bogolyubov theory. First, a brief review of Hartree-Fock-Bogolyubov formalism with density-dependent interactions is presented. Then the derivation of the effective interaction is explained and some details concerning the nuclear matter properties are given. Finally, we report the studies on spherical nuclei with special reference to the pairing properties. In order to demonstrate the versatility of our approach a comprehensive study of various nuclear properties is given. In view of the abundance of results obtained with our approach we plan to report the results on the deformed nuclei in a future publication.

Comparison with experimental odd-even mass difference

$$\Delta(N) \approx \frac{(-1)^N}{2}\left[B(N-1)+B(N+1)-2B(N)\right]$$

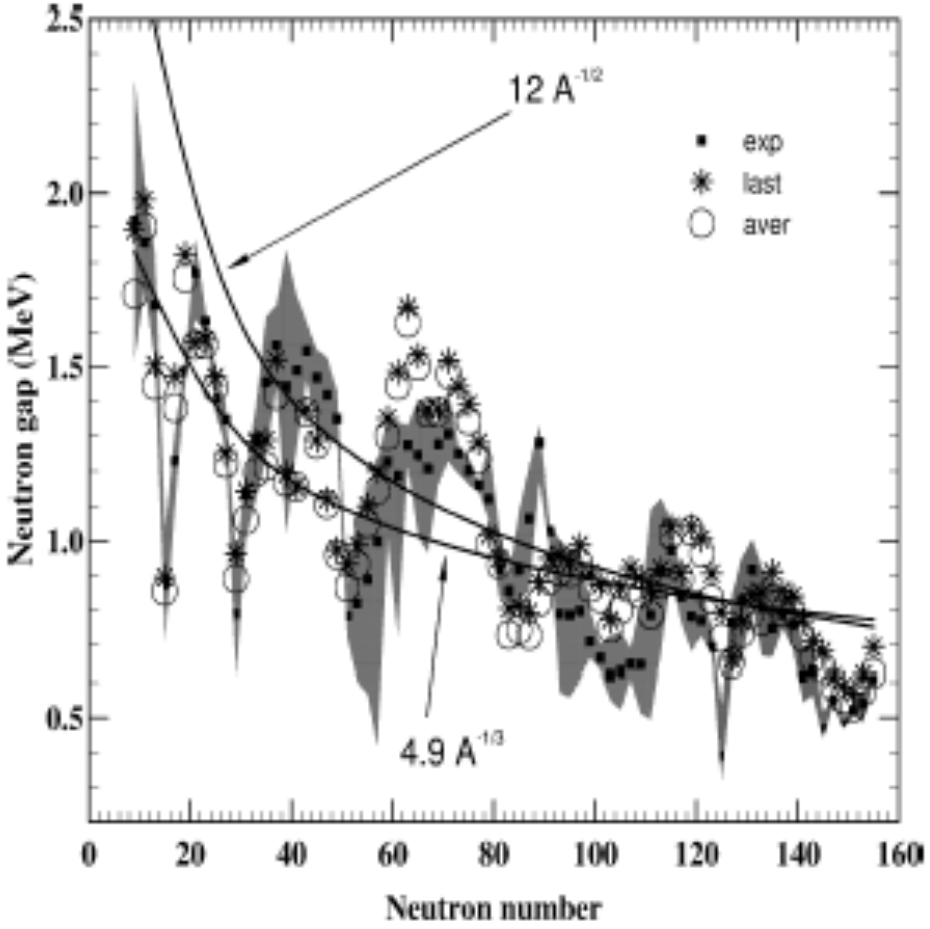

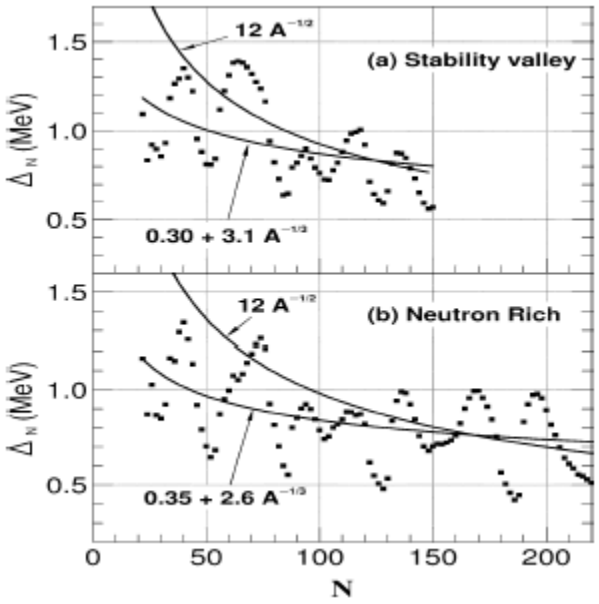

S. Hilaire, J.F. Berger, M. Girod, W. Satula, P. Schuck, Phys. Lett. B531(2002)61

$\rho = 0.16\ \text{fm}^{-3} = 2.8 \times 10^{14}\ \text{g cm}^{-3}$

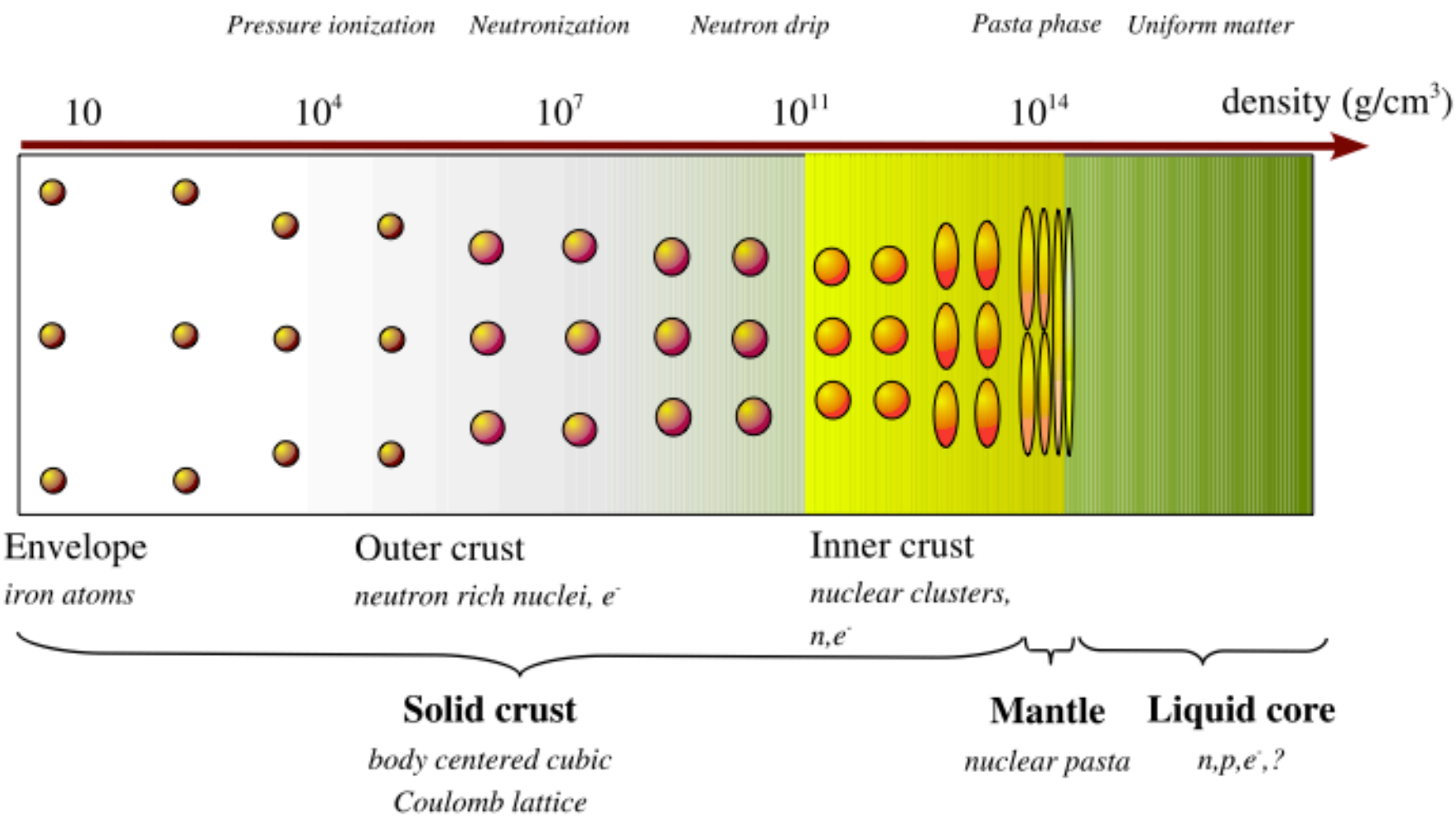

N. Chamel and P. Haensel, Living Rev. Relativity 11

The inner crust: coexistence of finite nuclei with a sea of free neutrons

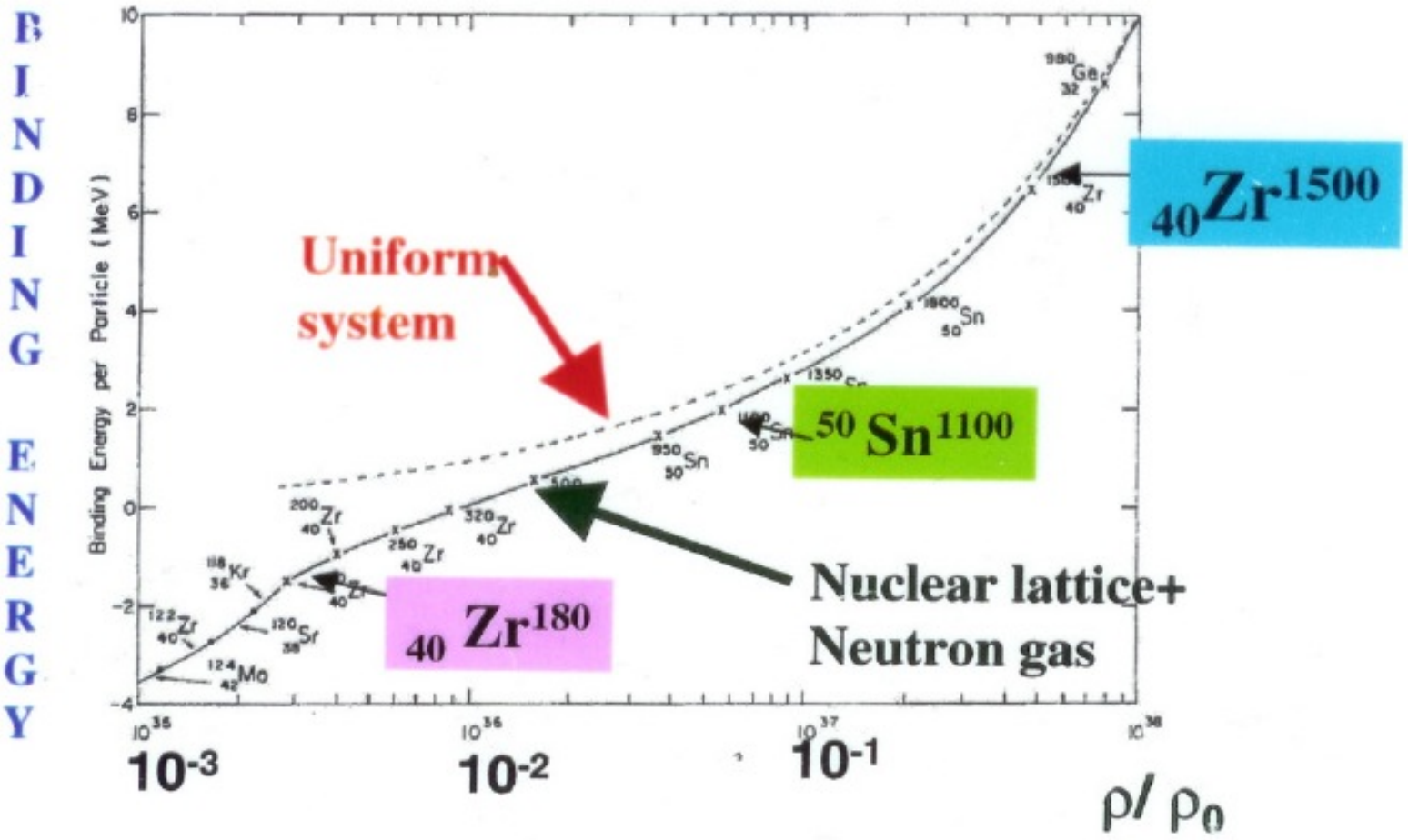

J. Negele, D. Vautherin
Nucl. Phys. A207 (1974) 298

Permanence of shell structure

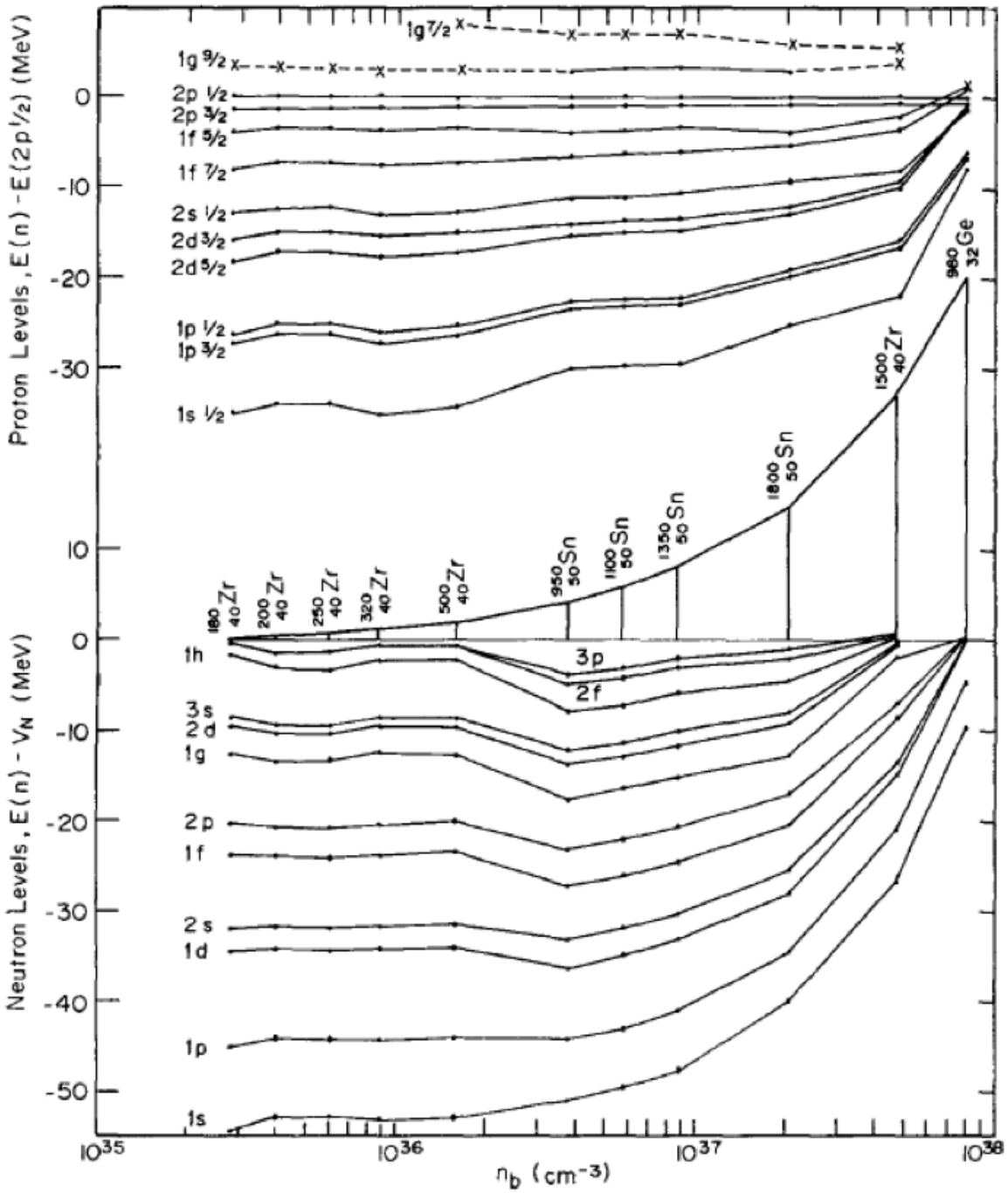

Fig 5. Single-particle spectrum of protons and neutrons

Reminder: the BCS equations

$$|BCS> = \prod_{k>0} u_k + v_k a_k^{+} a_{\bar{k}}^{+} \,|0> =$$

$$\sum_{k>0} \frac{v_k}{u_k} a_k^{+} a_{\bar{k}}^{+} \,|0> + \frac{1}{2} \sum_{kk'>0} \frac{v_k v_{k'}}{u_k u_{k'}} a_k^{+} a_{\bar{k}}^{+} a_{k'}^{+} a_{\bar{k}'}^{+} + ...$$

Gap equation

$$\Delta_k = -\sum_{k'>0} g_{k\bar{k}k'\bar{k}} u_{k'} v_{k'}$$

Number equation

$$2\sum_{k>0} v_k^{2} = N$$

Probability to be occupied

$$v_k^{2} = \frac{1}{2}\left(1 - \frac{\varepsilon_k - \lambda}{\sqrt{(\varepsilon_k - \lambda)^2 + \Delta_k^{2}}}\right)$$

Probability to be empty

$$u_k^{2} = \frac{1}{2}\left(1 + \frac{\varepsilon_k - \lambda}{\sqrt{(\varepsilon_k - \lambda)^2 + \Delta_k^{2}}}\right)$$

The simplest case: constant G

$$\hat{H} = \sum_{k>0} \varepsilon_k (a_k^+ a_k + a_{\bar{k}}^+ a_{\bar{k}}) - G \sum_{kk'>0} a_k^+ a_{\bar{k}}^+ a_{\bar{k}'} a_{k'}$$

$$v_k^{\,2} = \frac{1}{2}\left(1 - \frac{\varepsilon_k - \lambda}{\sqrt{(\varepsilon_k - \lambda)^2 + \Delta_k^{\,2}}}\right) \qquad u_k^{\,2} = \frac{1}{2}\left(1 + \frac{\varepsilon_k - \lambda}{\sqrt{(\varepsilon_k - \lambda)^2 + \Delta_k^{\,2}}}\right)$$

$$< BCS \mid \hat{H} - \lambda \hat{N} \mid BCS >= 2\sum_{k>0}\left((\varepsilon_k - \lambda - G v_k^{\,2}) v_k^{\,2} + \frac{1}{2} G v_k^{\,4}\right) - \frac{\Delta^2}{G}$$

$$\approx 2\sum_{k>0}\left((\varepsilon_k - \lambda) v_k^{\,2}\right) - \frac{\Delta^2}{G}$$

$$< BCS \mid + \sum_{k>0} a_k^+ a_{\bar{k}}^+ \mid BCS >= \frac{\Delta}{G} = \sum_{k>0} u_k v_k \rightarrow \textit{anomalous density}$$

^{120}Sn

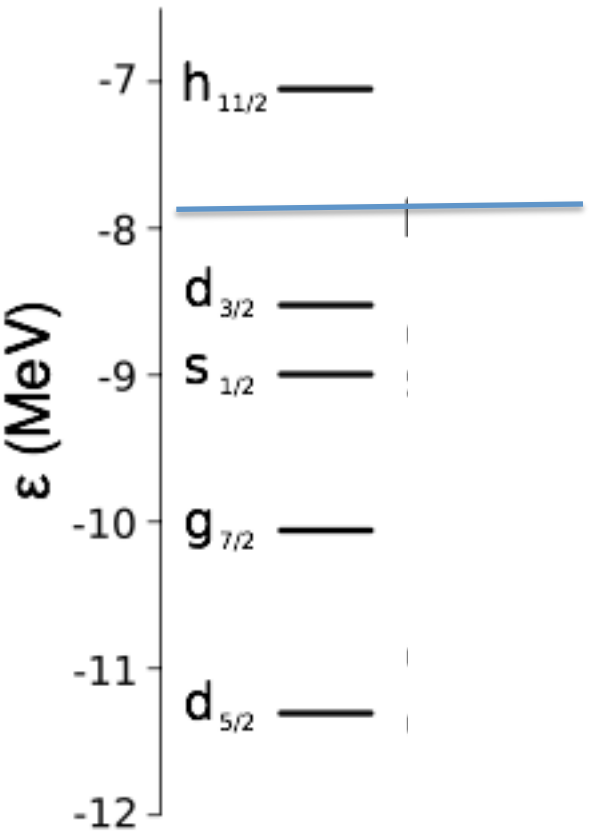

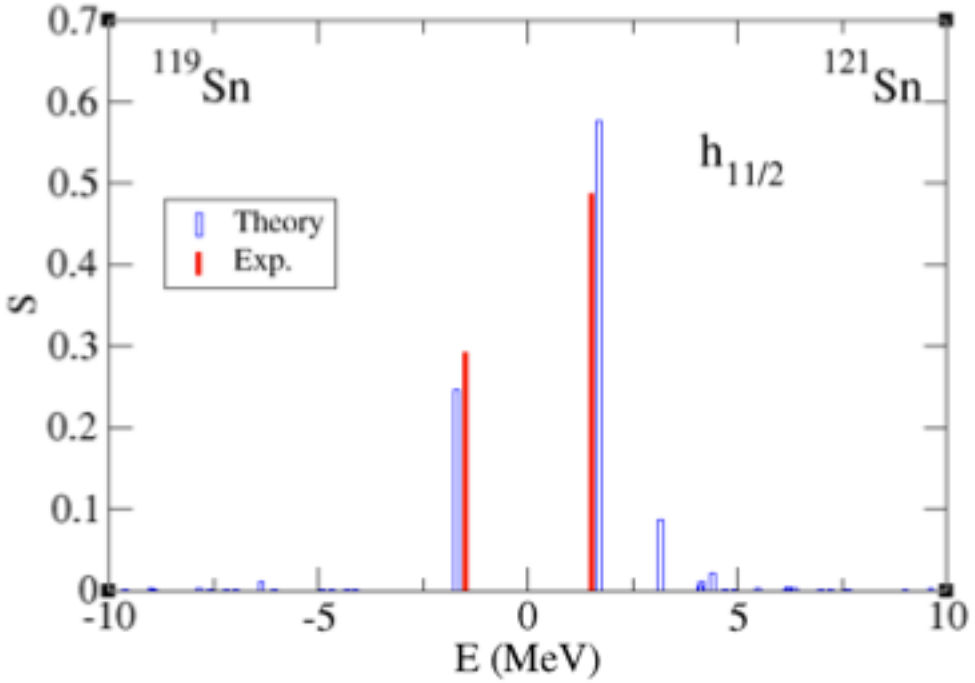

$$E_k = \sqrt{(\varepsilon_k - \lambda)^2 + \Delta^2}$$

$$v_k^{\,2} = \frac{1}{2}\left(1 - \frac{\varepsilon_k - \lambda}{\sqrt{(\varepsilon_k - \lambda)^2 + \Delta_k^{\,2}}}\right) \qquad u_k^{\,2} = \frac{1}{2}\left(1 + \frac{\varepsilon_k - \lambda}{\sqrt{(\varepsilon_k - \lambda)^2 + \Delta_k^{\,2}}}\right) \qquad v_k^2 + u_k^2 = 1$$

Spatial dependence of the wavefunction of Cooper pairs (pairing density)

UNIFORM MATTER

$$\kappa(r_1, r_2) = \sum_i U_i V_i \, \phi_i(\vec{r}_1)\phi_i^*(\vec{r}_2) = \sum_i U_i V_i \, e^{i\vec{k}_i \cdot \vec{r}} \qquad \left(k_i \approx k_F\right)$$

Oscillations of momentum k_F damped over a scale given by the coherence length:

$$\xi = h^2 k_F / m\pi\Delta \qquad \langle r_{12}^2 \rangle^{1/2} \sim \xi$$

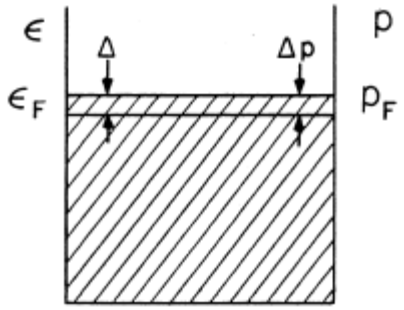

The wavefunction of the Cooper pair is built over waves of momentum $p \sim p_F$, which lie in an interval Δ around the Fermi energy.

$$\Delta \approx \frac{\Delta p \; p_F}{m} \rightarrow \frac{\Delta p}{p_F} \sim \frac{\Delta}{\epsilon_F}$$

The extension of the Cooper pair is

$$\xi \sim \frac{\hbar}{\Delta p} \sim \frac{\hbar p_F}{m\Delta}$$

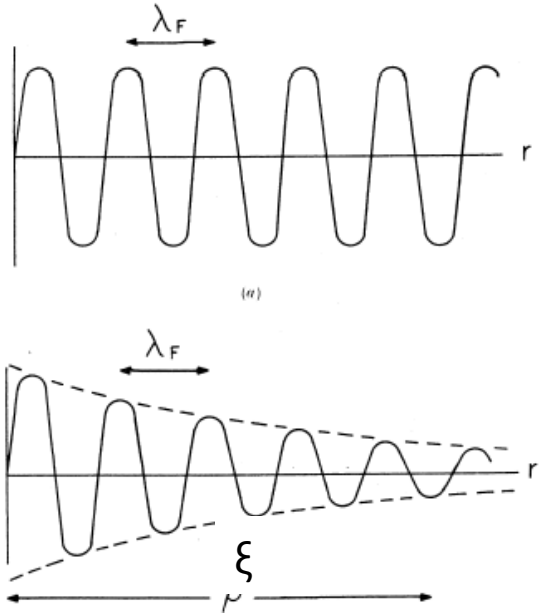

V.F. Weisskopf, Contemp. Phys. 22 (1981)375

Potential and density calculated in a WS cell at $n \cong 10^{13}$ g cm^{-3} (^{1364}Sn)

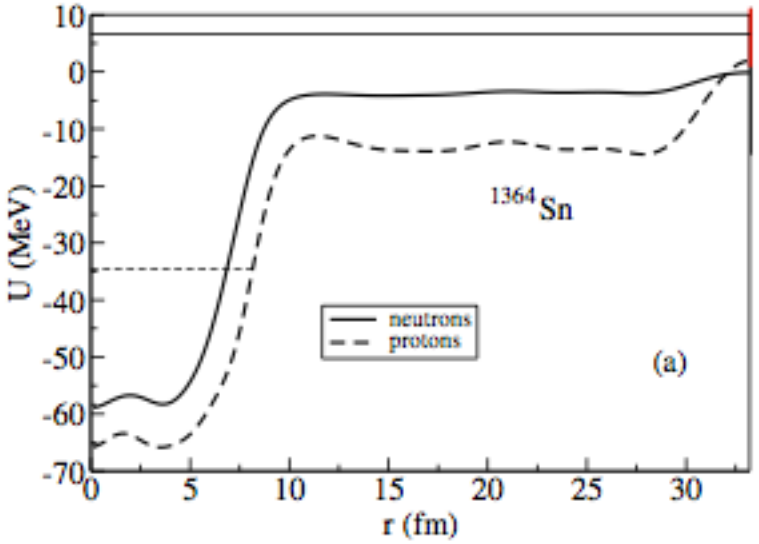

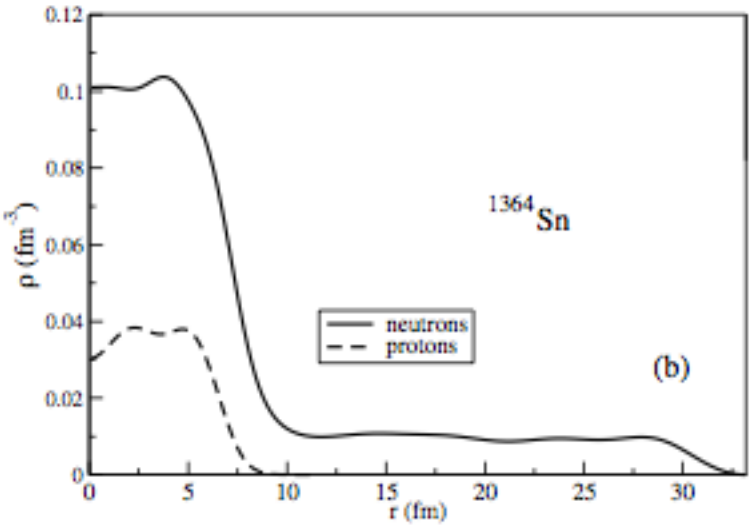

Gap equation

Single-particle wave functions used as a basis for simplified version of Hartree-Fock-Bogoliubov equation

$$\begin{pmatrix} (\epsilon_k - \epsilon_F) & \Delta \\ -\Delta & -(\epsilon_k - \epsilon_F) \end{pmatrix} \begin{pmatrix} U_k \\ V_k \end{pmatrix} = E_k \begin{pmatrix} U_k \\ V_k \end{pmatrix} \qquad \Delta_{a_1 a_2} = -\frac{1}{2} \sum_{b_1 b_2} \sum_k U^k_{b_1} V^k_{b_2} \langle a_1 \tilde{a}_2 | v(12) | b_1 \tilde{b}_2 \rangle$$

•Simplified because the self-consistency was considered only in the pairing channel.

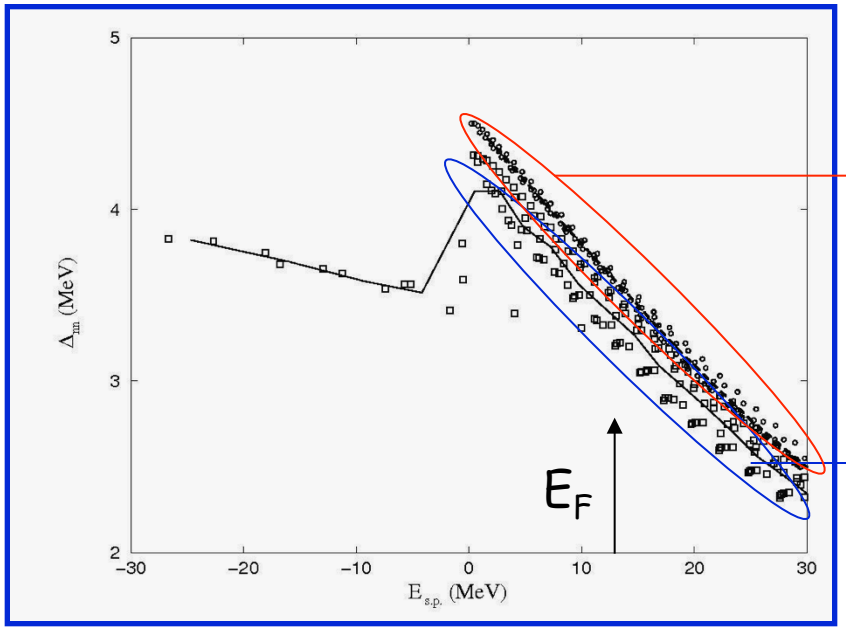

Calculated gaps for unbound states in a cell without nucleus

5-10% difference

Calculated gaps for unbound states in a cell with nucleus

Proximity effects at the mean field level

Potential in the Wigner cell

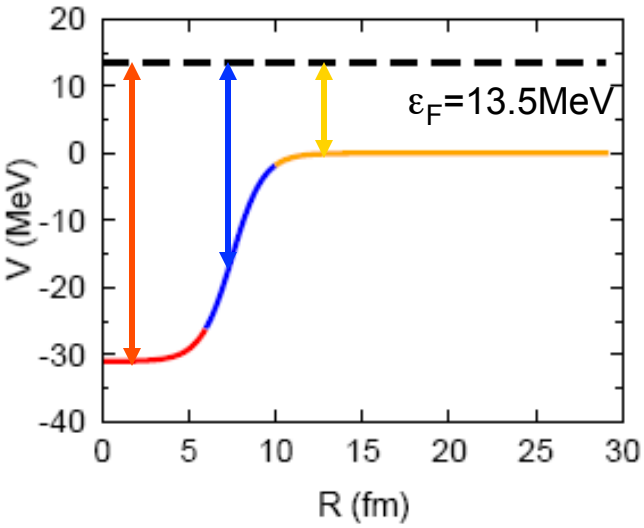

Pairing gap in uniform neutron matter

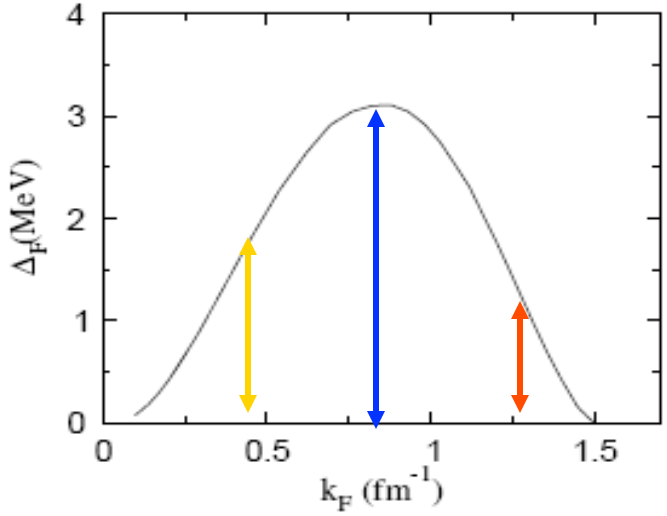

Pairing gap in the Wigner cell

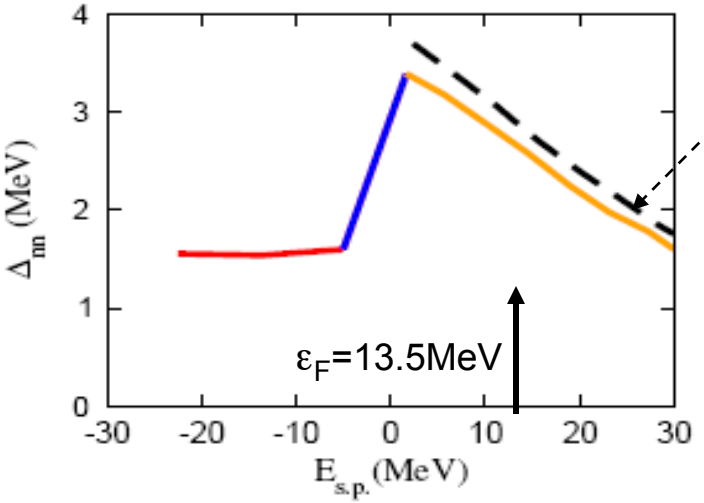

P.M. Pizzochero et al.,
APJ 569(2002)381

Spatial dependence of pairing densities and pairing gaps

FINITE NUCLEI, FINITE RANGE FORCE

HFB Equations are expanded on a basis

$$\begin{pmatrix} h_{nn'lj} - \lambda & \Delta_{nn'lj} \\ \Delta_{nn'lj} & -h_{nn'lj} + \lambda \end{pmatrix} \begin{pmatrix} U_{nlj}{}^{\alpha} \\ V_{nlj}{}^{\alpha} \end{pmatrix} = E_{lj}{}^{\alpha} \begin{pmatrix} U_{nlj}{}^{\alpha} \\ V_{nlj}{}^{\alpha} \end{pmatrix}$$

$$\kappa(R_{cm}, r_{12}) = \frac{1}{8\pi} \sum_{nn'lj} (2j+1)\, U_{nlj}{}^{\alpha *} V_{n'lj}{}^{\alpha} \varphi_{nlj}{}^{*}(r_1)\, \varphi_{n'lj}(r_2)\, P_l(\cos(\vartheta_{12}))$$

$$\Delta(R_{cm}, r_{12}) = -V_{eff}(r_{12}) \kappa(R_{cm}, r_{12})$$

Spatial description of (non-local) pairing gap

The range of the force is small compared to the coherence length, but not compared to the diffusivity of the nuclear potential

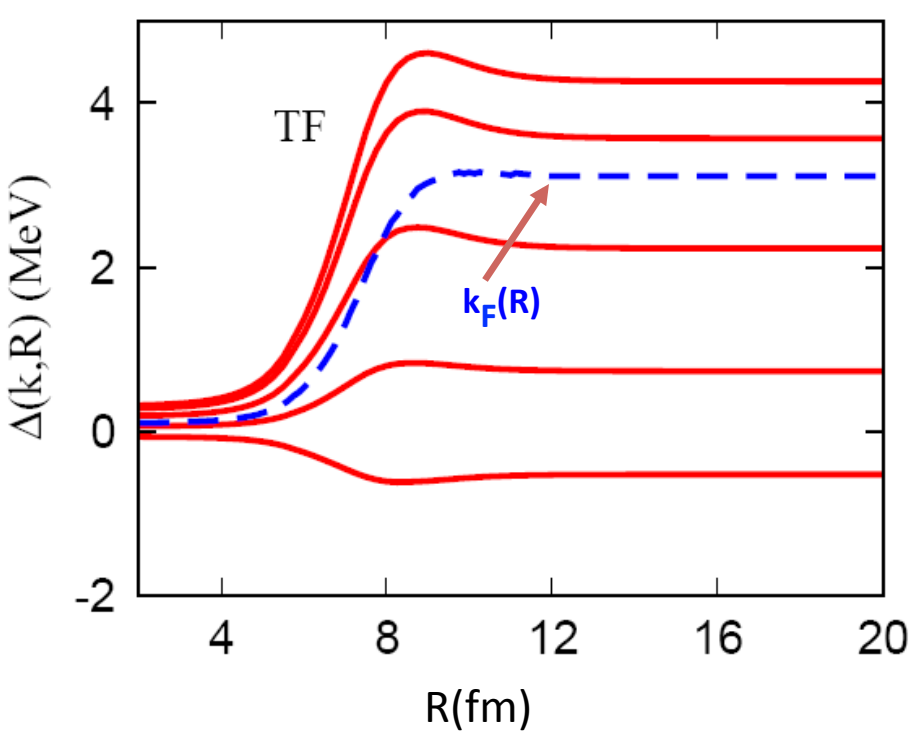

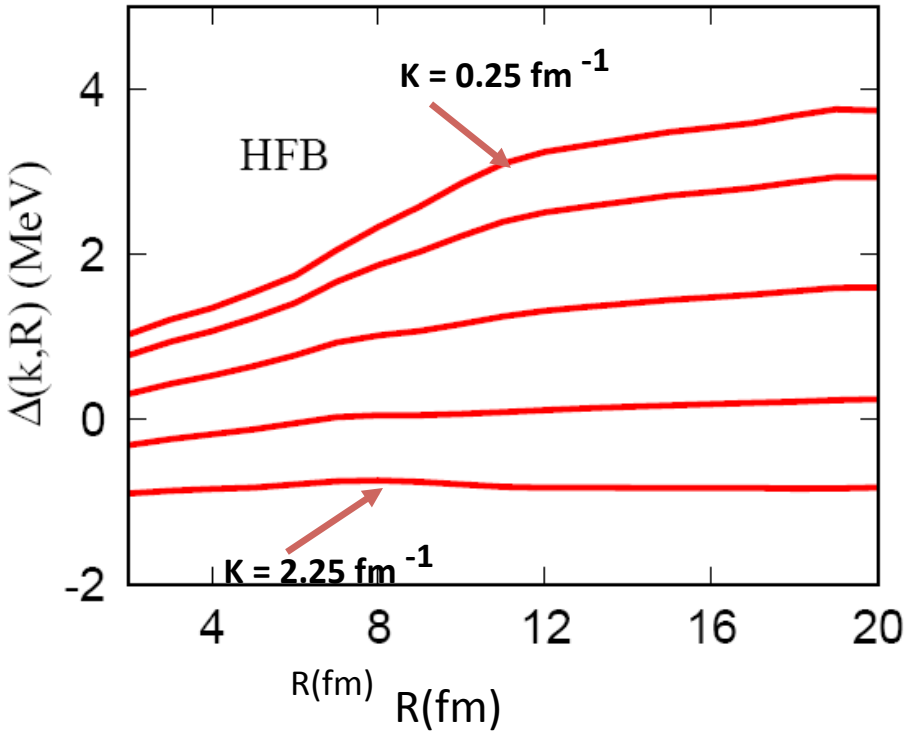

The local-density approximation overstimates the decrease of the pairing gap in the interior of the nucleus.

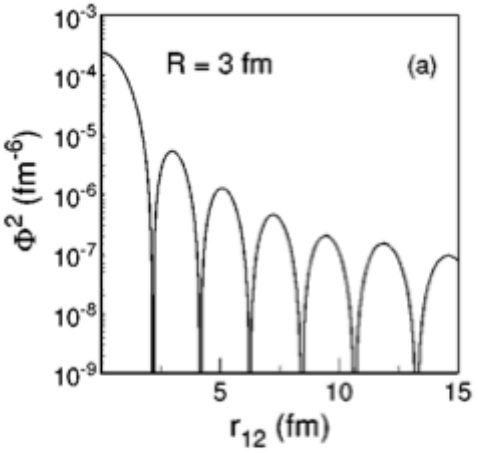

E_F (R)= 44.5 MeV
k_F (R)= 1.5 fm^{-1}
λ_F = 4.2 fm
Δ_{NM} (k_F) =1.6 MeV
ξ = 12 fm
$\langle r^2_{12}\rangle^{1/2}$ = 10.3 fm

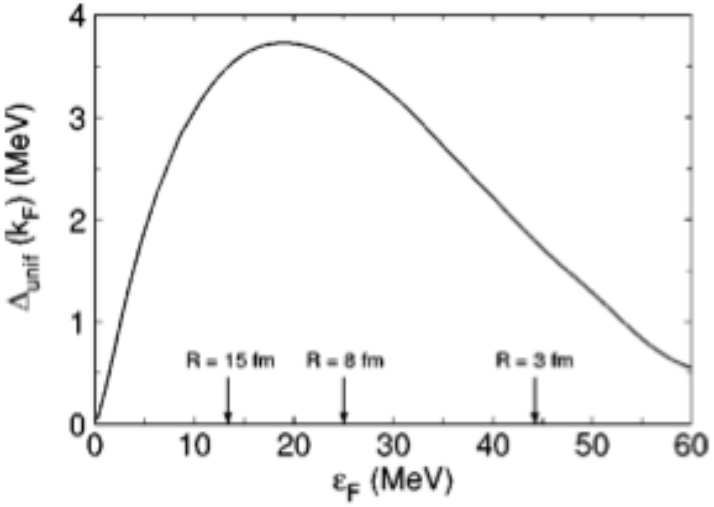

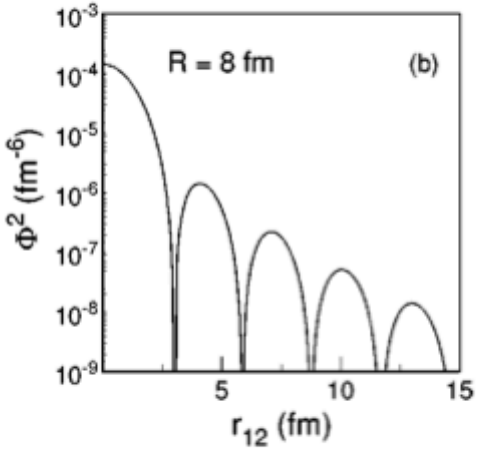

E_F = 25 MeV
k_F (R)= 1.1 fm^{-1}
λ_F = 5.7 fm
Δ_{NM} (k_F) =3.5 MeV
ξ = 4.1 fm
$\langle r^2_{12}\rangle^{1/2}$ = 3.8 fm

$\xi = h^2 k_F / m\pi\Delta$
$\lambda_F = 2\pi/k_F$

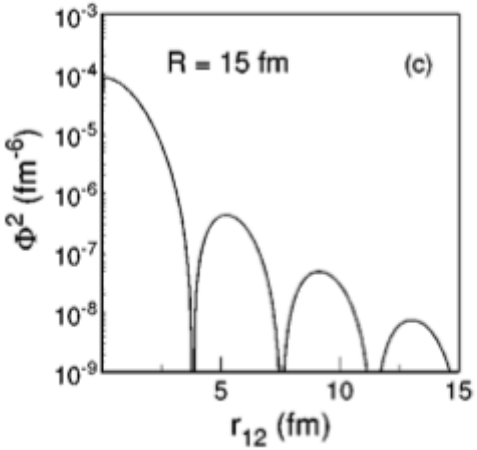

E_F = 13.5 MeV
k_F= 0.8 fm^{-1}
λ_F = 7.8fm
Δ_{NM} (k_F) =3.5 MeV
ξ = 3.2 fm
$\langle r^2_{12}\rangle^{1/2}$ = 4 fm

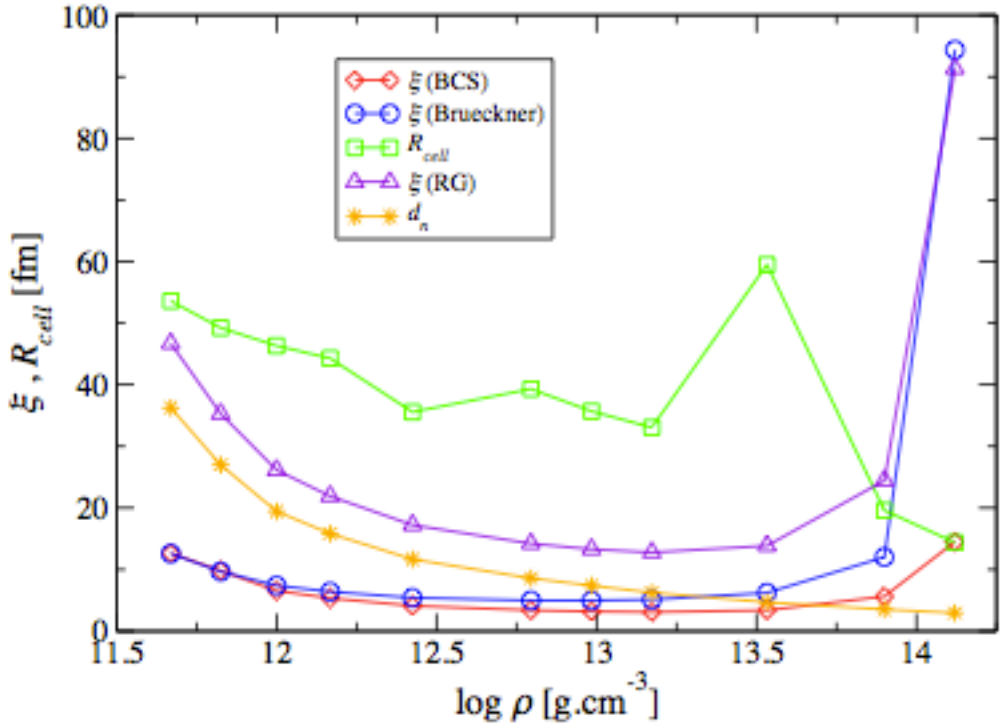

N. Chamel and P. Haensel, Living Rev. Relativity 11

The 'global' functional: matching Fayans functional (for finite nuclei) with Brückner calculations for neutron matter

$$F_m(r) = \left(1 + \exp\left((r - R_m)/d_m\right)\right)^{-1}.$$

$$\mathcal{E}\left(\rho_\tau(\mathbf{r}), \nu_\tau(\mathbf{r})\right) = \mathcal{E}^{\mathrm{ph}}\left(\rho_\tau(\mathbf{r}), \nu_\tau(\mathbf{r})\right) F_m(r) + \mathcal{E}^{\mathrm{mi}}\left(\rho_\tau(\mathbf{r}), \nu_\tau(\mathbf{r})\right)\left(1 - F_m(r)\right),$$

Phenomenological functional with gradient terms: 'knows how to deal With the surface'

Microscopic, 'exact' description of neutron matter

$$\rho_p(R_m) = 0.1\,\rho_p(0)$$

Matching condition

Simplified pairing description: constant G which reproduces the BCS gap in neutron matter

Making the connection with finite nuclei:
Microscopic functionals in neutron matter with gradient terms

$$\mathcal{H}(\rho) = \frac{\hbar^2}{2M}\sum_i (\nabla\psi_i)^2 + \left[U(\rho) + \eta(\nabla\rho)^2\right],$$

+ Spin Orbit, Coulomb

Micr. Correl. term

Phen. gradient. term

Table 1
Binding energy per particle and charge root mean square radius of some magic nuclei obtained with several values of the parameter η (see text). The same values computed with the SkM* force and the experimental ones are also given

	$\eta=-50$		$\eta=-53$		$\eta=-55$		SkM*		Exp	
	E/A	r_{ch}	E/A	r_{ch}	E/A	r_{ch}	E/A	r_{ch}	E/A	r_{ch}
^{16}O	−8.25	2.82	−8.10	2.83	−8.01	2.84	−7.98	2.81	−7.98	2.73
^{40}Ca	−8.63	3.52	−8.52	3.54	−8.45	3.55	−8.53	3.52	−8.55	3.49
^{48}Ca	−8.87	3.55	−8.76	3.56	−8.68	3.57	−8.75	3.54	−8.67	3.48
^{90}Zr	−8.73	4.31	−8.64	4.32	−8.58	4.33	−8.70	4.30	−8.71	4.27
^{208}Pb	−7.79	5.53	−7.73	5.54	−7.69	5.55	−7.87	5.51	−7.87	5.50

A related but different approach: constraining the parameters of Skyrme interaction with the results of Brueckner calculations in homogeneous matter

L.G. Cao, U. Lombardo, C.W. Shen, N.Van Giai, PRC73(2006)14313

New calculation of the optimal properties of the WIgner-Seitz cell including pairing

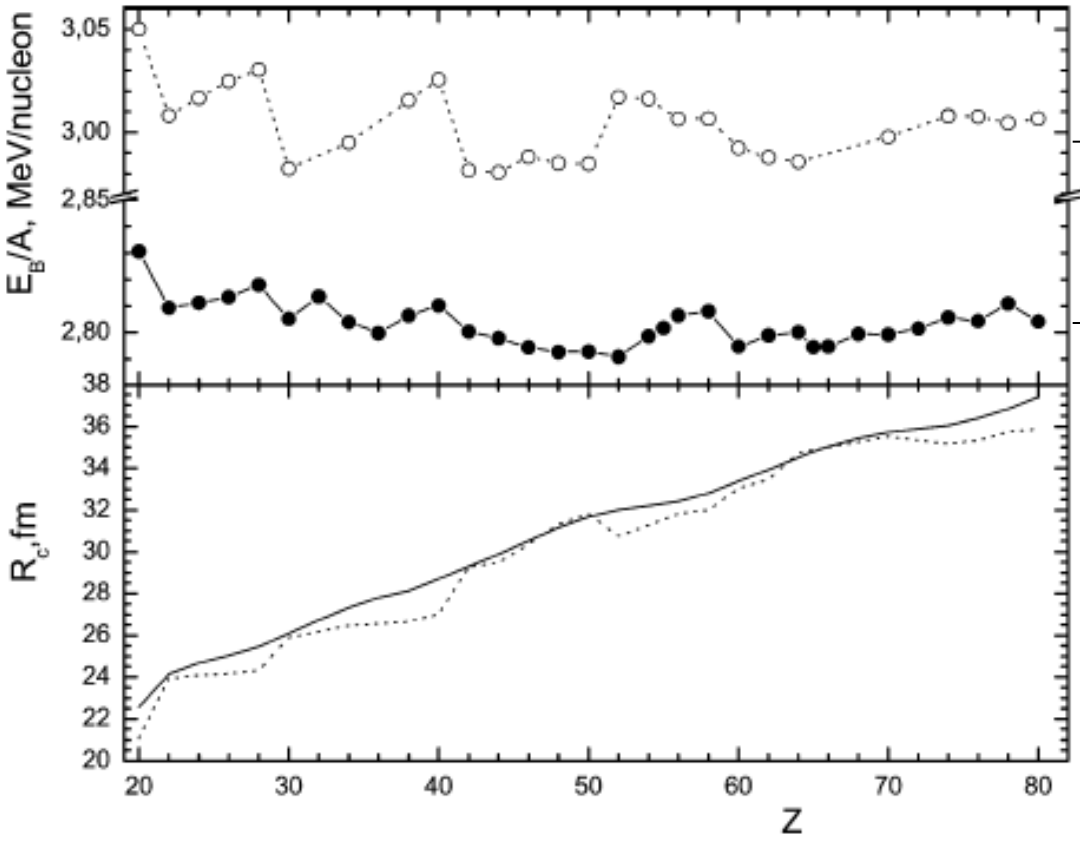

Without pairing

With pairing: smoothing of shell effects

M. Baldo, U. Lombardo, E.E: Saperstein, S.V. Tolokonnikov, Nucl. Phys. A736(2004)241

Including pairing in crust structure calculations

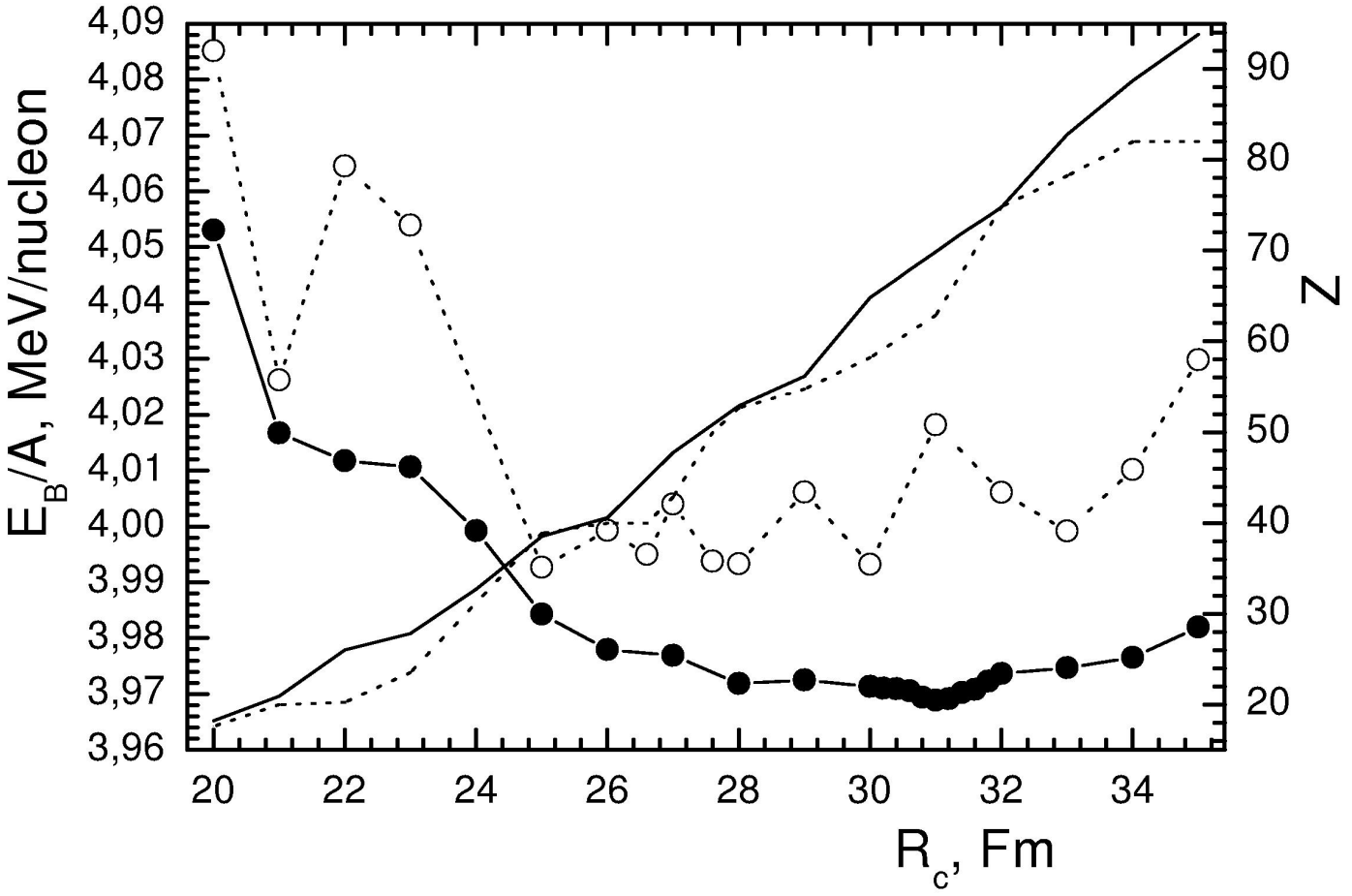

‘Smoothing’ of Z-shell effects due to neutron pairing

In search of the energy minimum as a function of the Z value inside the WS cell

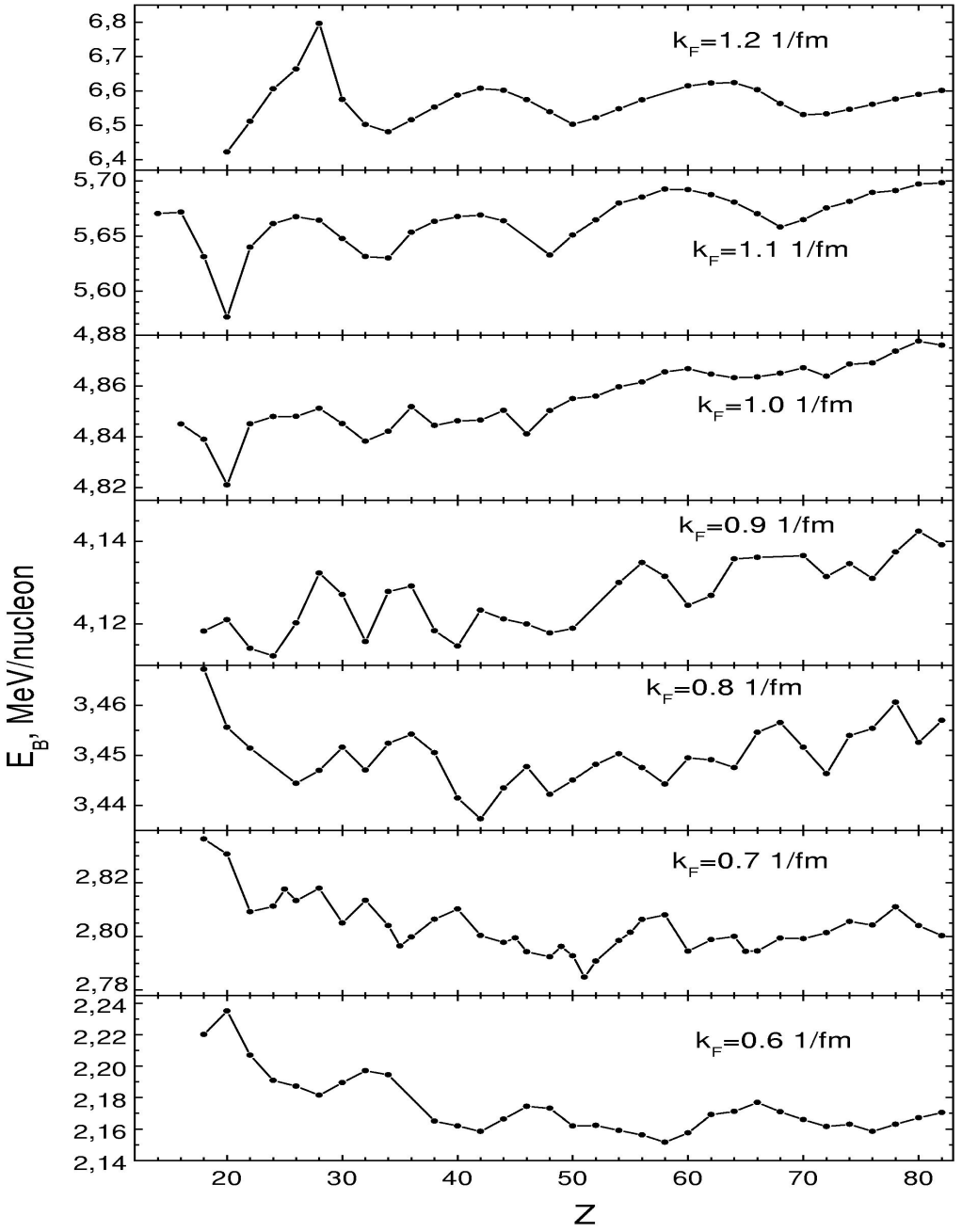

What is the reason for the shifts in energy and in the optimal Z ?

i) Smoothing of shell effects
ii) Pairing energy is different for different configurations (for the "nucleus")
iii) Shifts in the chemical potentials, both in the nucleus and in the dripped neutron gas

A complete search for the most stable configuration of the inner crust should include also the comparison of different lattice structures (Carter, Haensel and Chamel) beyond the Wigner-Seitz approximation.
However, if pairing is present with the expected strength, band structures will be smoothed within an energy interval of the order of the gap value.

A similar situation can occur in the borderline region between the inner crust and the liquid phase, where extended structures (rods, layers and so on) can exist.
However the pairing gap is expected to be much smaller.

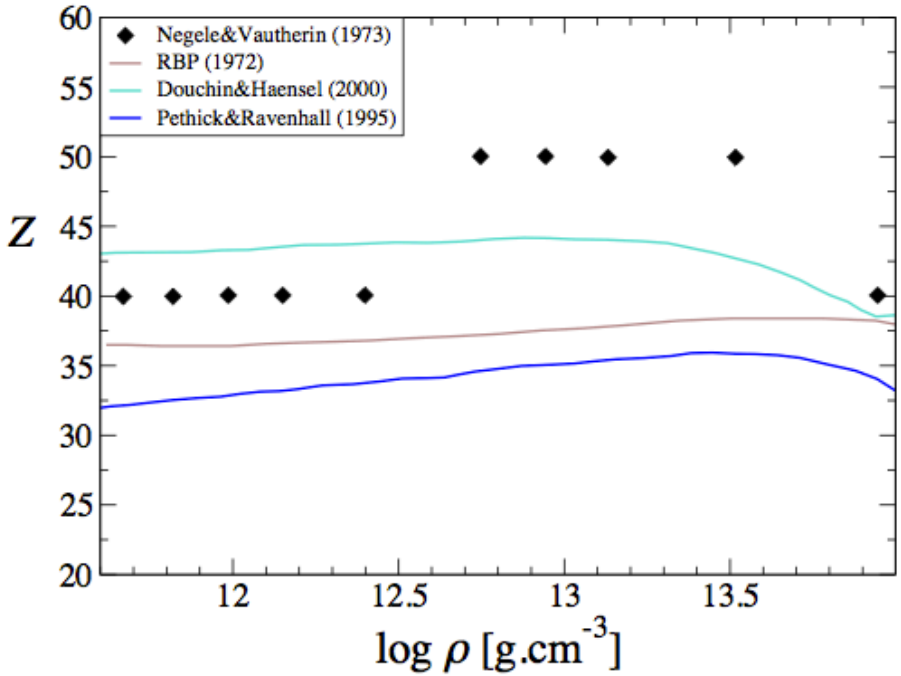

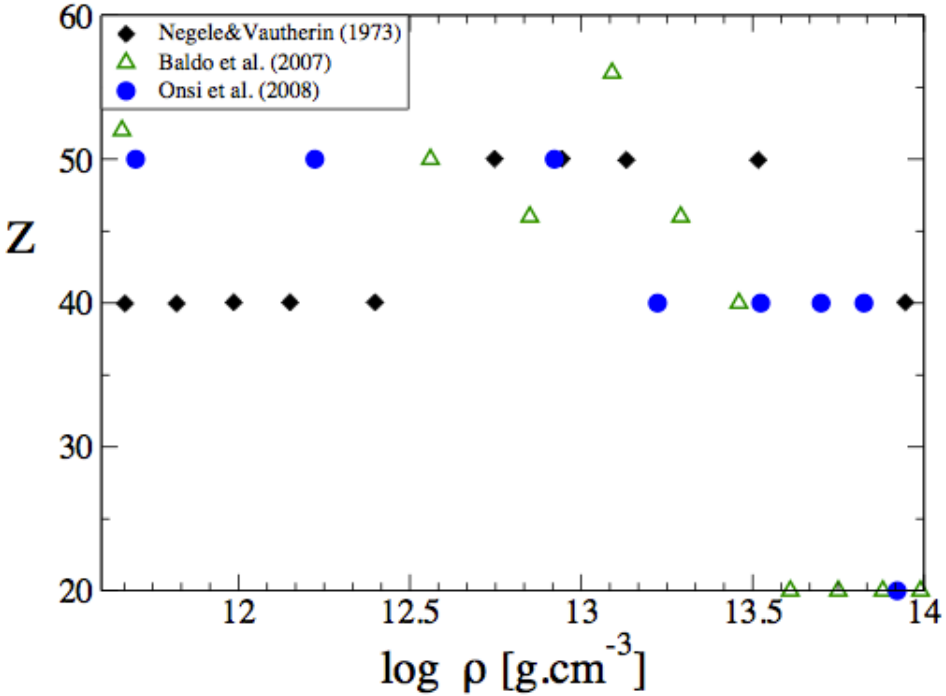

N. Chamel and P. Haensel, Living Rev. Relativity 11

A few basic questions about pairing correlations

1. **Does superfluidity affect the results found by Negele and Vautherin?**

2. **What is the spatial dependence of the pairing gap?**

   How important are the nuclear clusters?

3. **How much are the gaps affected by many-body processes ?**

4. **Can we prove experimentally that the crust is really superfluid?**

BEC

BCS

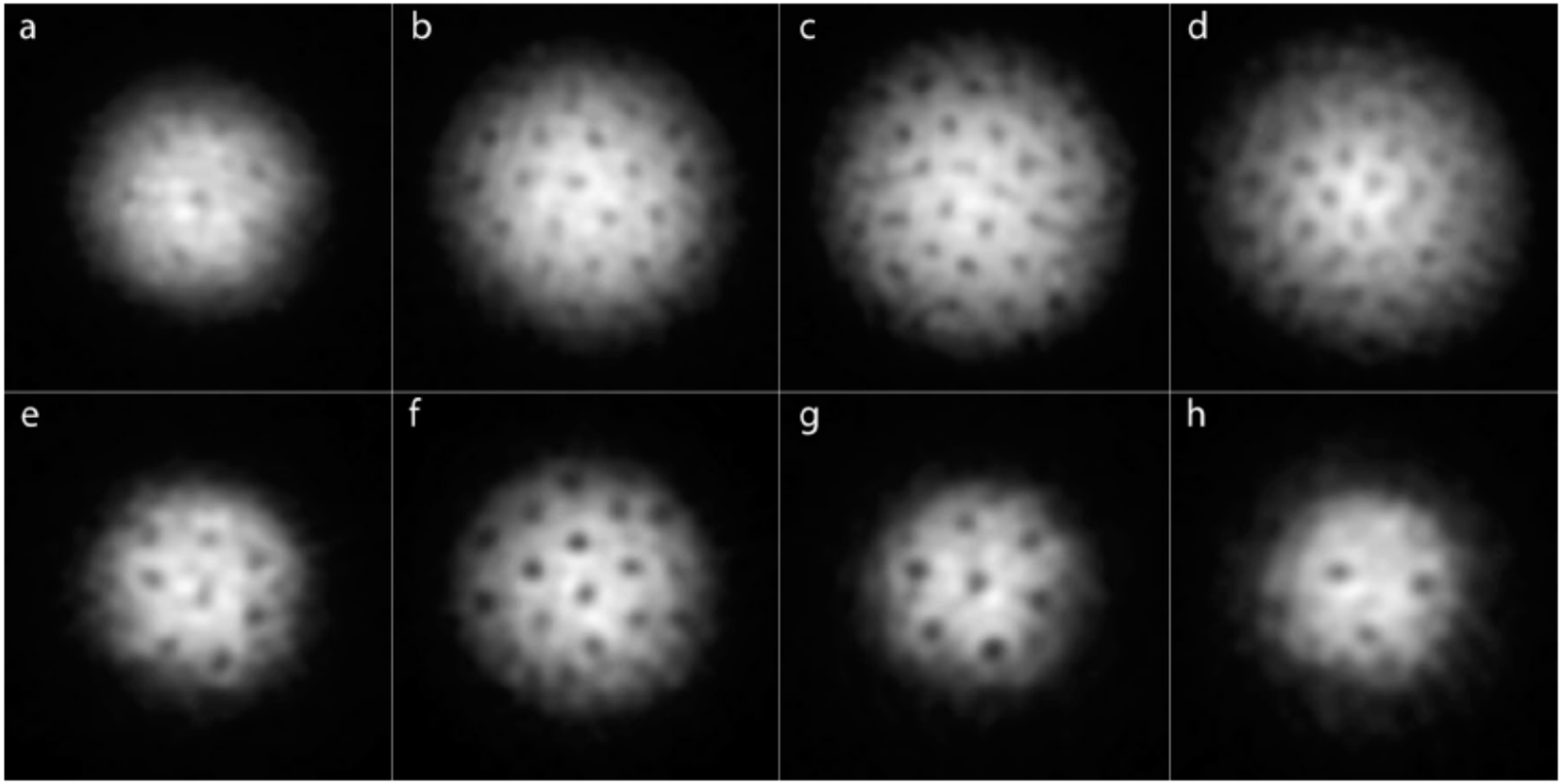

Fig. 2: Vortices in a strongly interacting gas of fermionic atoms on the BEC- and the BCS-side of the Feshbach resonance. At the given field, the cloud of lithium atoms was stirred for 300 ms (a) to 500 ms (b-h) followed by an equilibration time of 500 ms. After 2 ms of ballistic expansion, the magnetic field was ramped to 735 G for imaging (see text for details). The magnetic fields were (a) 740 G, (b) 766 G, (c) 792 G, (d) 812 G, (e) 833 G, (f) 843 G, (g) 853 G and (h) 863 G. The field of view of each image is $880\ \mu\mathrm{m} \times 880\ \mu\mathrm{m}$.

Zwierlein et al. Nature 435(2005)1047

The neutron superfluid's rotation

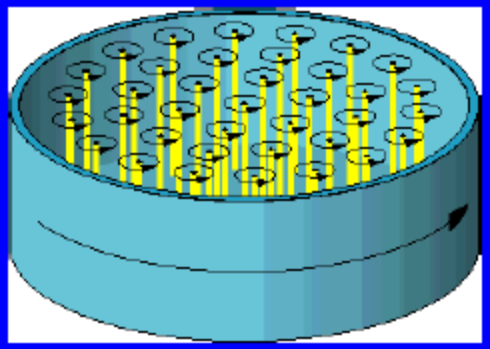

Rotating superfluid He

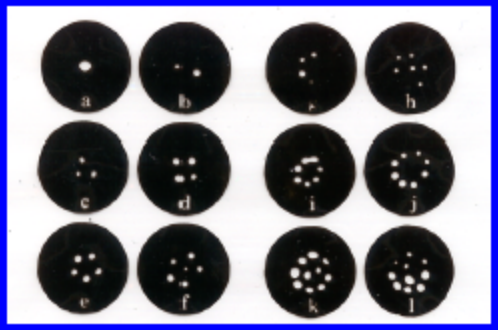

Distribution of vortices determines the fluid's angular momentum.

A typical neutron star contains ~10^{17} neutron vortices.

Glitches

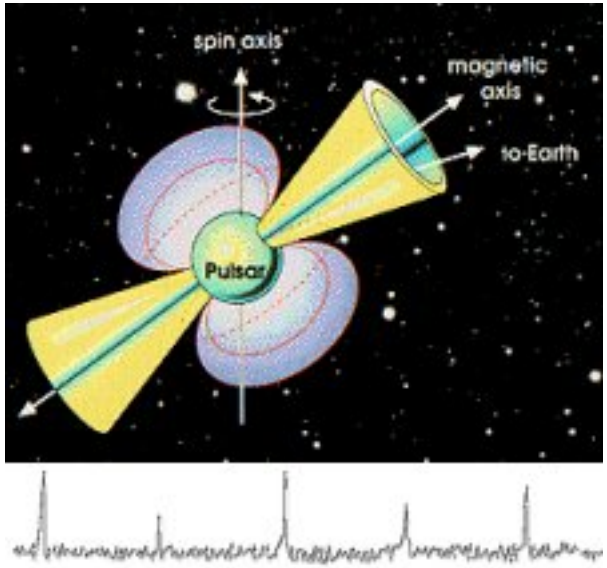

As a rule, rotational period of a neutron star slowly increases because the system loses energy emitting electromagnetic radiation.

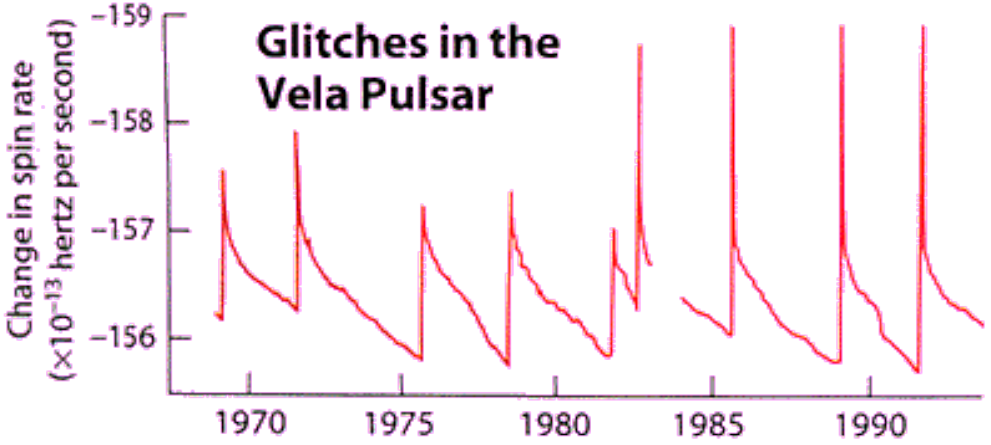

One of the proposed explanations

→ Superfluid nature of nucleons in the inner crust

P.W. Anderson and N.Itoh, Nature 256(1975)25

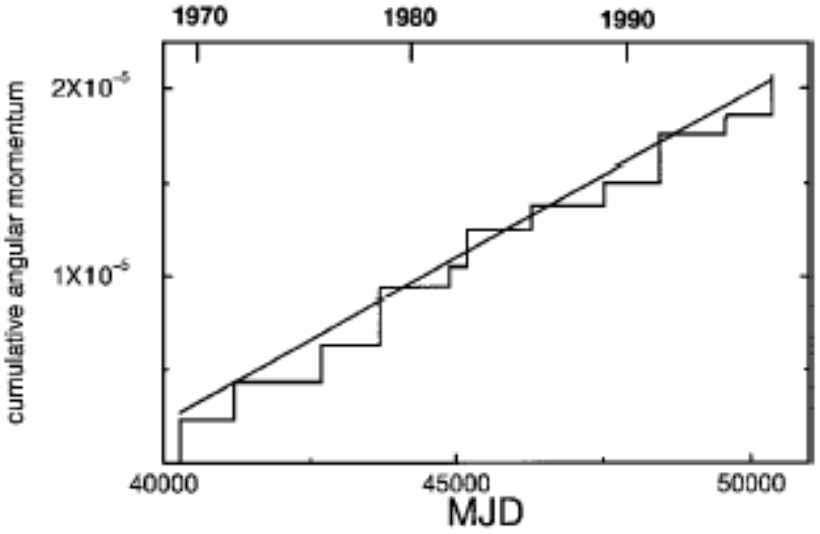

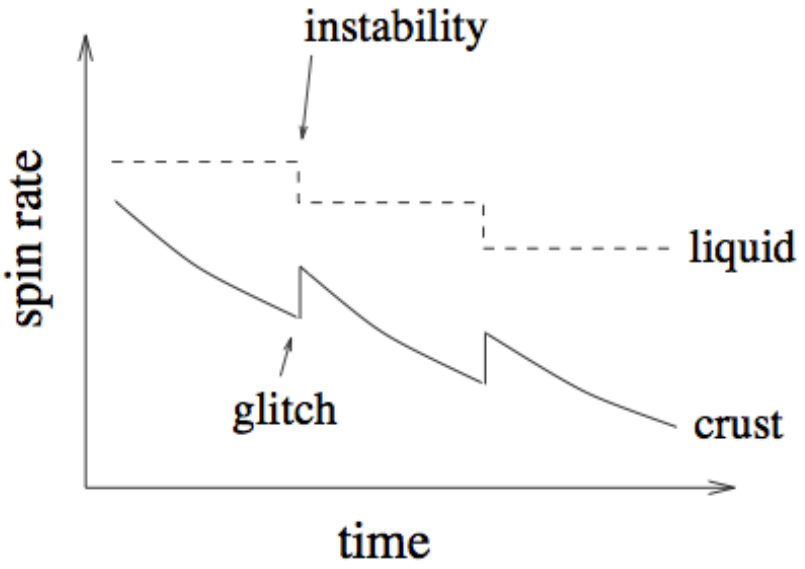

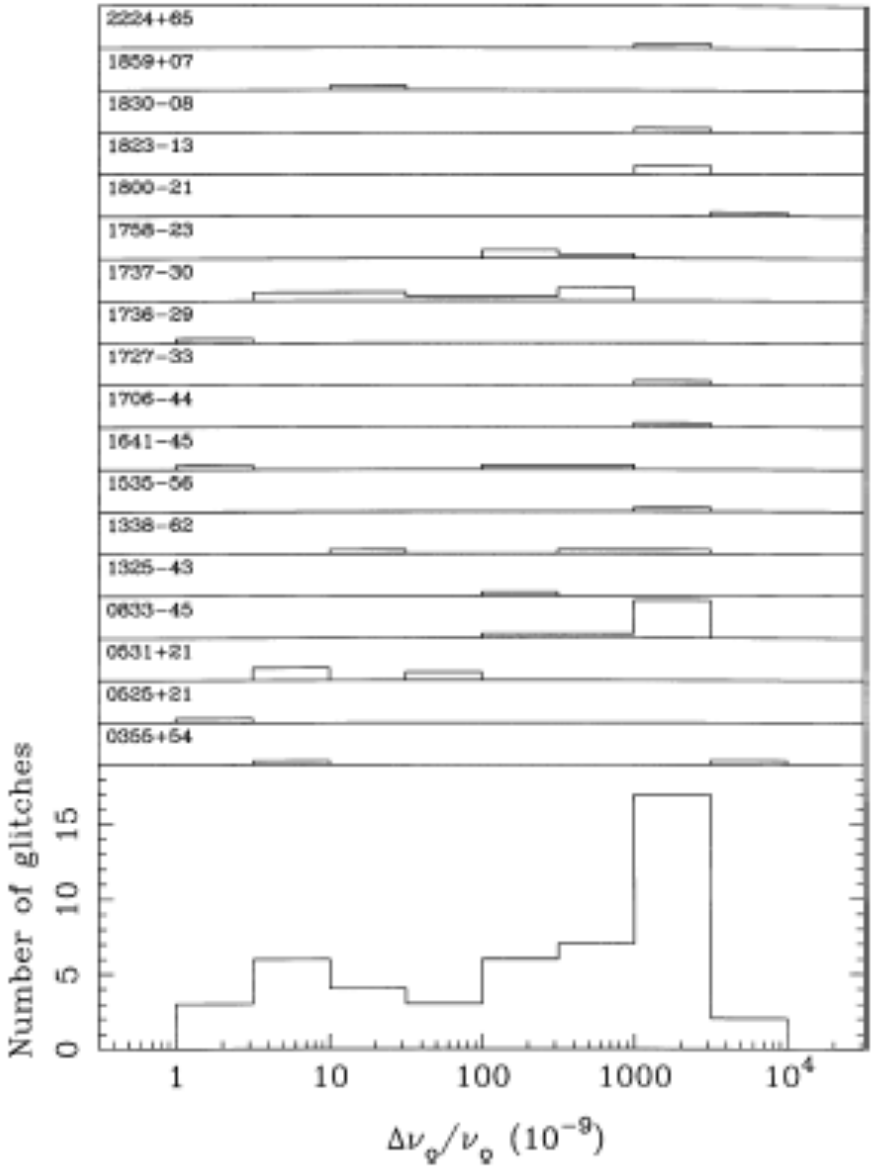

A.G. Lyne, S.L.Shemar, F. Graham Smith,
Mon. Not. Roy. Soc. 315(2000)534

Glitches

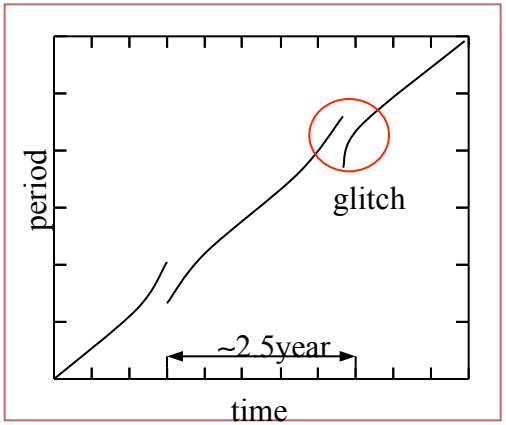

As a rule, rotational period of a neutron star slowly increases because the system loses energy emitting electromagnetic radiation.

Sudden spin ups are measured, at regular intervals

One of the accredited explanations

→ Superfuid nature of nucleons in the inner crust

P.W. Anderson and N.Itoh, Nature 256(1975)25

P.W. Anderson and N.Itoh, Nature 256(1975)25

neutron matter of the inner crust → superfluid in a rotating container

in order to minimize the energy of the system → it develops an array of microscopic linear vortices of superfluid matter

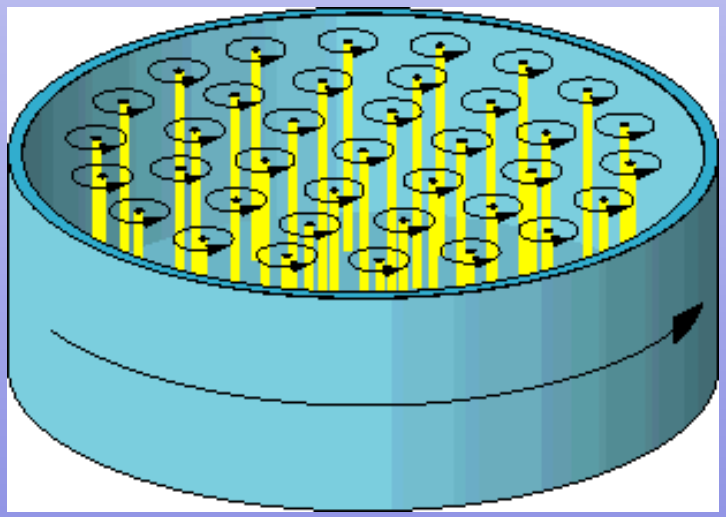

Each vortex line carries angular momentum

A superfluid in a rotating container develops an array of microscopic linear vortices

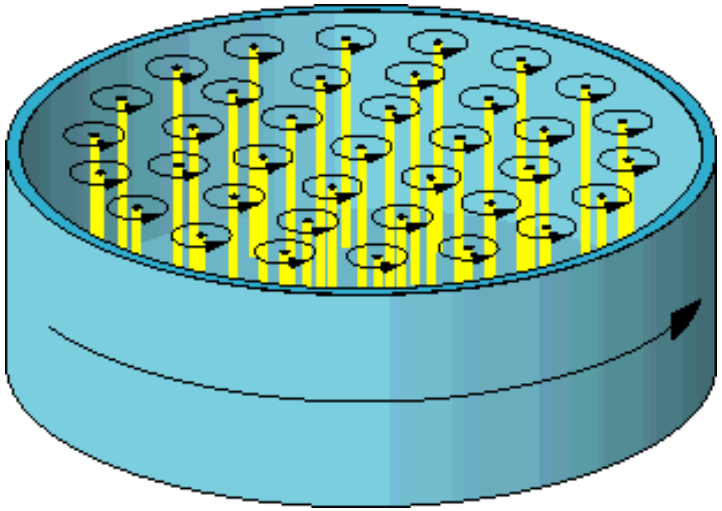

Vortices may pin to **container impurities**, what may modify their dynamics. Sudden unpinning at critical period difference, due to Magnus force, would cause the glitch.

P.W. Anderson and N.Itoh, Nature 256(1975)25

Rotations of a superfluid

Irrotational macroscopic motion

superfluid at rest $\rightarrow$ condensate wavefunction $\rightarrow$ Ψ_0

macroscopic motion $\rightarrow$ phase $\Phi(\vec{x},t)$ $\rightarrow$ $\Psi = \Psi_0 e^{i\Phi}$

macroscopic velocity field $\rightarrow$ $\vec{v}_s = \frac{\hbar}{2m_N}\nabla\Phi$

$\Downarrow$

irrotational flow $\rightarrow$ $\nabla \times \vec{v}_s = 0$

$\Downarrow$

$\nabla \times (\vec{\Omega} \times \vec{r}) = 2\vec{\Omega} \neq 0$ $\rightarrow$ no rigid rotations $\vec{\Omega}$

Vortex lines

classical vortex $\rightarrow$ $\vec{v}_s = \frac{C}{r}\hat{e}_\theta$ $\rightarrow$ $\nabla \times \vec{v}_s = 2\pi C\, \delta^{(2)}(\vec{r})$

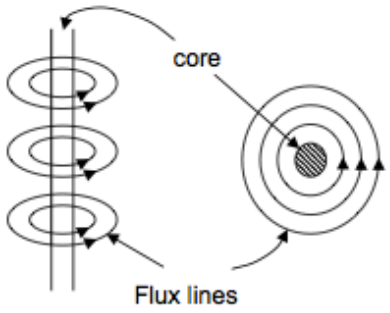

$\vec{v}_s$ minimizes $E_\Omega = E_{lab} - \vec{L}_{lab} \cdot \vec{\Omega}$ (if $\Omega > \Omega_{cr}$)

$\vec{v}_s$ singular at $r = 0$ $\rightarrow$ vortex core (empty or normal matter)

P.M. Pizzochero, Orsay 2005

Quantization of vorticity

$\Psi = \Psi_0 e^{i\Phi}$ single valued $\rightarrow$ $\oint \nabla\Phi \cdot d\vec{l} = 2\pi k \quad (k = 1,2,\cdots)$

$\Downarrow$

quantized vortex lines $\rightarrow$ $C = k \dfrac{\hbar}{2m_N} \quad (k = 1,2,\cdots)$

quantized vorticity $\rightarrow$ $\oint \vec{v}_s \cdot d\vec{l} = k \dfrac{h}{2m_N} \quad (k = 1,2,\cdots)$

Rotating vessel: Feynman-Onsager formula

array of parallel vortices (if $\Omega >> \Omega_{cr}$) $\rightarrow$ $\langle \vec{v}_s \rangle = \Sigma_i \vec{v}_{si}$

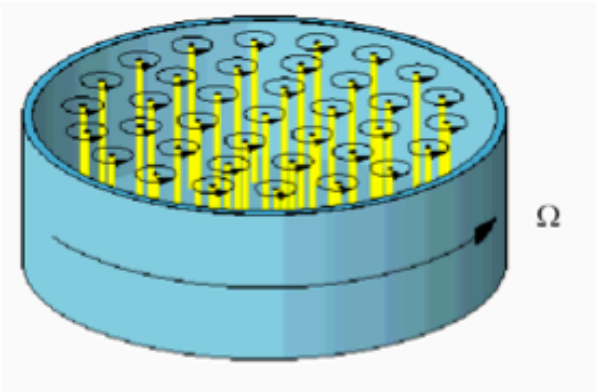

E_Ω minimized by $\langle \vec{v}_s \rangle = \vec{\Omega} \times \vec{r} \Leftrightarrow \nabla \times \langle \vec{v}_s \rangle = 2\vec{\Omega}$

$\Downarrow$

uniform density of vortices $\rightarrow$ $n_v = \dfrac{N_v}{\pi R^2} = \dfrac{4m_N}{h}\Omega$

Vortex spacing:

$$d_v \simeq 3.4 \times 10^{-3} \sqrt{\frac{10^2\ \mathrm{s}^{-1}}{\Omega}}\ \mathrm{cm}\,,$$

Vortex pinning and Magnus force

if superfluid vortices are pinned $\rightarrow \quad \dot{n}_v = 0 \quad \rightarrow \quad \dot{\Omega}_s = 0$

but slow-down of normal component $\rightarrow \quad \dot{\Omega}_n < 0$

$\Downarrow$

rotational lag of components $\rightarrow \quad \Delta\Omega = \Omega_s - \Omega_n > 0$

$\Downarrow$

outward drag force on vortex $\rightarrow \quad f_{mag} \propto \left| \vec{v}_s - \vec{v}_n \right| \propto \Delta\Omega$

Vortex un-pinning and glitches

since $\Delta\dot{\Omega} > 0 \quad \rightarrow \quad f_{mag}$ increases with time

pinning energy $\rightarrow$ maximum pinning force f_{pin}

$\Downarrow$

when $f_{mag} \geq f_{pin} \quad \rightarrow$ unpinning of many vortices

$\Downarrow$

transfer of angular momentum to the star surface

The Magnus force

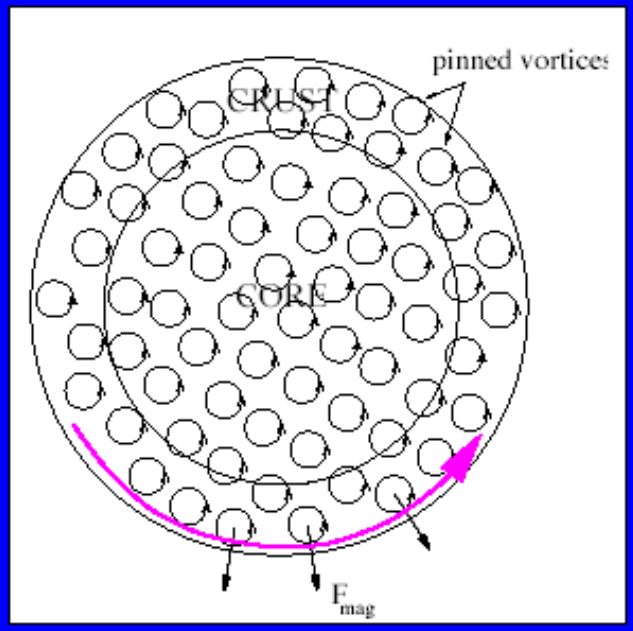

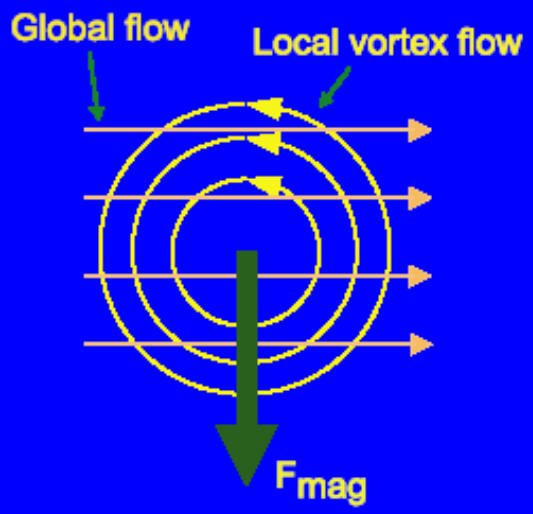

Inner-crust SF store angular momentum as star spins down.

A simple argument:

For sufficiently large densities, pairing is smaller within the nuclear volume than outside;

Vortex destroys pairing within its core;

Then it is energetically convenient for the vortex to be placed on top of the nucleus, rather than far from it: in this way, one saves pairing energy.

$$\Delta E_{pin} \equiv \left[\varepsilon_{cond}(n_N) - \varepsilon_{cond}(n_G)\right] \cdot V_N$$

But we need a realistic estimate of the vortex-nucleus interaction

Much progress since 1995 ….

Since, as we have seen, the spatial variation of superfluid gaps in the inner crust is not well understood theoretically, even in the absence of superfluid flow, the properties of vortices in such an inhomogeneous medium are even less well understood from basic theory. Consequently the dependence of the energy of a vortex line on its location relative to nuclei, which is the essential ingredient in calculations of pinning energies, is also poorly known. Even if the bulk superfluid properties are assumed to be known, estimates of pinning energies that have been made to date are at best indicative and cannot be regarded as quantitatively reliable because they do not take into account the fact that the size of the vortex core is expected to be comparable to the characteristic dimensions of nuclei and the distances between them. Consequently simple

…. But many important open problems remain

C.J. Pethick, D.G.Ravenhall, Annu. Rev. Nucl. Sci. 45 (1995) 429

According to the model, vortex lines are pinned (bound) to nuclei of the lattice

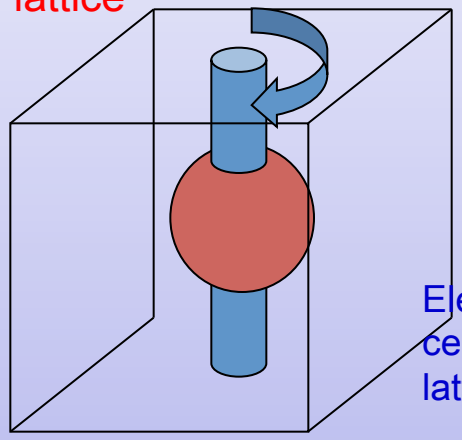

Elementary cell of nuclear lattice

Under certain conditions, the vortices can be unpinned from the lattice and deliver their angular momentum to the whole system: The star spins up.

Angular momentum is transferred to star rotation.

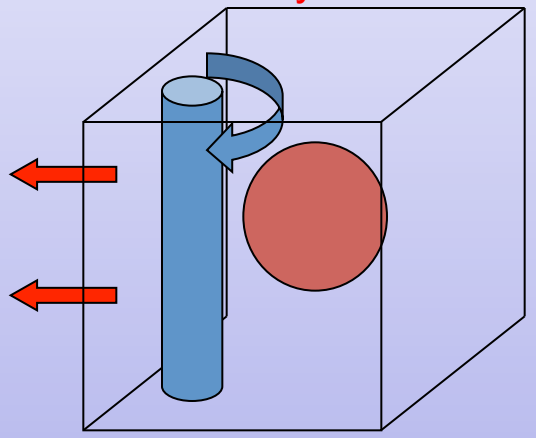

Crucial step: Calculation of the force which binds vortex to nuclei

Pinning force

$$\Delta E = E_{dec} - E_{cen}$$

$E_{tot}=E_{kin}+E_{pot}+E_{pair}$

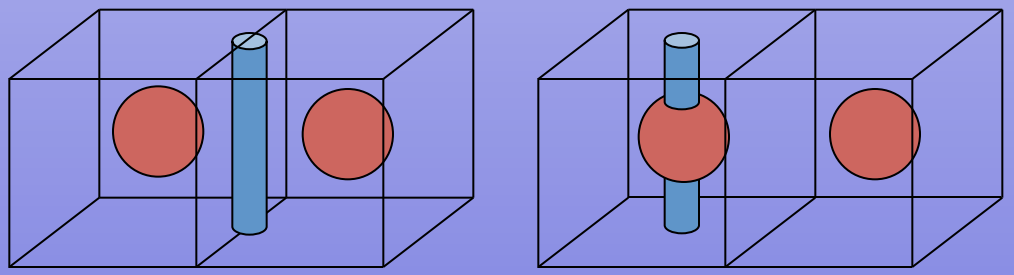

A basic issue for a model of glitches based on vortex unpinning
To determine the favoured vortex configuration

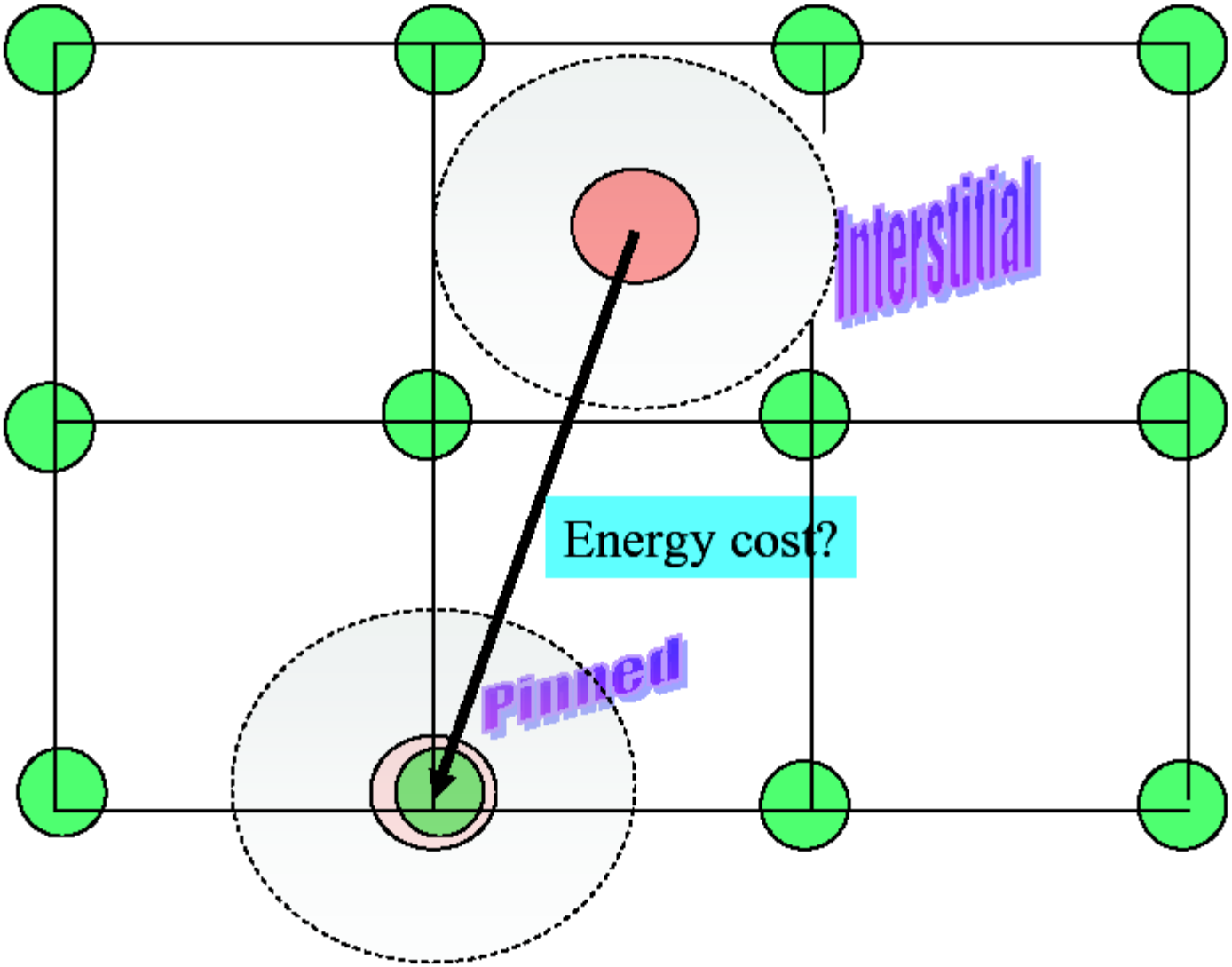

Trapping of atoms by vortices in ^{4}He

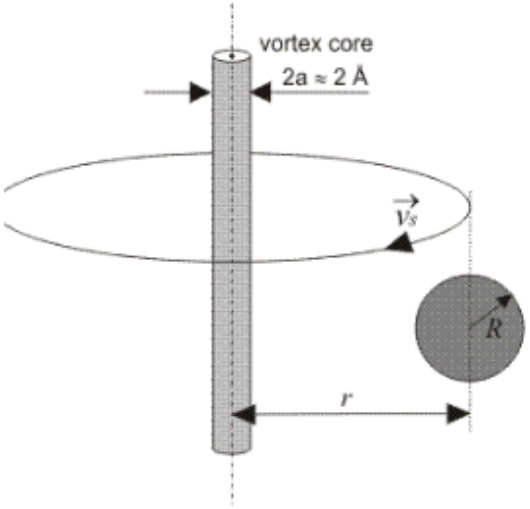

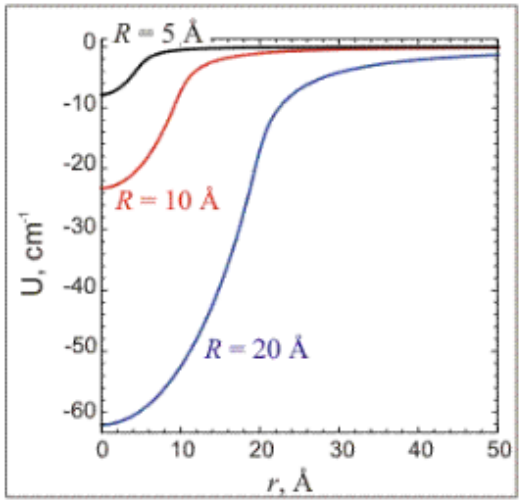

Nanofilaments

Metal atoms trapped at the vortices aggregate into filaments with nanometer thickness.

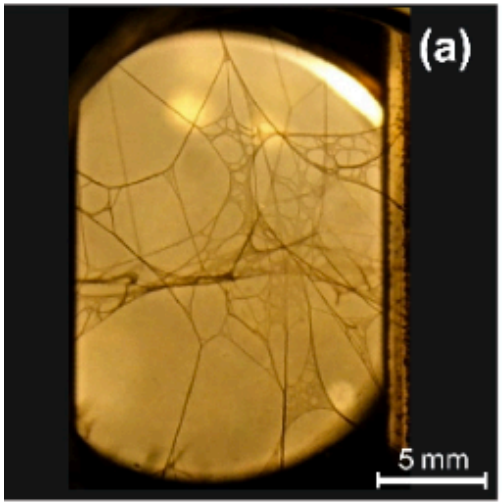

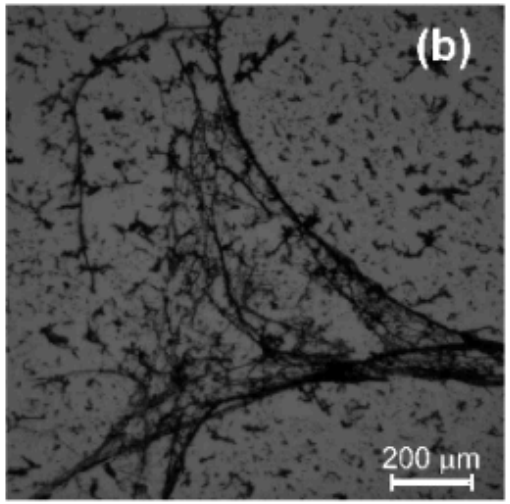

P. Moroshkin et al.,
EPL 90 (2010) 34002

Microscopic quantum calculation of the vortex-nucleus system

The ansatz for the study of a vortex is $\Delta(\rho, z, \phi) = \Delta(\rho, z) e^{i\nu\phi}$

where $\Delta(\rho, z)$ is a real function and $\nu = 0,1,2,..$ is the vortex index.

Because of the symmetry of the problem $\Delta(\rho, z) = \Delta(\rho, -z)$. The pairing gap is an eigenstate of the parity operator with eigenvalue $(-1)^{\nu}$

Vortices are expected to be formed from Cooper pairs carrying each 1 quantum of angular momentum, for this reason they must be formed of **single particle levels of opposite parity.**

We solve the HFB (De Gennes) equations expanding on a single-particle basis in cylindrical coordinates

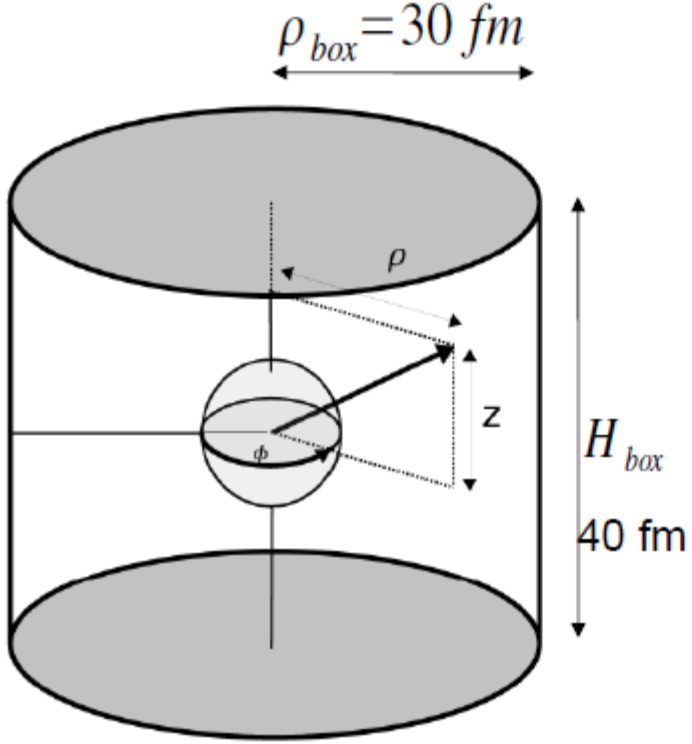

- The expanded on single particle basis
- we used SLy4, SkM*, SII and SGII Skyrme for the single particle levels.
- we constrained protons to keep spherical symmetry.
-we neglected spin-orbit interaction

$$\begin{pmatrix} \varepsilon_i-\lambda & \Delta \\ \Delta & -(\varepsilon_i-\lambda) \end{pmatrix}\begin{pmatrix} U_i \\ V_i \end{pmatrix}=E_i\begin{pmatrix} U_i \\ V_i \end{pmatrix}$$

The solution of the HFB equations expanded on the single particle basis read:

$$u_{qm}(\rho,z,\phi)=\Sigma_{nk}\,U_{nk}^{qm}\,J_{nm}(\rho)\sin(kz)\,e^{im\phi}$$

$$v_{qm}(\rho,z,\phi)=\Sigma_{nk}\,V_{nk}^{qm}\,J_{n(m-\nu)}(\rho)\sin(kz)\,e^{i(m-\nu)\phi}$$

PAIRING INTERACTION

Ecut = 60 MeV

$$V_{pair}(\mathbf{x},\mathbf{x}') = V_0 \cdot \left(1 - 0.7 \cdot \left(\frac{n(\mathbf{x})}{n_0}\right)^{0.45}\right) \delta(\mathbf{x}-\mathbf{x}') \quad MeVfm^3$$

With a HF field based on the Skyrme interaction.

Results in neutron matter

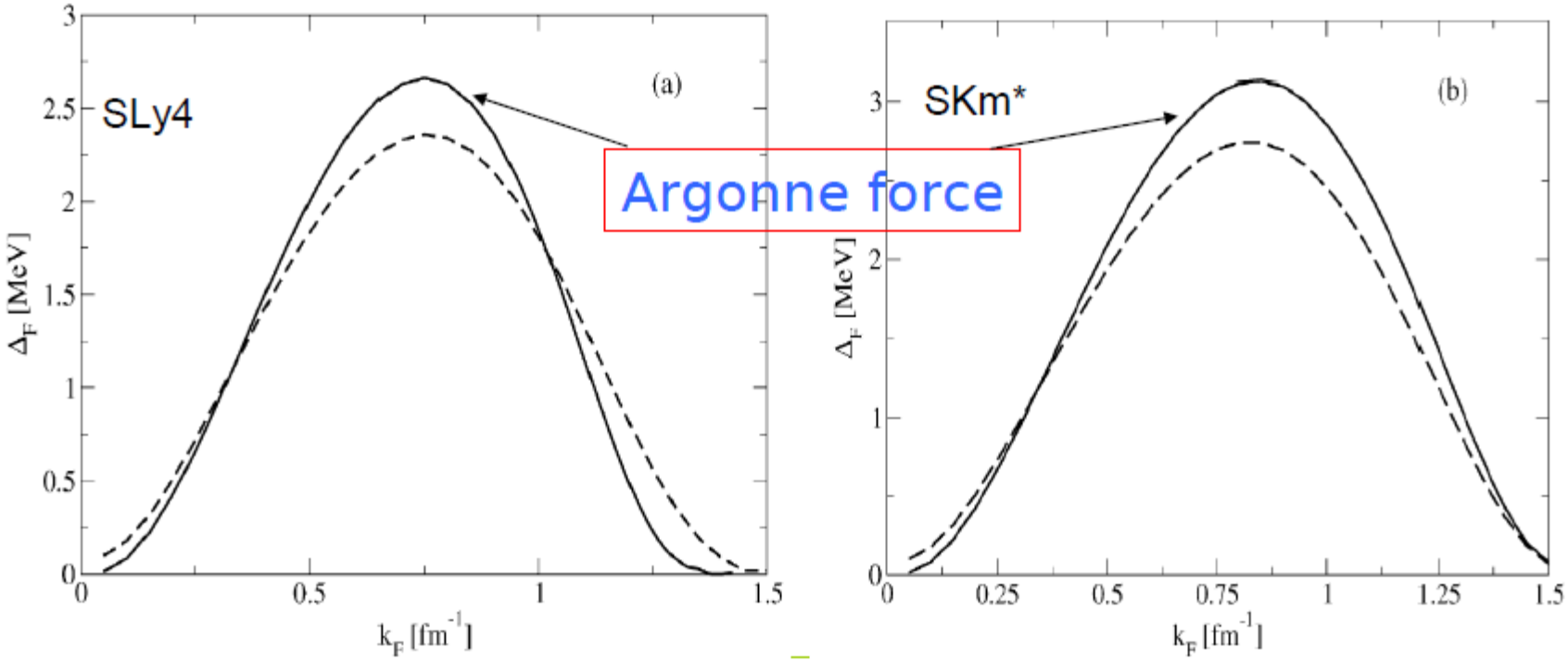

E. Garrido et al. Phys. Rev. C60(1999)64312

A vortex in uniform neutron matter (inside the cell)

SLy4

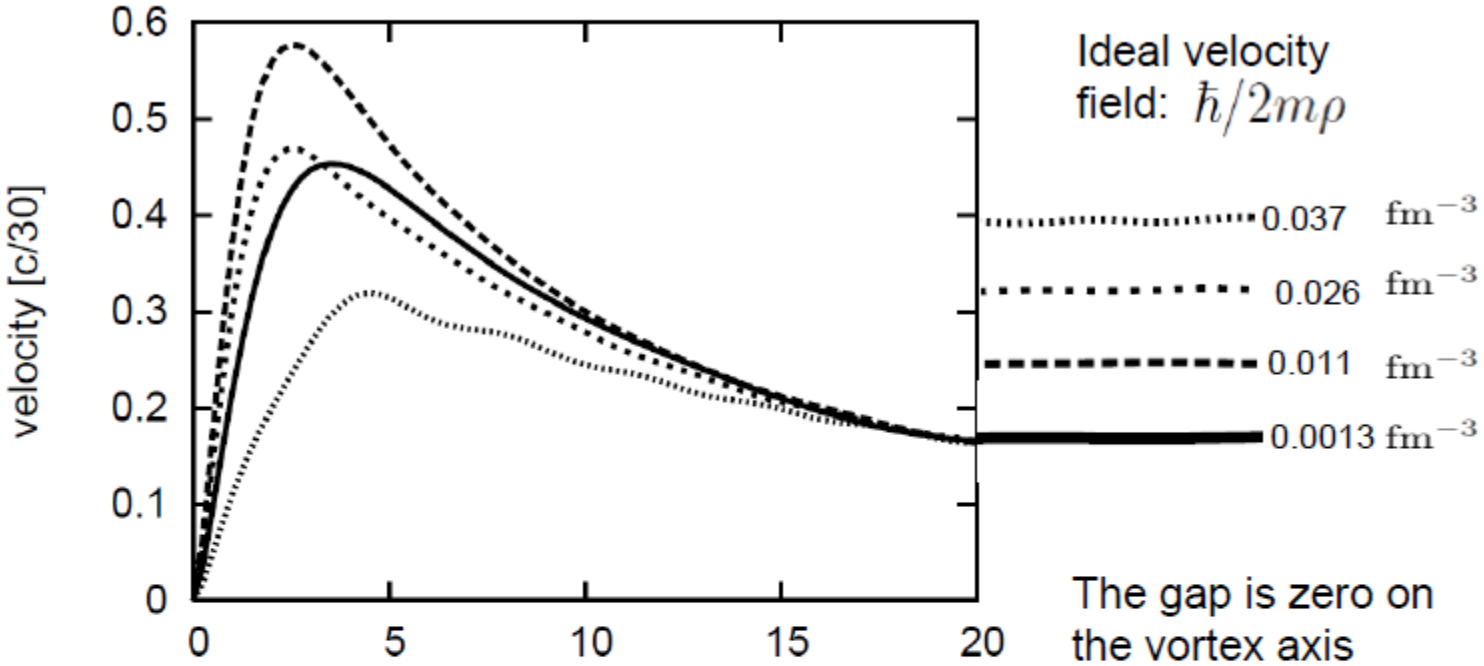

The density drops on the vortex axis

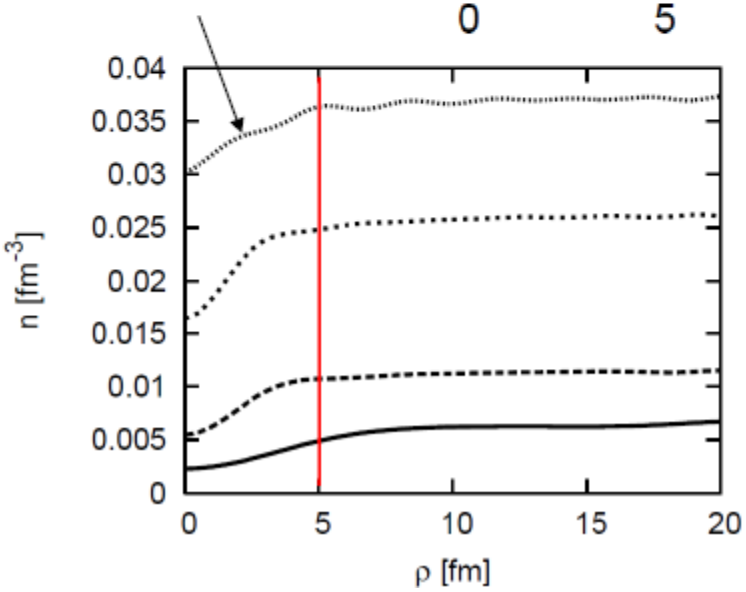

The gap is zero on the vortex axis

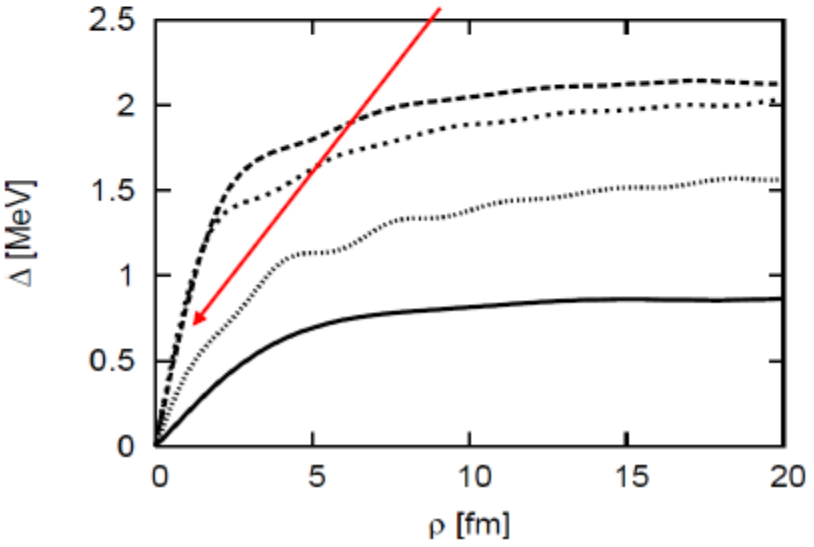

Pairing gap of pinned vortex

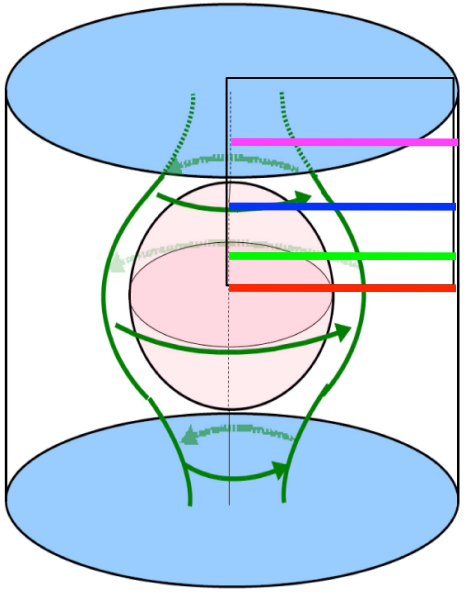

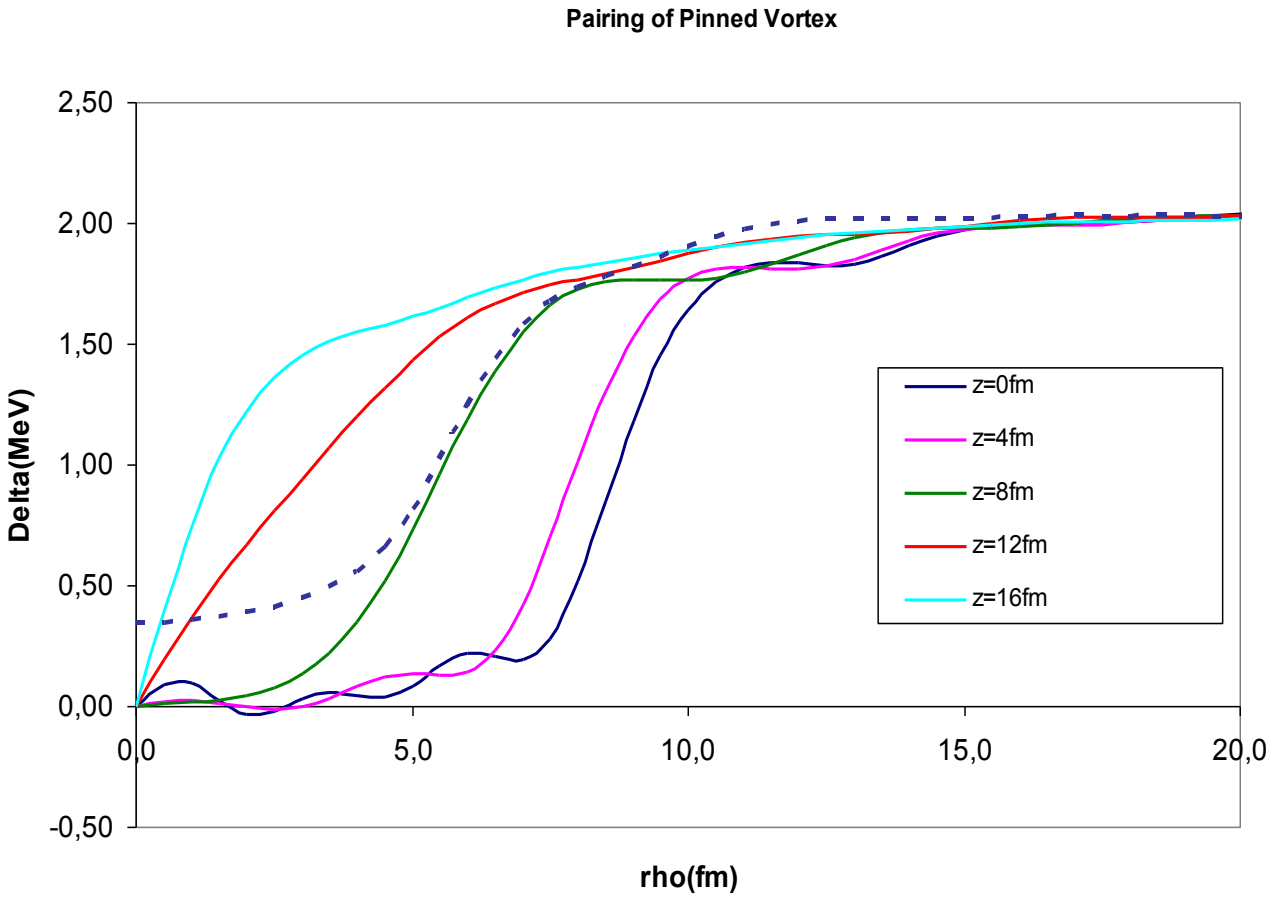

Velocity of pinned vortex

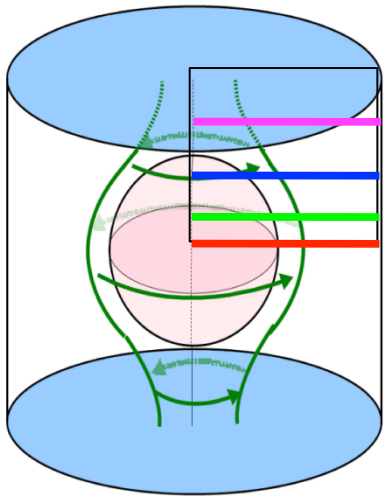

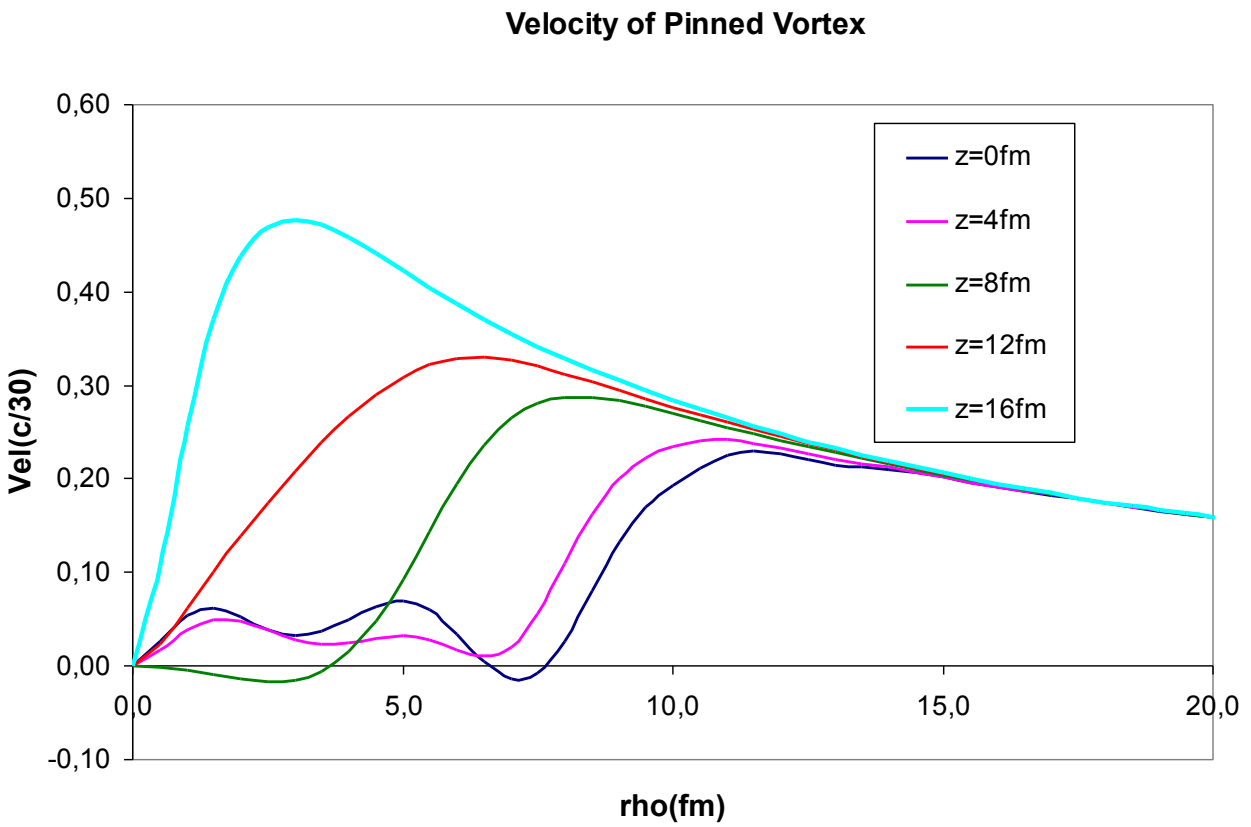

Sly4 5.8MeV

nucleus

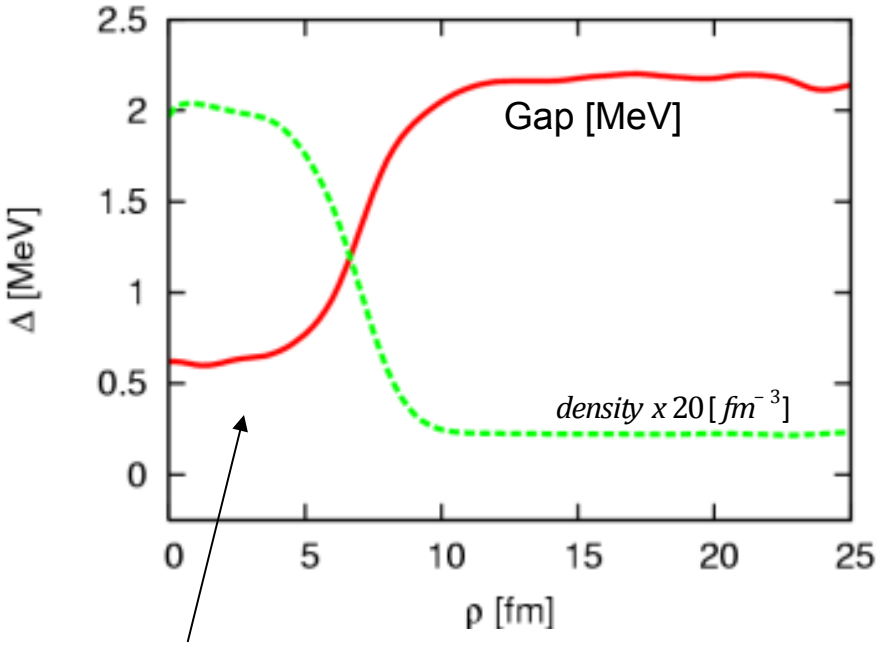

vortex pinned on a nucleus

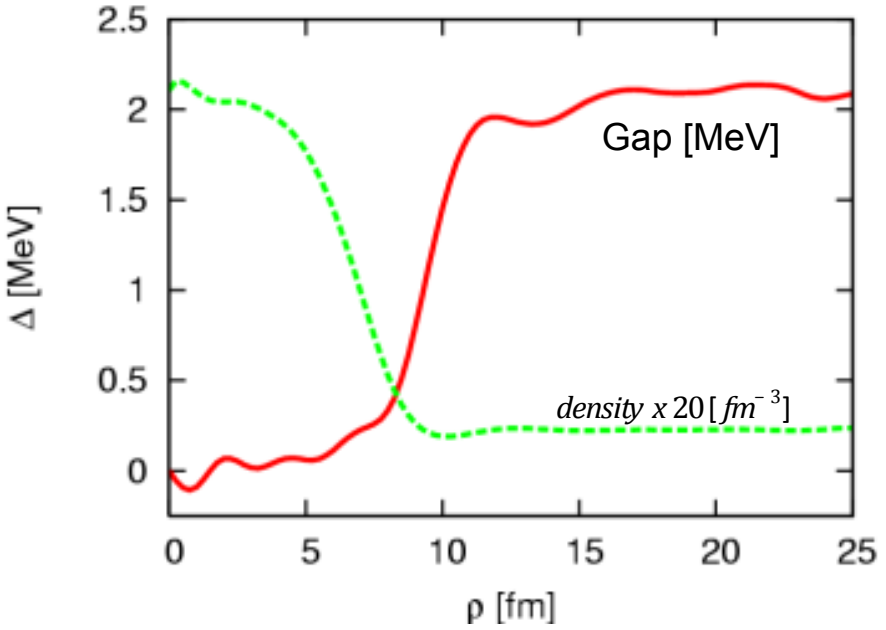

In this region the gap is not completely suppressed

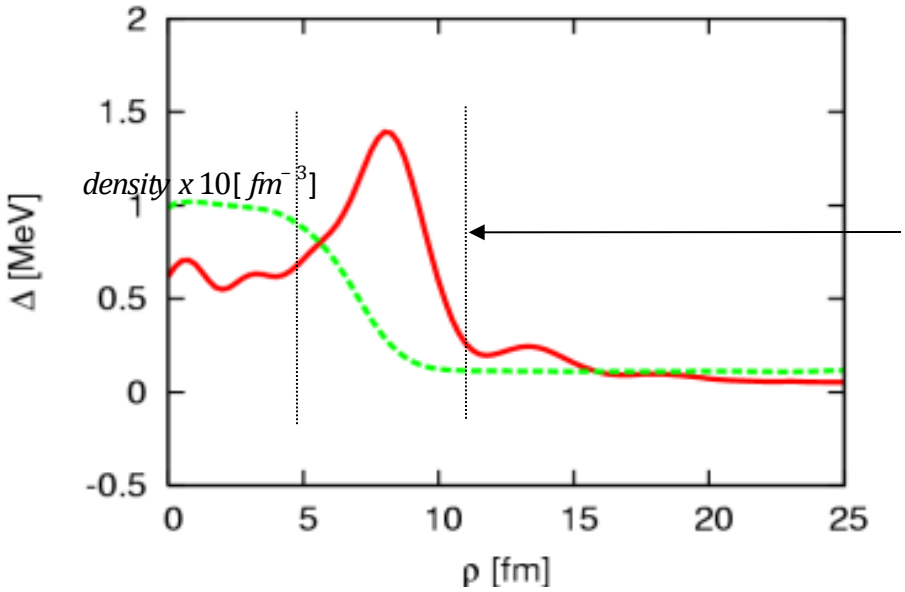

the gap of a nucleus minus the gap of a vortex on a nucleus: on the surface there is the highest reduction of the gap.

The velocity field is suppressed in the nuclear region

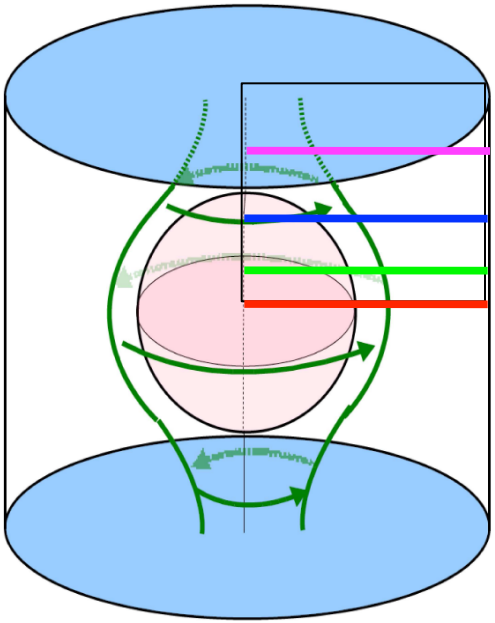

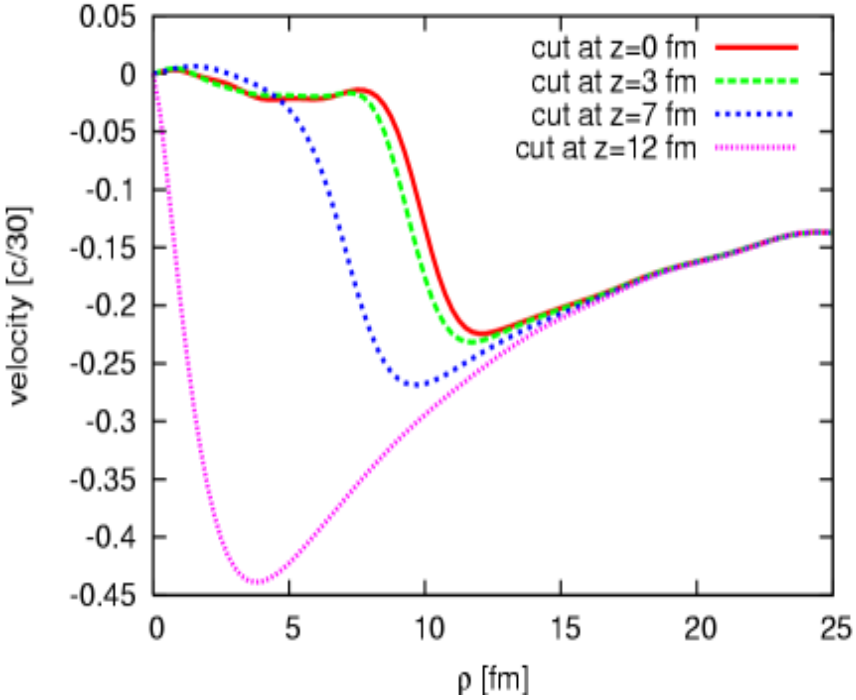

$$Vel = -\frac{i\hbar}{m\rho n(\rho,z)} \sum_{qm} v^*_{qm}(\rho,z,\phi) \frac{\partial v_{qm}(\rho,z,\phi)}{\partial \phi}$$

The superfluid flow is destroyed in the nuclear volume.

Vortex in uniform matter

Nucleus

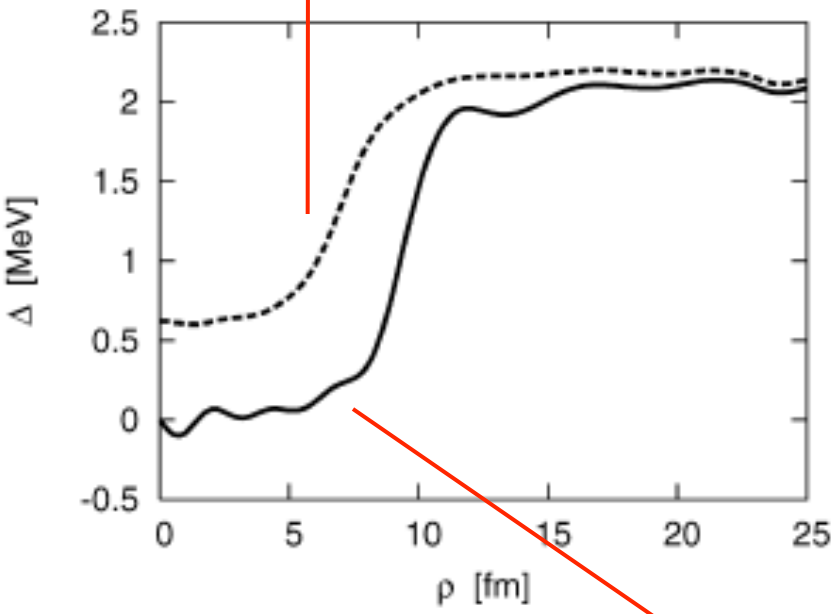

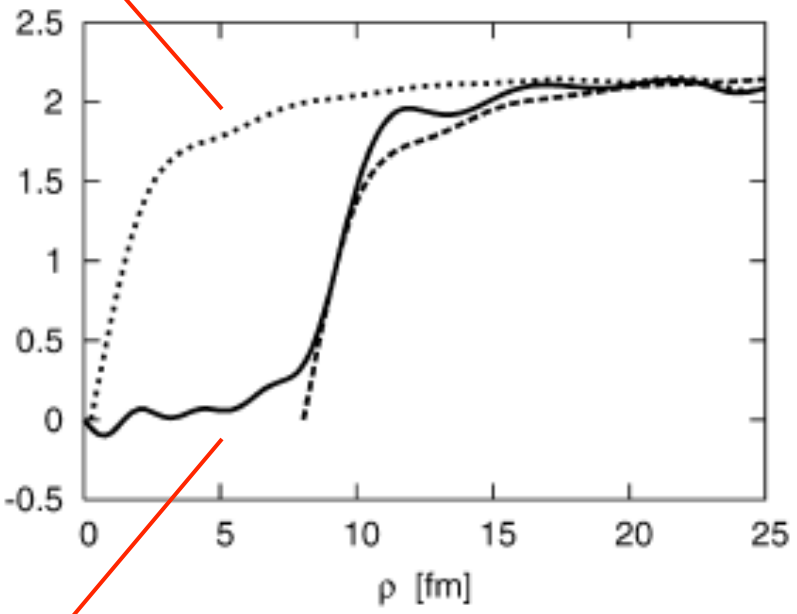

Pinned vortex

$\nu = 2$ Pinned Vortex

In this case Cooper pairs are made of single particle levels of the same parity

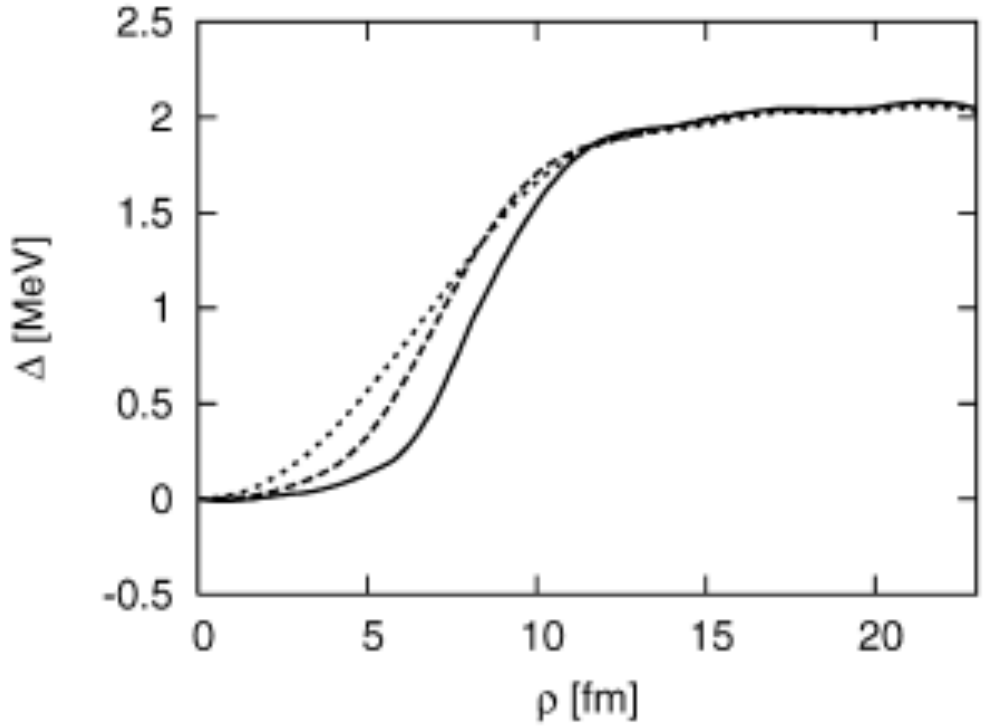

Vortex radii

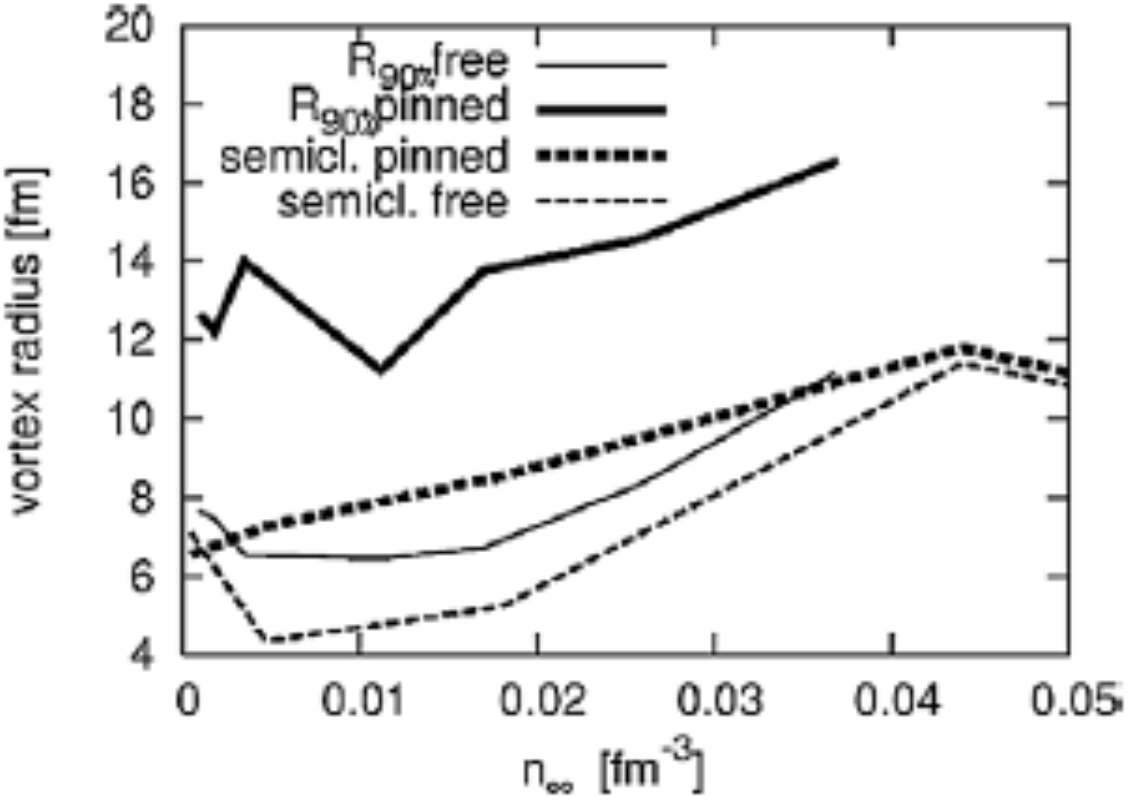

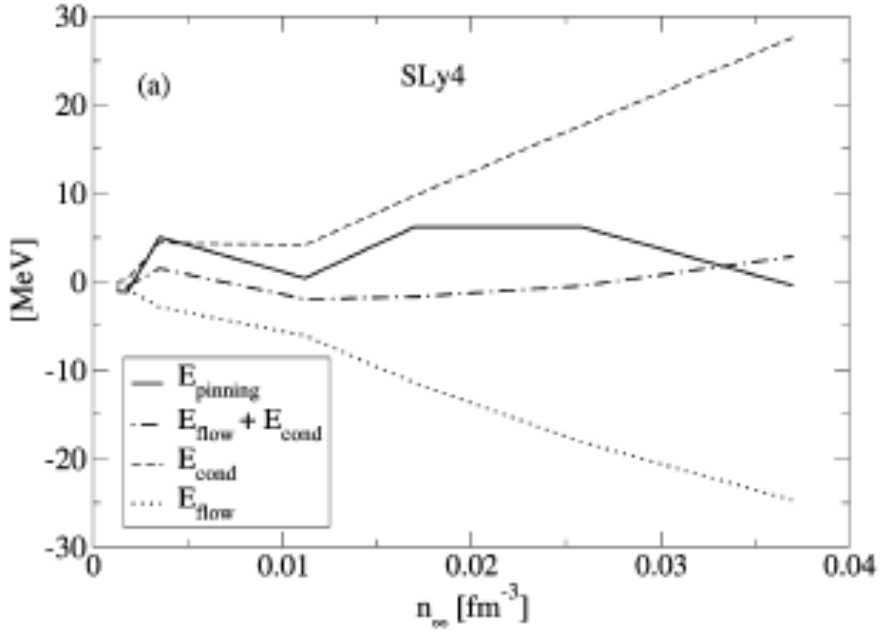

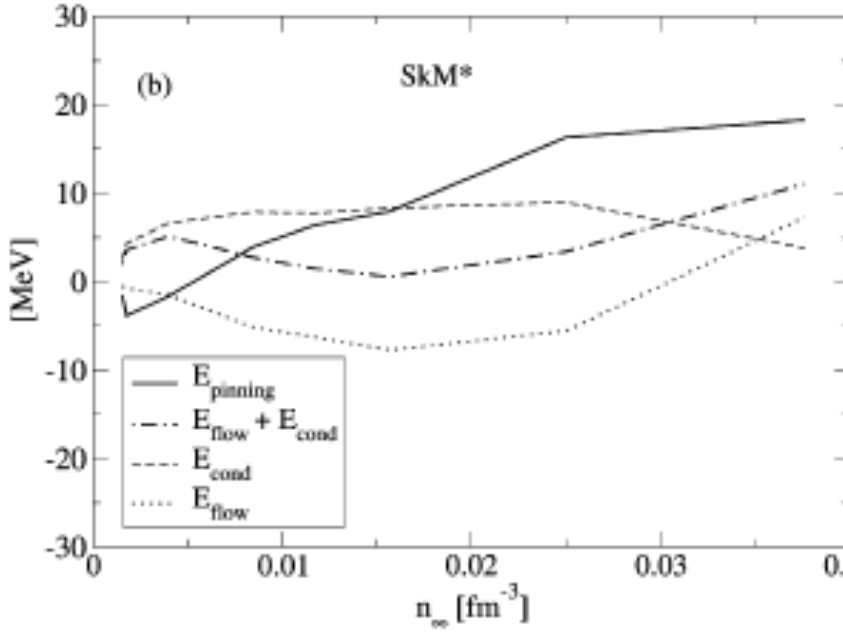

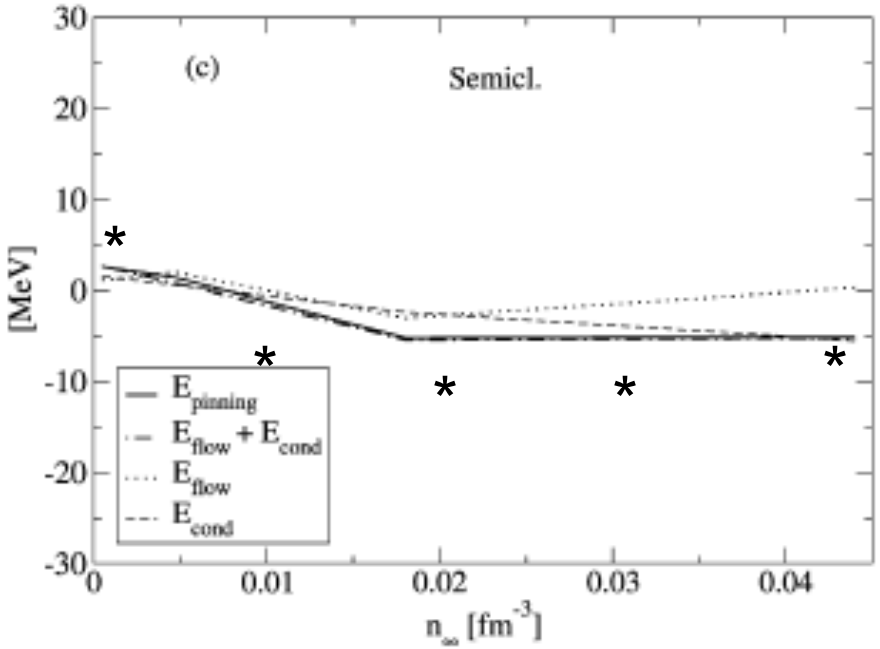

P.M. Pizzochero and Donati,
Nucl. Phys. A742,36 (2004) Semiclassica model with spherical nuclei.

Conclusions and perspectives

-We have solved the HFB equations for a single vortex in the crust of neutron stars, considering explicitly the presence of a spherical nucleus, generalizing previous studies in uniform matter.

-We have found that finite size effects are important, (v=1) vortex (at low and medium density) stays outside of the nuclear volume, where the pairing goes to zero. At high density the vortex expulsion can be cancelled (Skm* and SGII) and a situation similar to the semiclassical approximation is found.

-Numerical results at different densities with SII, Sly4, Skm* and SGII interaction indicate that the pinning energy is very small and of the order of a few MeV. In particular pinning is found at low asymptotic neutron density.

-Adoption of the more recent calculations for the inner crust nuclei.
-Which interactions to adopt to describe the mean field.
-Which is the role of medium polarization effects for the pairing?
-Vortex dynamics

A few basic questions about pairing correlations

1. **Does superfluidity affect the results found by Negele and Vautherin?**

2. **What is the spatial dependence of the pairing gap?**

   How important are the nuclear clusters?

3. **How much are the gaps affected by many-body processes ?**

4. **Can we prove experimentally that the crust is really superfluid?**

Pairing interaction in neutron and nuclear matter and exchange of p.h. excitations

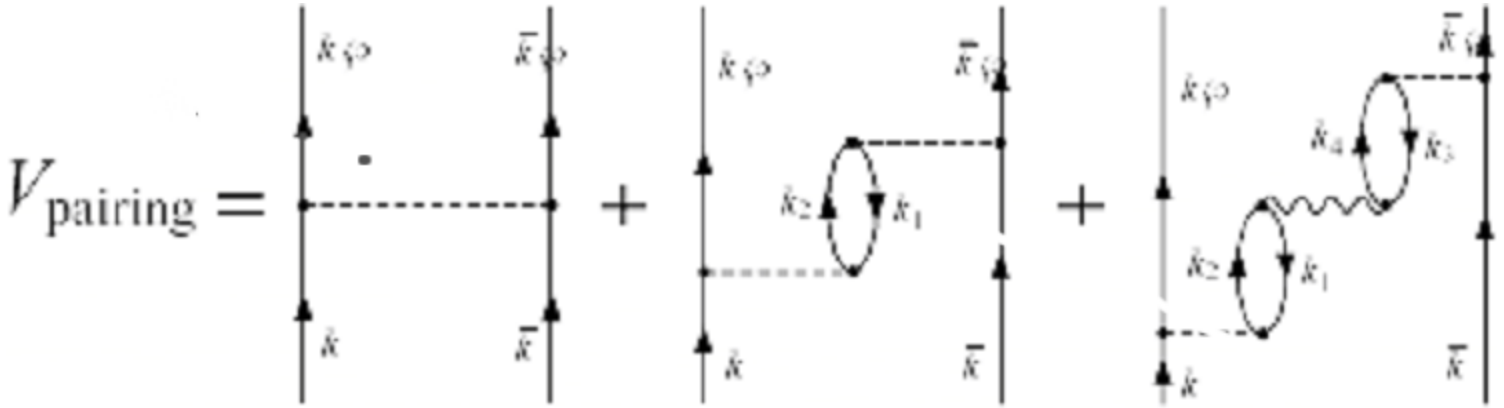

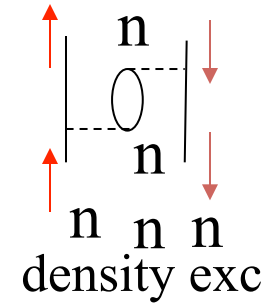

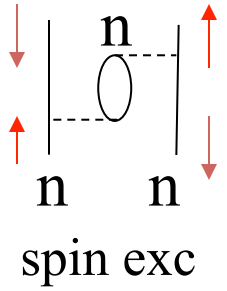

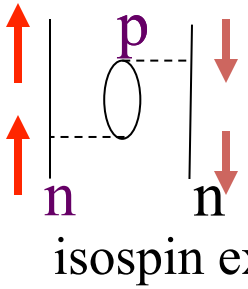

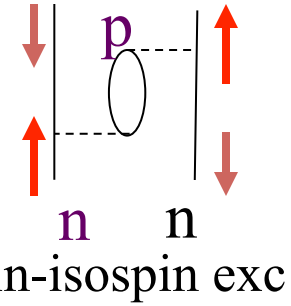

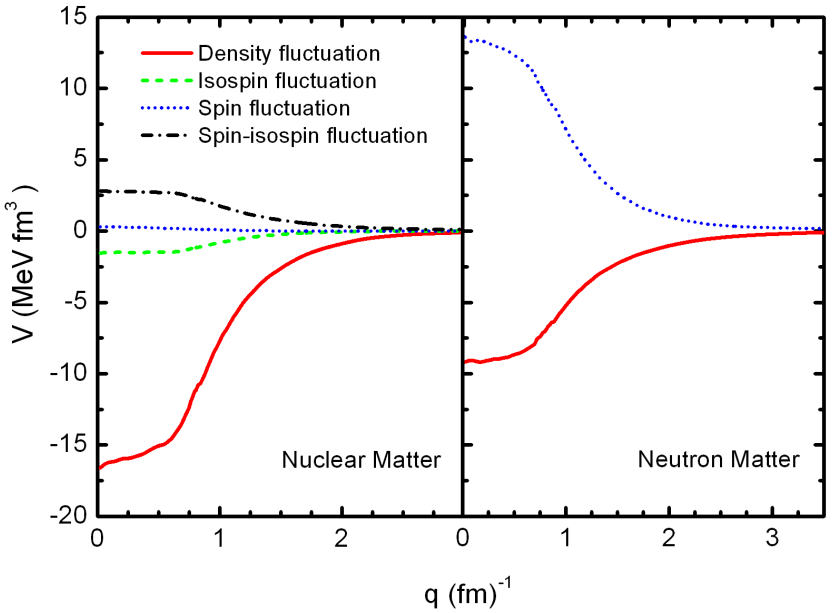

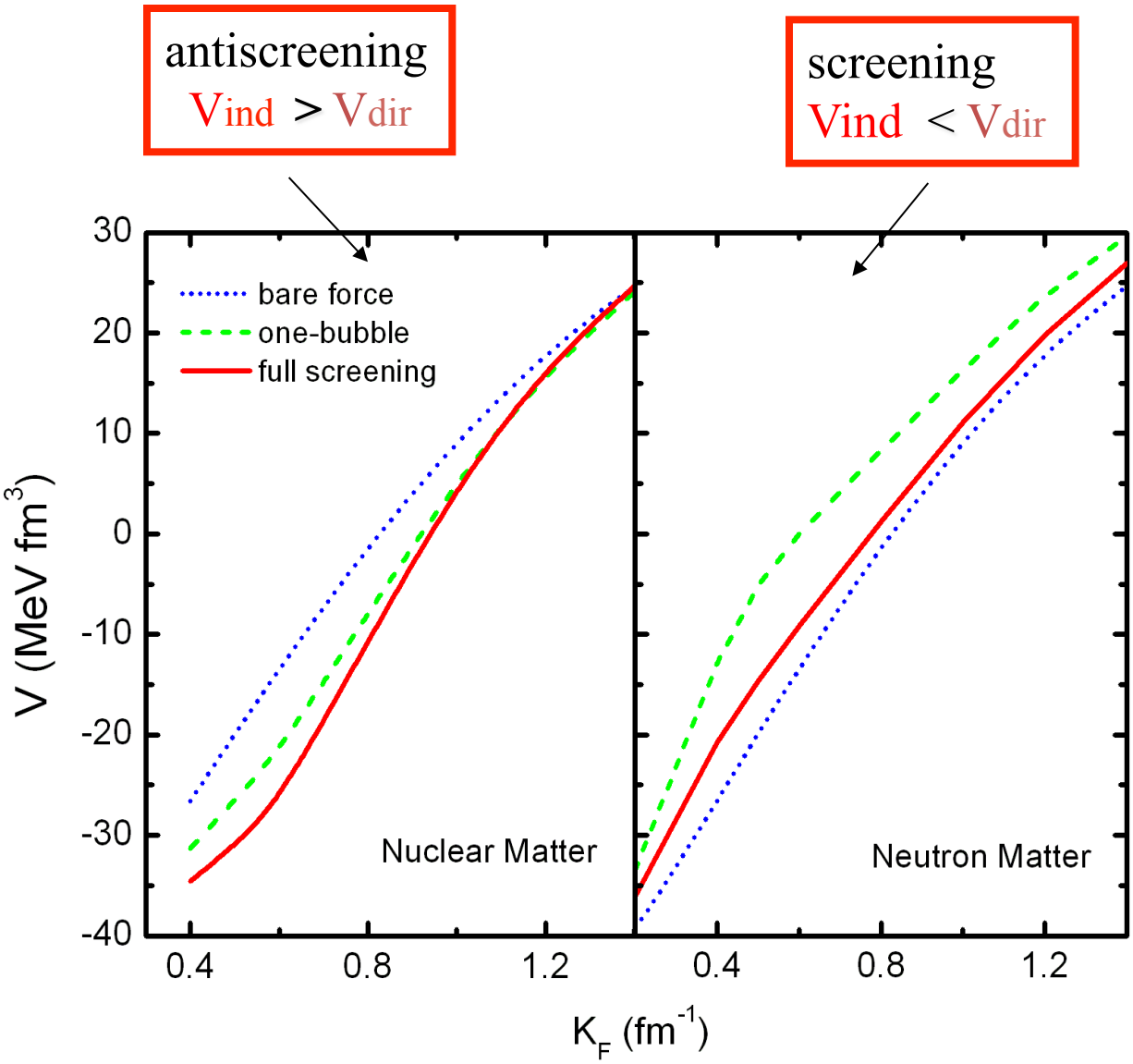

L.G. Cao, U. Lombardo, P. Schuck

Z=1 free Fermi gas

Z<1 correlated Fermi system

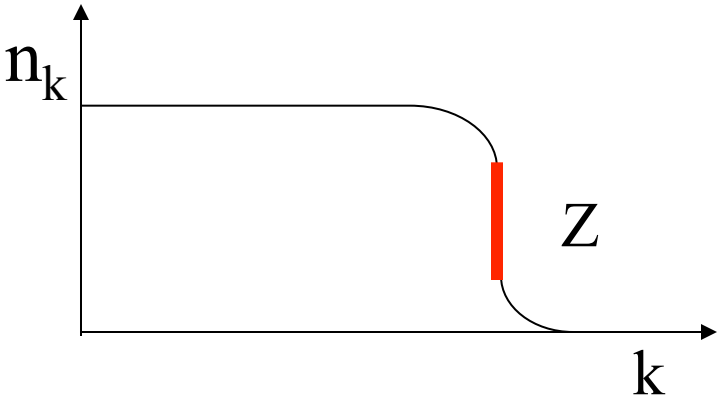

Gap Equation

$$\Delta_p = -\frac{1}{2}\int d^3p' \frac{Z_p V_{pp'} Z_{p'}}{\sqrt{(\varepsilon_{p'} - \varepsilon_F)^2 + \Delta_{p'}^2}} \Delta_{p'}$$

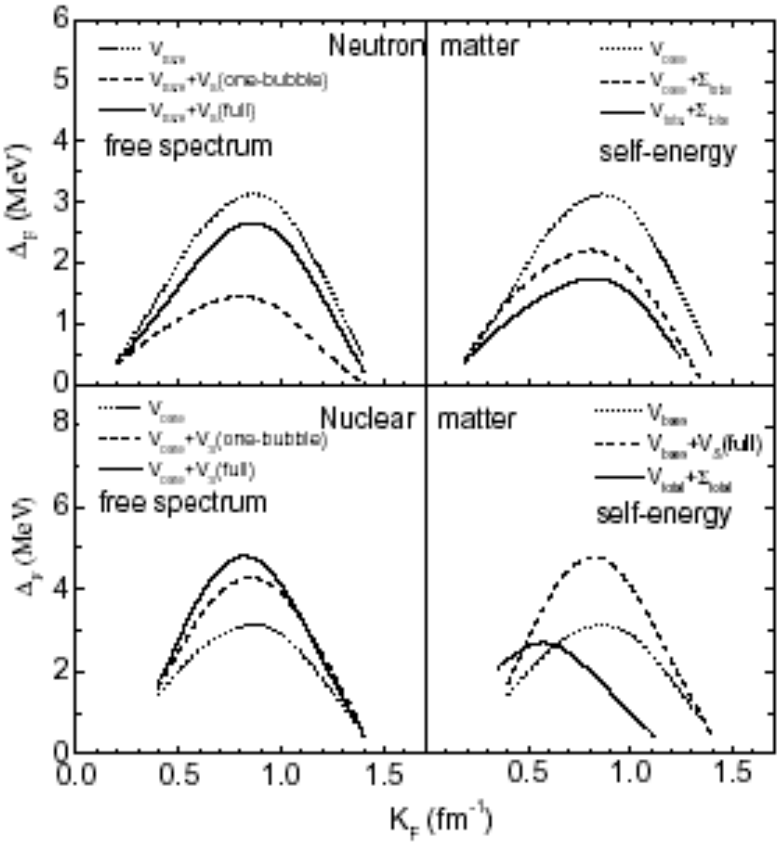

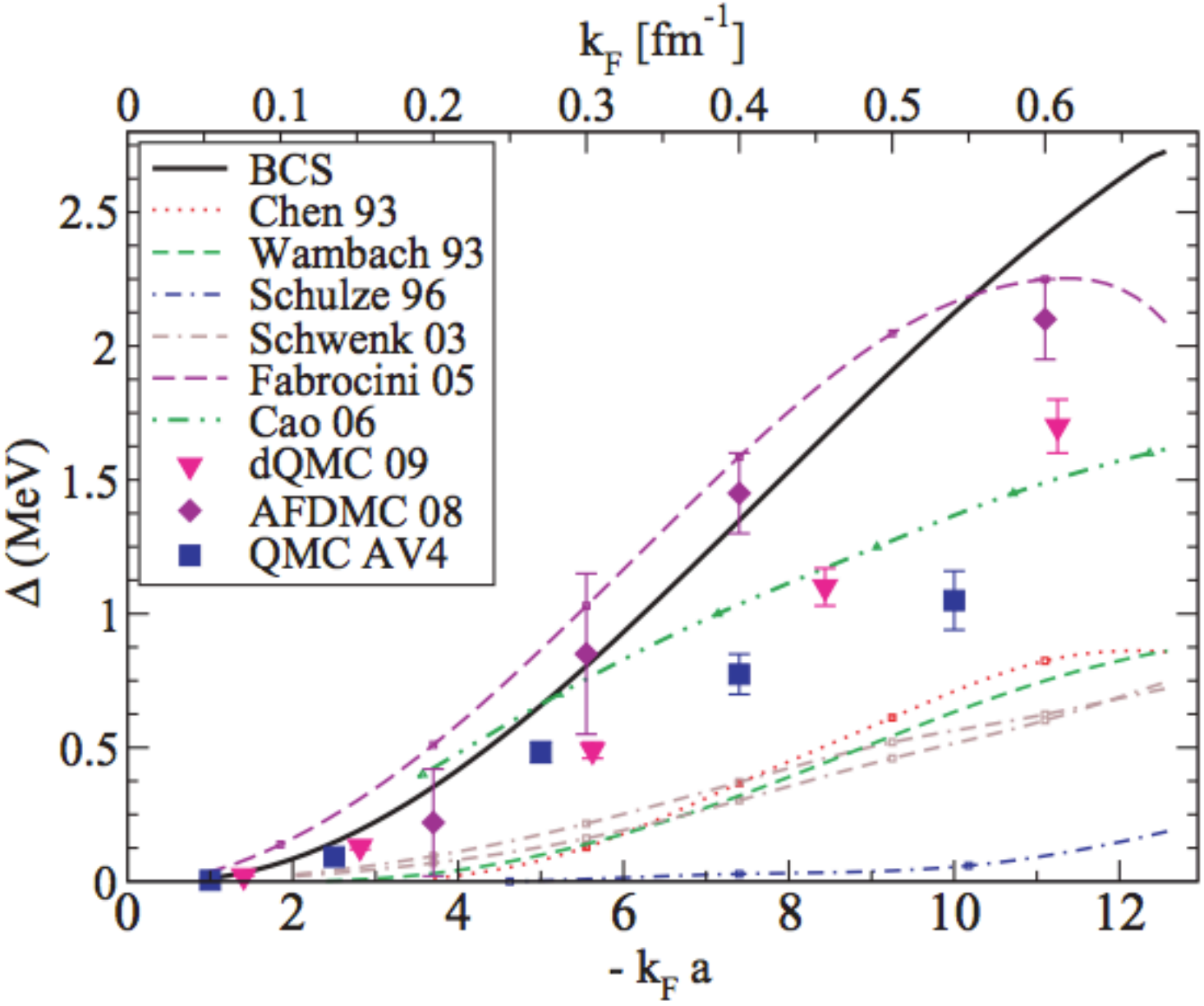

A. Gezerlis, J. Carlson PRC 81 (2010) 025803

PAIRING GAP IN FINITE NUCLEI

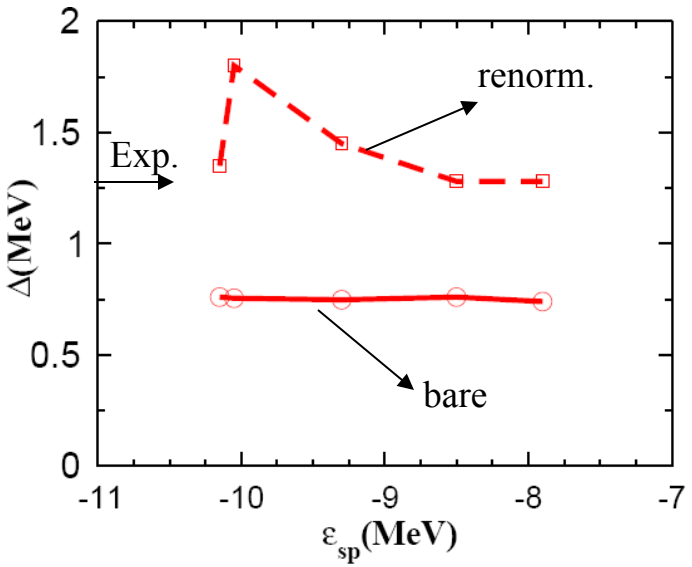

Medium effects **increase** the gap in ^{120}Sn

F. Barranco et al., Eur. J. Phys. A21(2004) 57

PAIRING GAP IN NEUTRON MATTER

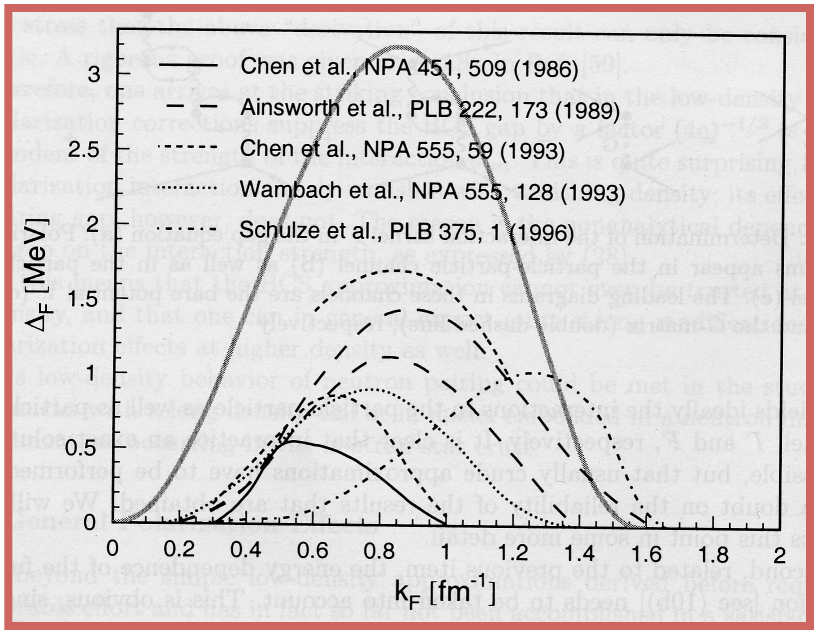

Medium effects **decrease** the gap

Connection with Self-consistent Green Function

J. Terasaki et al., Nucl.Phys. **A697**(2002)126;

cf. C.Barbieri, M. Hjorth-Jensen, PRC79 (2009)064313

by extending the Dyson equation…

$$G_\mu^{-1} = (G_\mu^o)^{-1} - \Sigma_\mu(\omega)$$

$$\Sigma_\mu(\omega) = \int_{-\infty}^{+\infty} \frac{d\omega'}{2\pi} \sum_{\mu'} \frac{1}{\hbar} G_{\mu'}(\omega') \sum_{\alpha} \frac{1}{\hbar} D^o_\alpha(\omega-\omega') * V^2_{\mu\mu',\alpha}$$

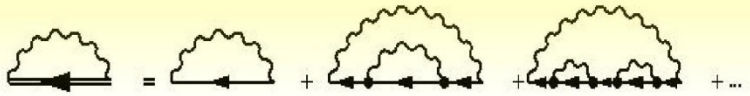

to the case of superfluid nuclei (Nambu-Gor'kov), it is possible to consider both:

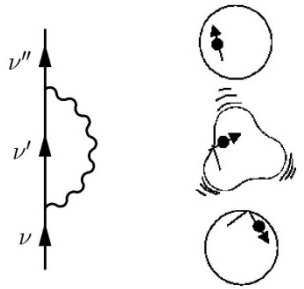

and

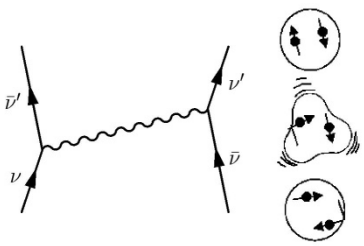

USED FORMALISM

(cf. Van der Sluys et al., NPA551(1993)210)

$$\begin{pmatrix} E_a + \Sigma_{11}(\tilde{E}_{a(n)}) & \Sigma_{12}(\tilde{E}_{a(n)}) \\ \Sigma_{12}(\tilde{E}_{a(n)}) & -E_a + \Sigma_{22}(\tilde{E}_{a(n)}) \end{pmatrix} \begin{pmatrix} x_{a(n)} \\ y_{a(n)} \end{pmatrix} = \tilde{E}_{a(n)} \begin{pmatrix} x_{a(n)} \\ y_{a(n)} \end{pmatrix} \quad (10)$$

where one has introduced the normal and abnormal self-energies $\Sigma_{11}(E)$ (being $\Sigma_{22}(E) = -\Sigma_{11}(-E)$) and $\Sigma_{12}(E)$, given by

$$\Sigma_{11} = \sum_{b,m,J,\nu} \frac{V^2(a(n)b(m)J\nu)}{\tilde{E}_{a(n)} - \tilde{E}_{b(m)} - \hbar\omega_{J\nu}} + \sum_{b,m,J,\nu} \frac{W^2(a(n)b(m)J\nu)}{\tilde{E}_{a(n)} + \tilde{E}_{b(m)} + \hbar\omega_{J\nu}} \quad (11)$$

and

$$\Sigma_{12} = \Sigma^{\text{pho}}{}_{12} + \Sigma^{\text{bare}}{}_{12}$$

$$\Sigma^{\text{pho}}{}_{12} = -\sum_{b,m,J,\nu} V(a(n),b(m),J,\nu) W(a(n),b(m),J,\nu) \left[\frac{1}{\tilde{E}_a(n) - \tilde{E}_b(m) - \hbar\omega_{J,\nu}} - \frac{1}{E_a(n) + \tilde{E}_b(m) + \hbar\omega_{J,\nu}} \right].$$

$$\Sigma_{12}^{bare} = \pm \sum_{b,n} V_{bare}(a,b) \frac{(2j_b+1)}{2} \tilde{u}_{b(n)} \tilde{v}_{b(n)}.$$

$V(jj'\lambda) = \beta\lambda(2\lambda+1)^{-1/2} \langle j||\text{Ro } dU/dr\ Y_\lambda||j'\rangle (u_j \tilde{u}_{j'} - v_j v_{j'}) (2j+1)^{-1/2}$

$W(jj'\lambda) = \beta\lambda(2\lambda+1)^{-1/2} \langle j||\text{Ro } dU/dr\ Y_\lambda||j'\rangle (u_j v_{j'} + v_j \tilde{u}_{j'}) (2j+1)^{-1/2}$

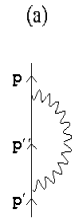

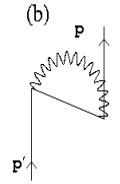

The presence of the nucleus lowers the pairing gap around the Fermi energy….

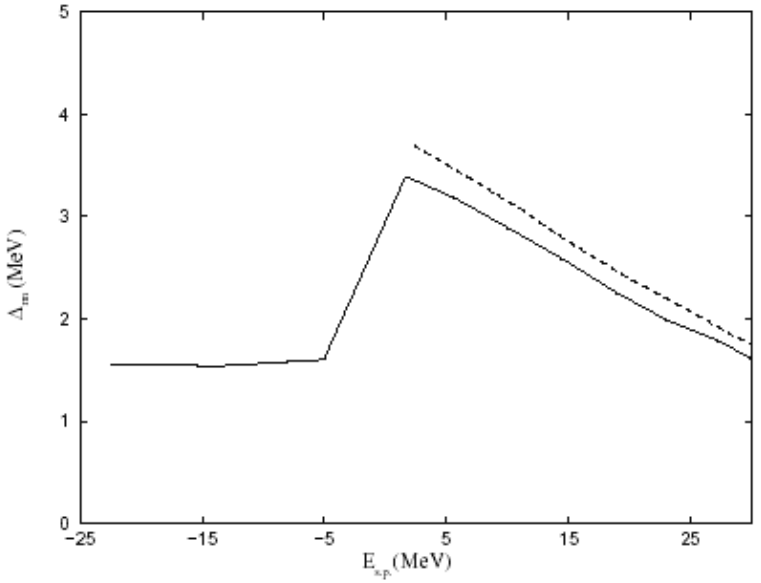

… increasing the specific heat of the system

For a superfluid system,

$$C_V^{(\mathrm{sf})} = C_V^{(\mathrm{norm})} \frac{\sqrt{2}}{\pi^{3/2}} \left(\frac{\Delta_F}{T}\right)^{5/2} e^{-\Delta_F/T}$$

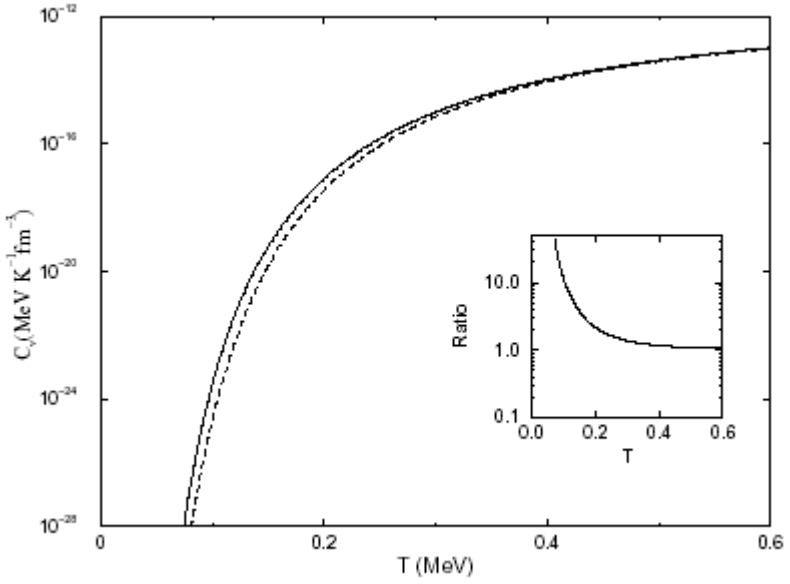

Specific heat along the inner crust

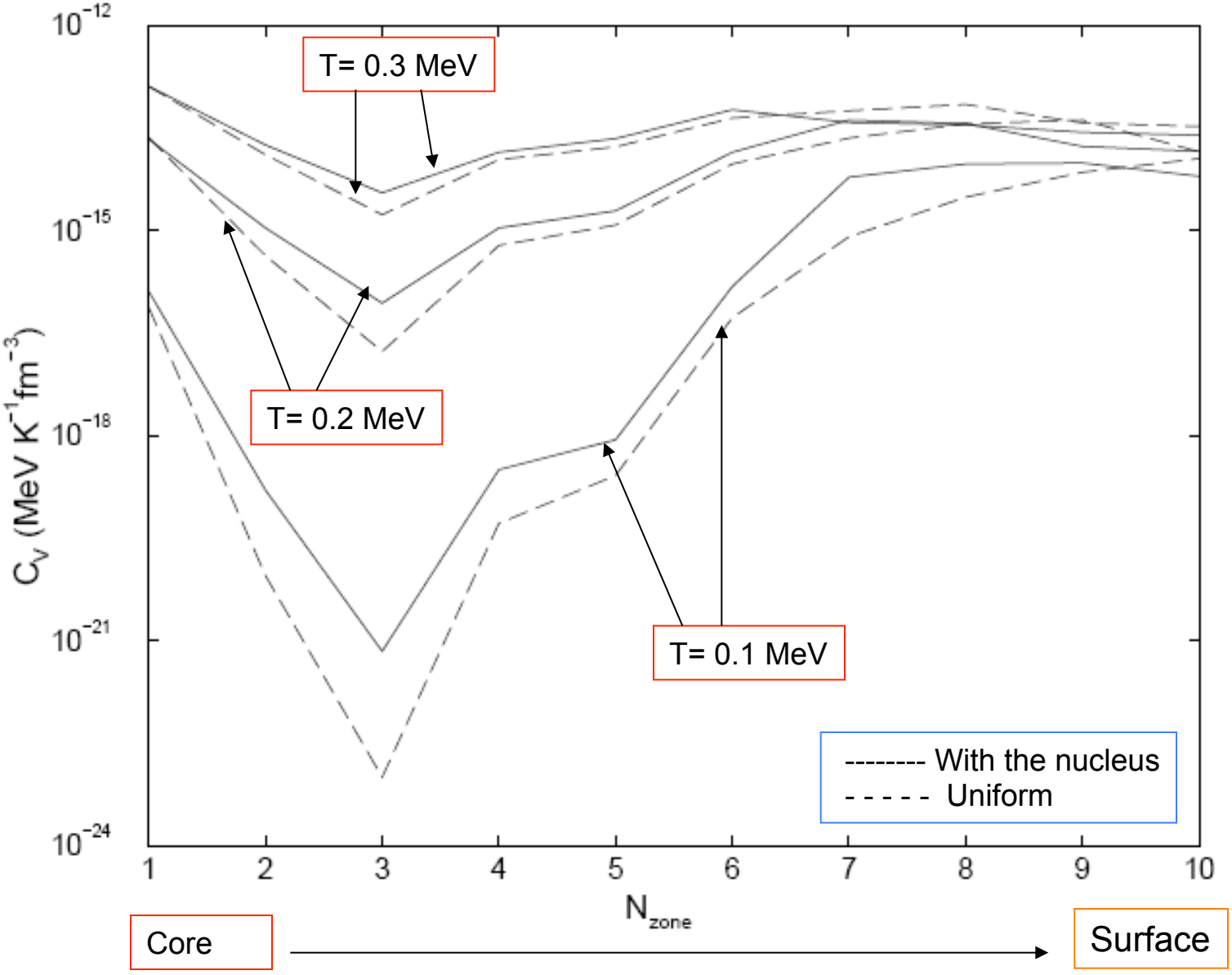

Neutron and electron specific heat going from the core to the surface of the star

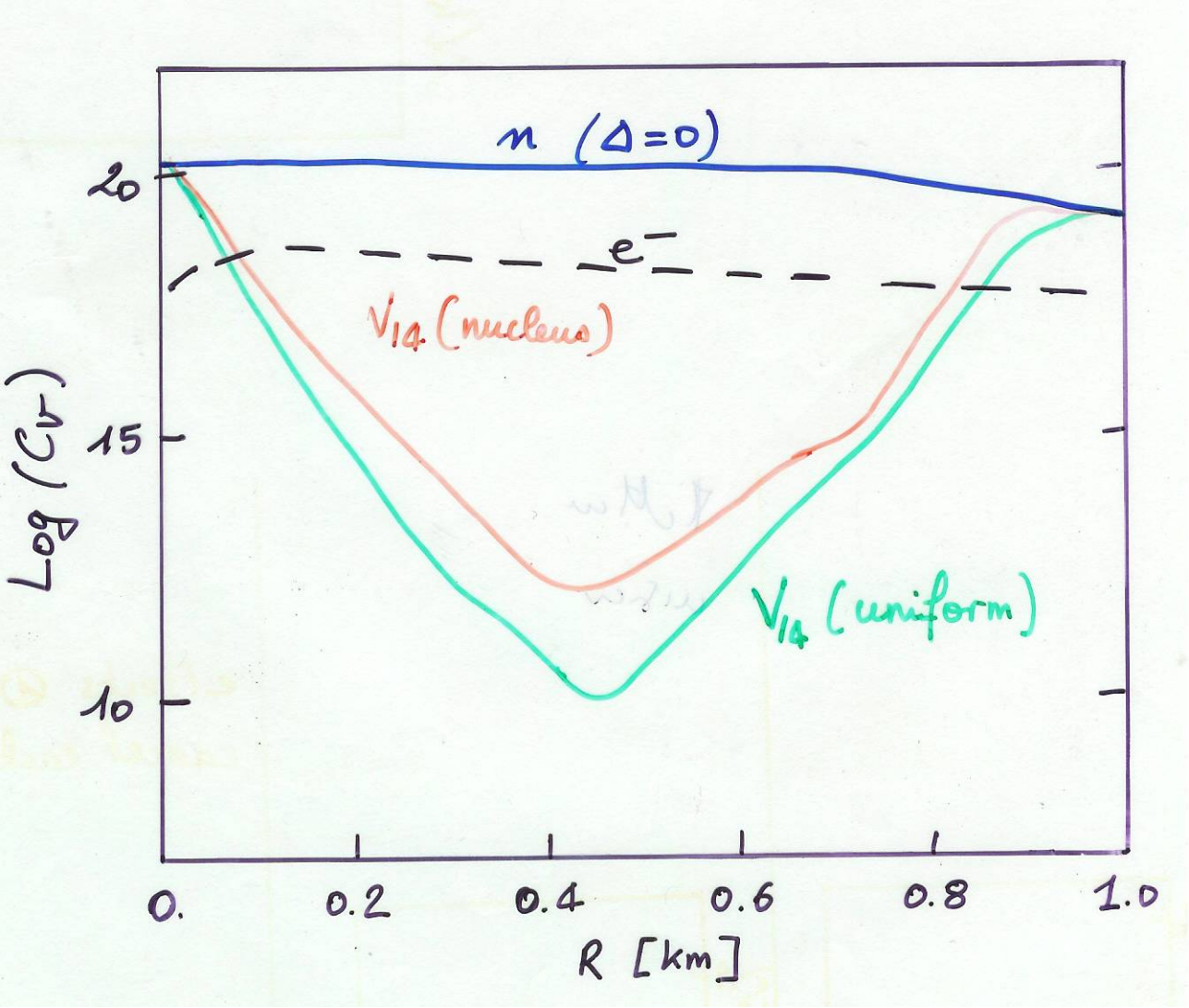

The presence of the nucleus increases Cv but the electronic contribution is dominant.
But: effects beyond mean field can reduce the gap and change this picture…

Application : effect of superfluidity on neutron-star cooling.

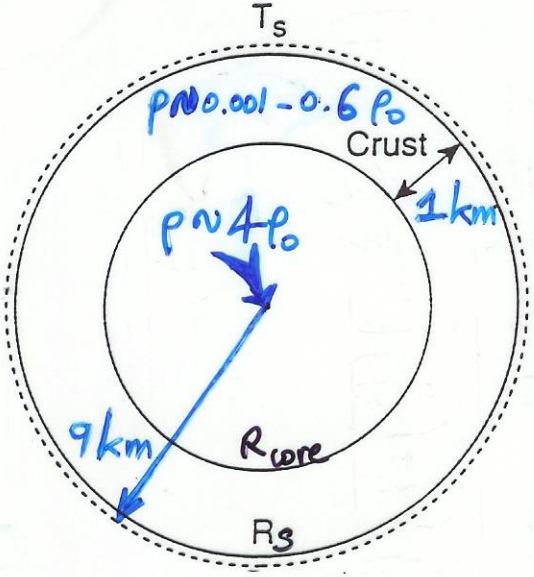

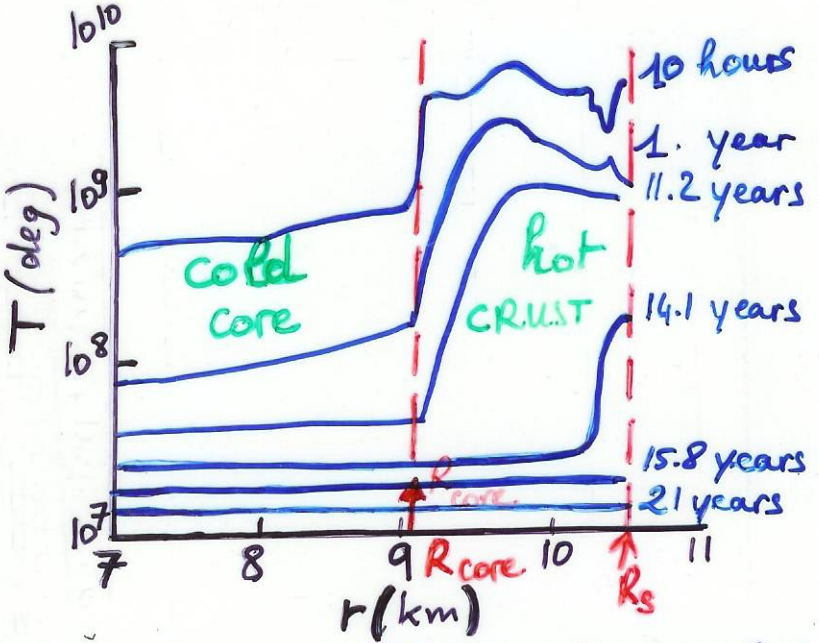

Neutron star Temperature versus Time after explosion

Temperature inversion ➔ $T_{crust} \sim 0.1$ MeV
$\sim 10^9$ degrees

J. Lattimer et al.
APJ 425 (1994) 802

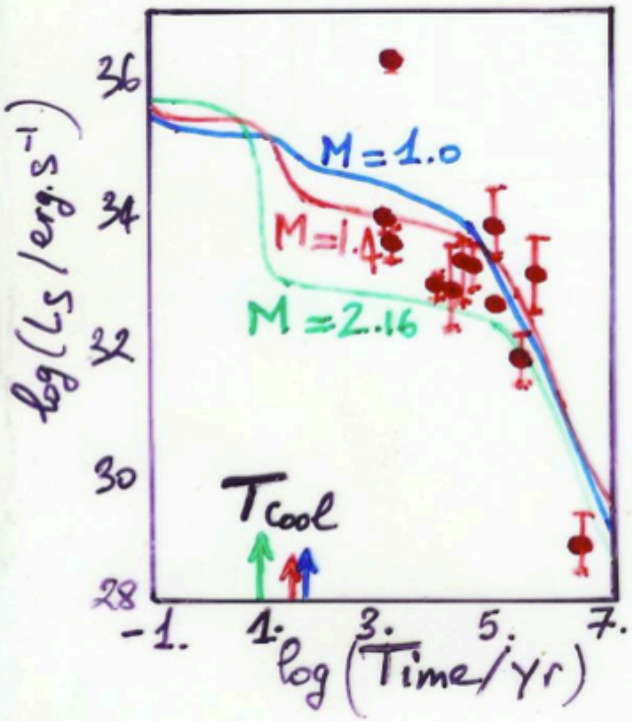

T_{cool} : Time to reach same temperature in core and in crust.

$T_{cool} \propto \frac{R^2_{crust}}{D}$ (diffusion)

$D = \frac{K}{C_v}$ (conductivity / specific heat)

C. Schaab et al. NPA 605 (1996) 531

Rapid cooling scenario

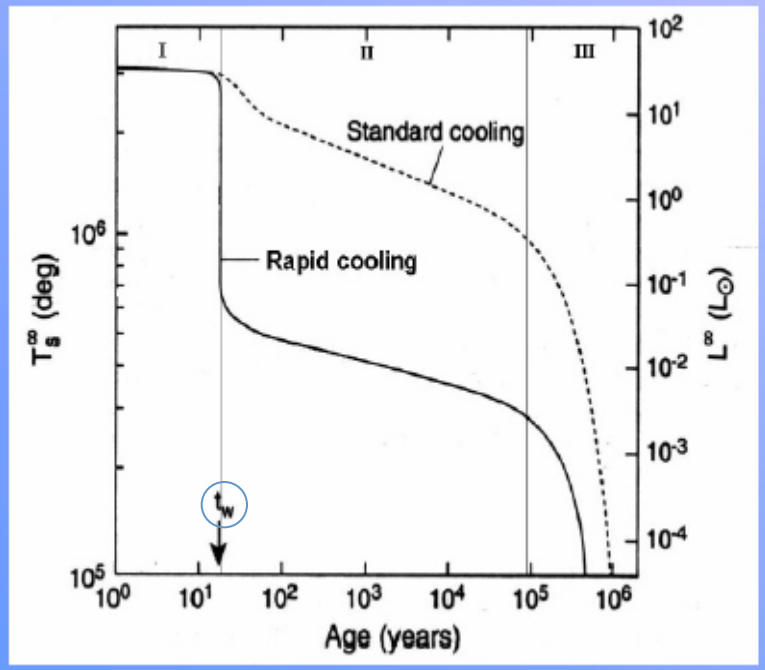

I. Core relaxation epoch
II. Neutrino cooling epoch
III. Photon cooling epoch

J. Lattimer et al., APJ 425(1994)802

The time t_w is sensitive to the specific heat of the crust.
Superfluidity tends to decrease C_v and to decrease t_w ;
proximity effects act against this tendency.

Results from a recent detailed cooling calculation

M. Fortin et al., PRC 82 (2010) 065804

Contributions to the specific heat

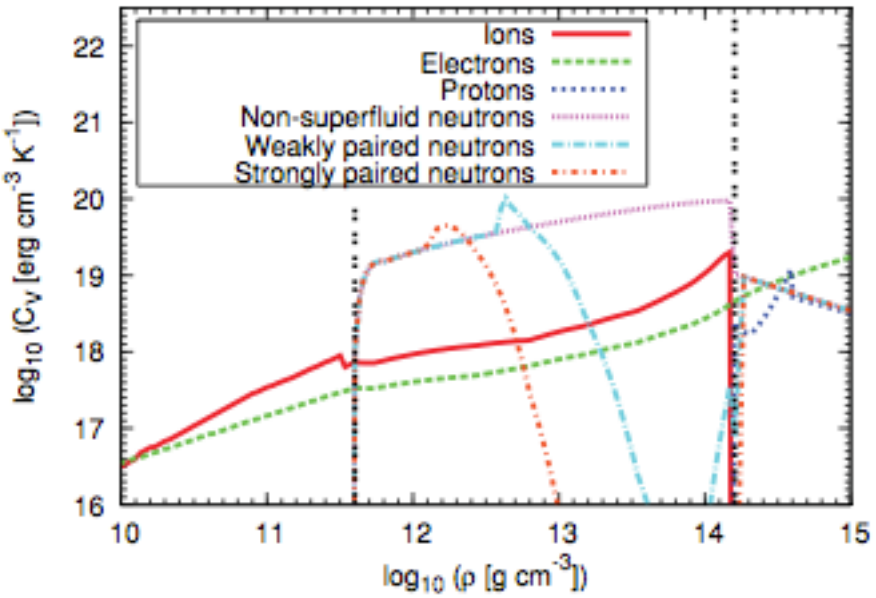

Temperature evolution in the crust

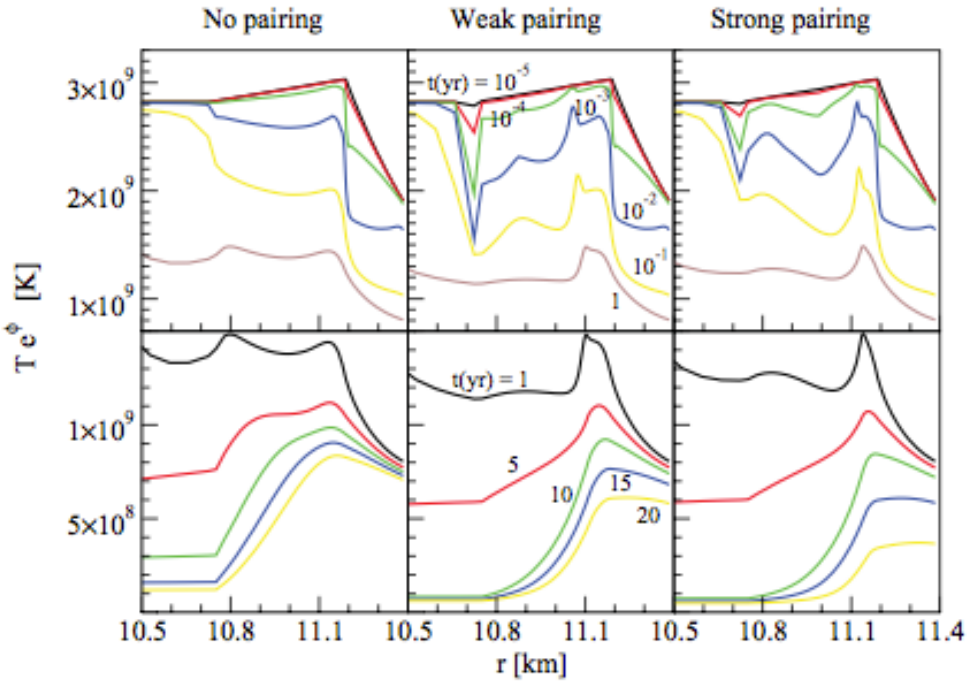

Temperature at the surface

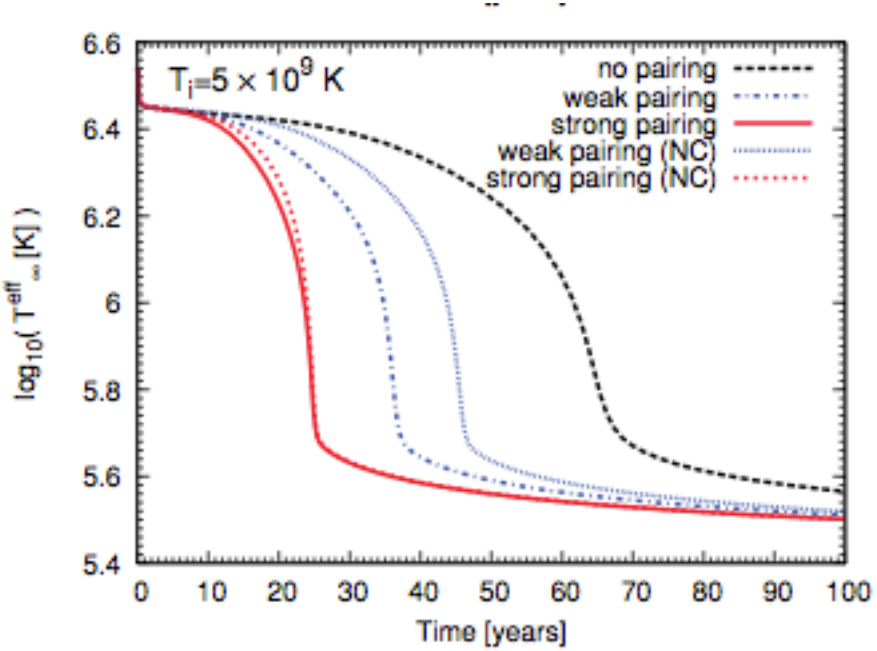

The simplest process for neutrino emission is

$$n \rightarrow p + e^- + \bar{\nu}_e. \tag{1}$$

To fulfill beta equilibrium,

$$\mu_n = \mu_p + \mu_e. \tag{2}$$

Process (1) must take place at finite temperature in a range kT around the Fermi energy. The neutrino momentum is small, and neglecting it momentum conservation at the Fermi energy $\vec{p}_{F_n} = \vec{p}_{F_p} + \vec{p}_{F_e}$ implies that

$$p_{F_p} + p_{F_e} > p_{F_n}. \tag{3}$$

Charge neutrality requires $p_{F_p} = p_{F_e}$, so that

$$p_{F_p} > p_{F_n}/2. \tag{4}$$

But the density of particles $n_i = p_{F_i}^3/3\pi^2\hbar^3$, so that

$$n_p > n_n/8, \tag{5}$$

and the proton fraction $x = n_p/n$ must be larger than $1/9$.

The direct Urca process

Basic mechanism: β and inverse β decays:

$$n \longrightarrow p + e^- + \overline{\nu}_e \quad \text{and} \quad p + e^- \longrightarrow n + \nu_e$$

Energy conservation:

$$E_{Fn} = E_{Fp} + E_{Fe}$$

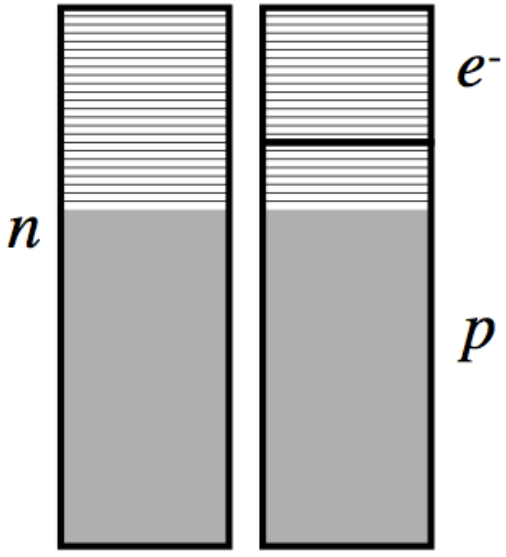

Momentum conservation:

"Triangle rule": $p_{Fn} < p_{Fp} + p_{Fe}$

$$n_i = \frac{k_{F\,i}^3}{3\pi^2} \Rightarrow n_n^{1/3} \leq n_p^{1/3} + n_e^{1/3} = 2n_p^{1/3}$$

$$x_p \equiv \frac{n_p}{n_n + n_p} \geq \frac{1}{9} \approx 11\%$$

"Direct URCA process in neutron stars", JM Lattimer, CJ Pethick, M Prakash & P Haensel, 1991 PhRvL 66, 2701

Neutrino emission on a napkin (III)

Name	Process	Emissivity (erg cm^{-3} s^{-1})	
Modified Urca cycle (neutron branch)	$n+n \to n+p+e^- + \bar{\nu}_e$ $n+p+e^- \to n+n+\nu_e$	$\sim 2{\times}10^{21}\, R\, T_9^8$	Slow
Modified Urca cycle (proton branch)	$p+n \to p+p+e^- + \bar{\nu}_e$ $p+p+e^- \to p+n+\nu_e$	$\sim 10^{21}\, R\, T_9^8$	Slow
Bremsstrahlung	$n+n \to n+n+\nu+\bar{\nu}$ $n+p \to n+p+\nu+\bar{\nu}$ $p+p \to p+p+\nu+\bar{\nu}$	$\sim 10^{19}\, R\, T_9^8$	Slow
Cooper pair formations	$n+n \to [nn]+\nu+\bar{\nu}$ $p+p \to [pp]+\nu+\bar{\nu}$	$\sim 5{\times}10^{21}\, R\, T_9^7$ $\sim 5{\times}10^{19}\, R\, T_9^7$	Medium
Direct Urca cycle (nucleons)	$n \to p+e^- + \bar{\nu}_e$ $p+e^- \to n+\nu_e$	$\sim 10^{27}\, R\, T_9^6$	Fast
Direct Urca cycle (Λ hyperons)	$\Lambda \to p+e^- + \bar{\nu}_e$ $p+e^- \to \Lambda+\nu_e$	$\sim 10^{27}\, R\, T_9^6$	Fast
Direct Urca cycle (Σ^- hyperons)	$\Sigma^- \to n+e^- + \bar{\nu}_e$ $n+e^- \to \Sigma^-+\nu_e$	$\sim 10^{27}\, R\, T_9^6$	Fast
π^- condensate	$n+<\pi^->\to n+e^-+\bar{\nu}_e$	$\sim 10^{26}\, R\, T_9^6$	Fast
K^- condensate	$n+<K^->\to n+e^-+\bar{\nu}_e$	$\sim 10^{25}\, R\, T_9^6$	Fast

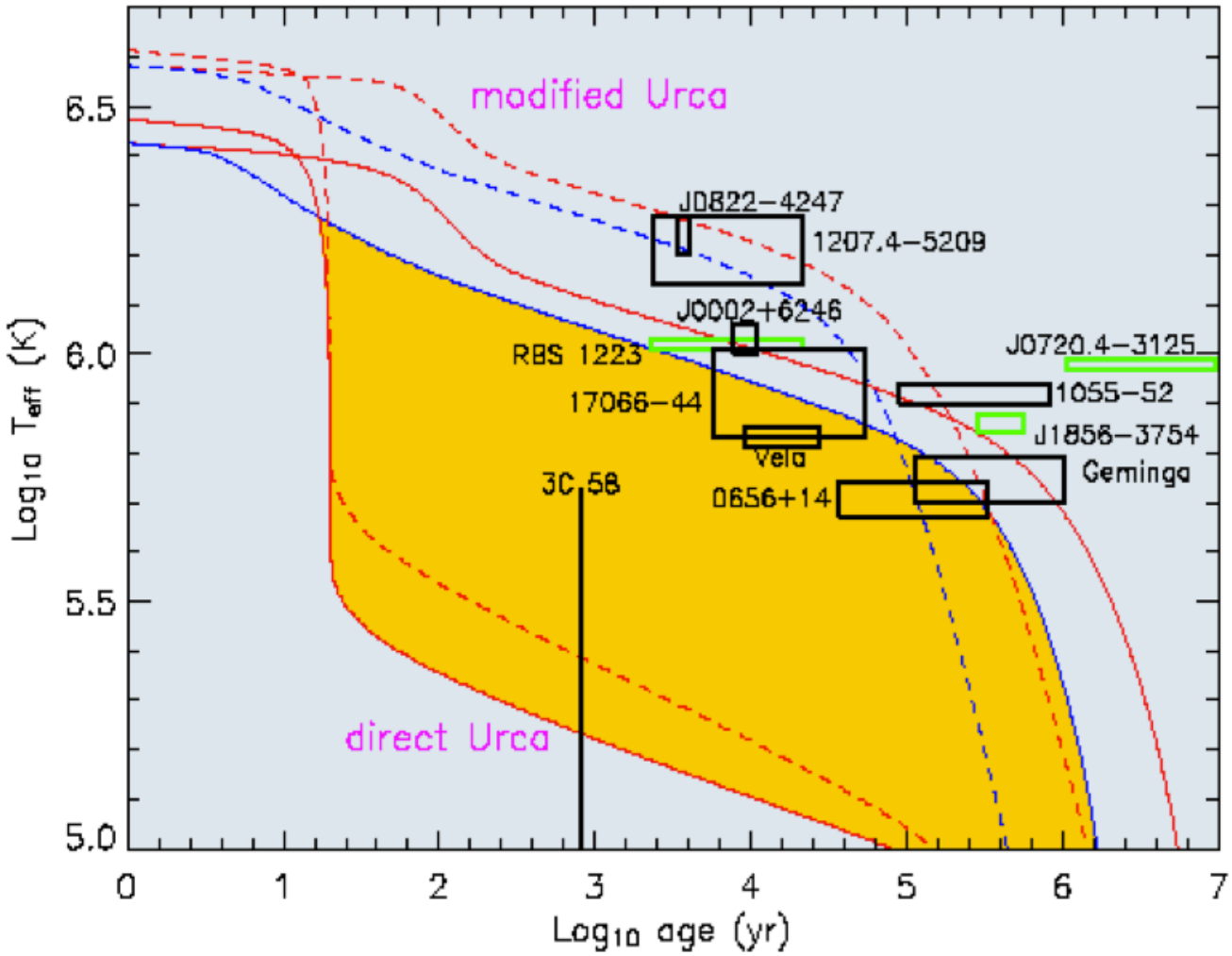

Fig. 4. Observational estimates of neutron star temperatures and ages together with theoretical cooling simulations for $M = 1.4\,M_{\odot}$. Models (solid and dashed curves) and data with uncertainties (boxes) are described in (*43*). The green error boxes indicate sources from which thermal optical emissions have been observed in addition to thermal x-rays. Simulations with Fe (H) envelopes are displayed by solid (dashed) curves; those including (excluding) the effects of superfluidity are in red (blue). The upper four curves include cooling from modified Urca processes only; the lower two curves allow cooling with direct Urca processes and neglect the effects of superfluidity. Models forbidding direct Urca processes are relatively independent of M and superfluid properties. The yellow region encompasses cooling curves for models with direct Urca cooling including superfluidity.

Minimal Cooling or, do we need fast cooling ?

Minimal Cooling assumes:
nothing special happens in the core, i.e.,
no direct URCA, no π^- or K^- condensate,
no hyperons, no deconfined quark matter, no ...

(and no medium effects enhance the
modified URCA rate beyond its standard value)

Minimal Cooling is not naive cooling:

it takes into account uncertainties due to

- Large range of predicted values of T_c for n & p.
- Enhanced neutrino emission at $T \leq T_c$ from the Cooper pair formation mechanism.
- Chemical composition of upper layers (envelope), i.e., iron-peak elements or light (H, He, C, O, ...) elements, the latter significantly increasing T_e for a given T_b.
- Equation of state.
- Magnetic field.

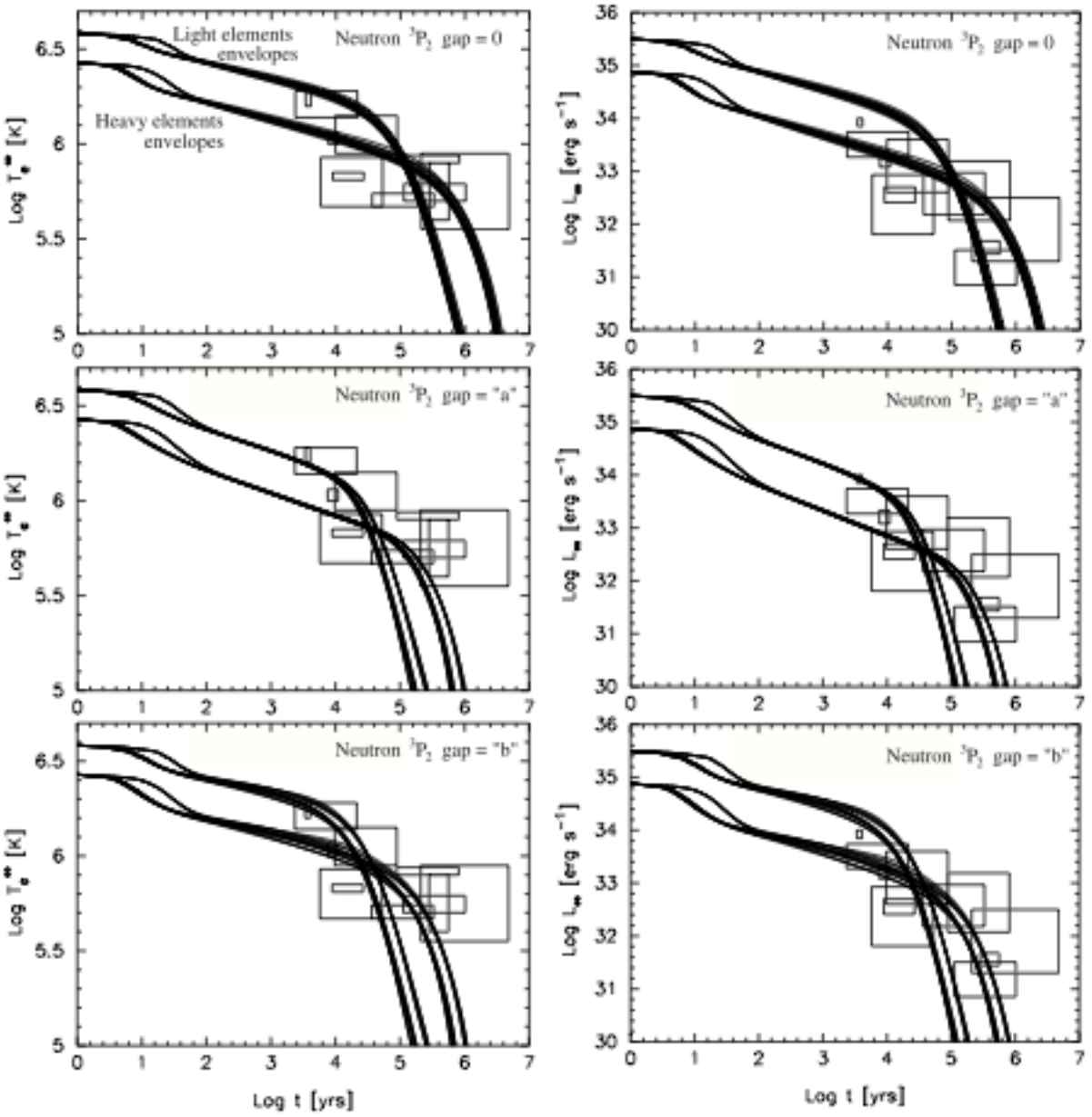

D. Page et al. APJ Suppl. 155 (2004)623

Observed cooling of a young neutron star (Cassiopeia A)

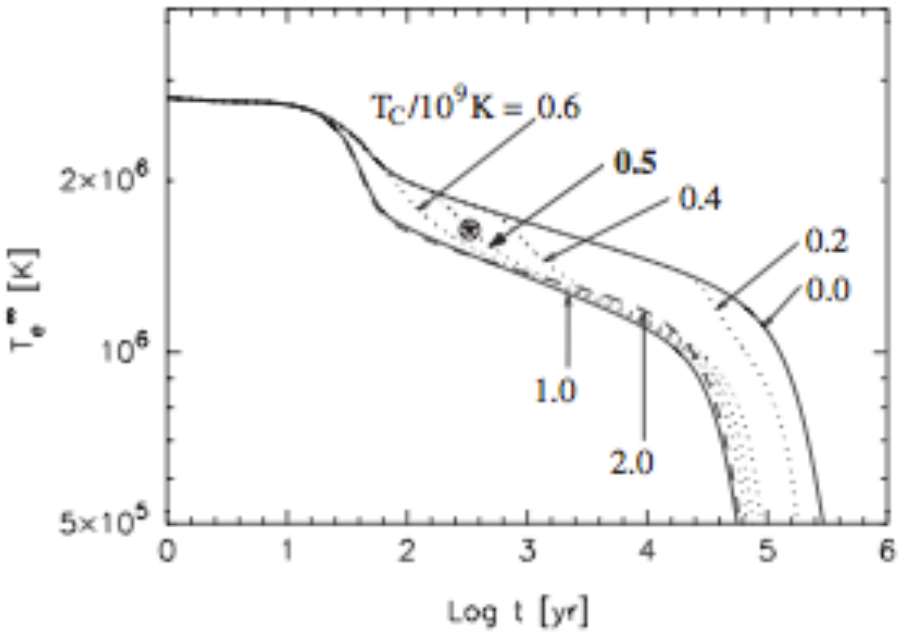

D. Page et al., PRL106 (2011)081101

Freezing on Accreting Neutron Stars

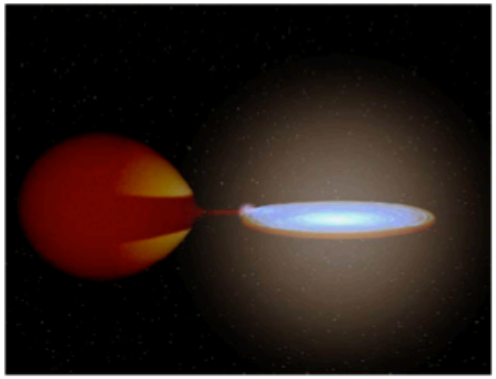

- Material falling on NS can undergo rapid proton capture nucleosynthesis and electron capture to produce a range of n rich elements from ~ O to ~ Se.
- Material is compressed by further accretion and freezes at ~10^{10} g/cm^3.
- We performed large scale MD simulations of how this complex rp ash freezes.
- We find chemical separation where liquid ocean is greatly enriched in low Z elements while the solid crust is enriched in high Z elements.
- We find a regular crystal forms even with large numbers of impurities. We do not find an amorphous solid.
- X-ray observations of rapid crust cooling, following extended periods of accretion, strongly favor a crystalline crust, with a high thermal conductivity, over a low conductivity amorphous phase.
- *See talk by Ed Brown in Nuc Astro 5.*

C.H. Horowitz

A review on the crust

N. Chamel and P. Haensel, Living Rev. Relativity 11
(www.livingreviews.org/lrr-2008-10)

Neutron star biology

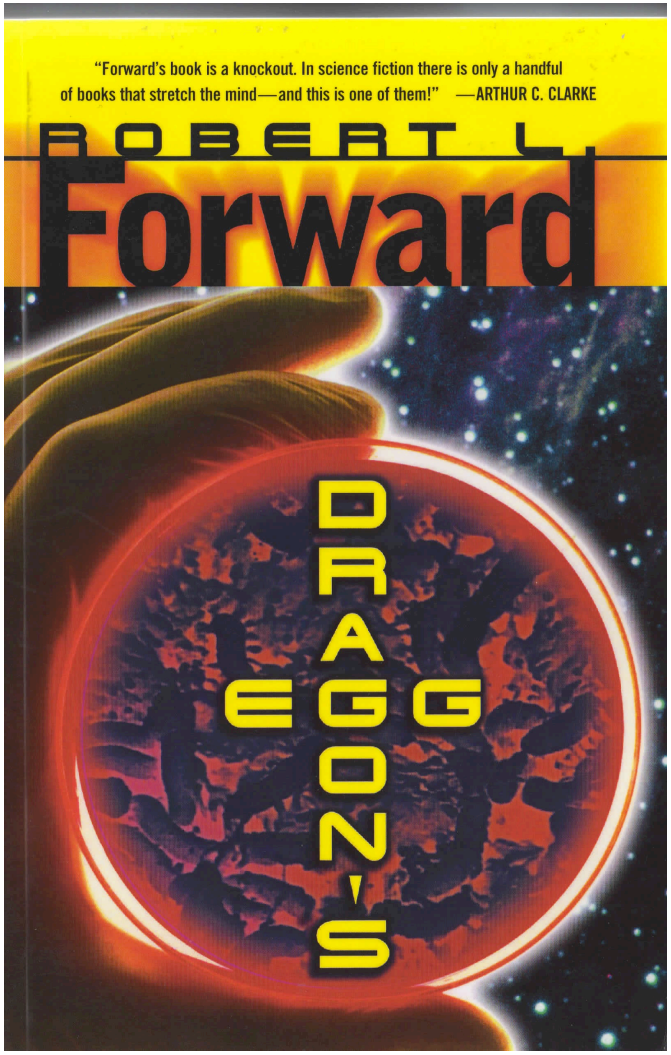

The Cheela civilization

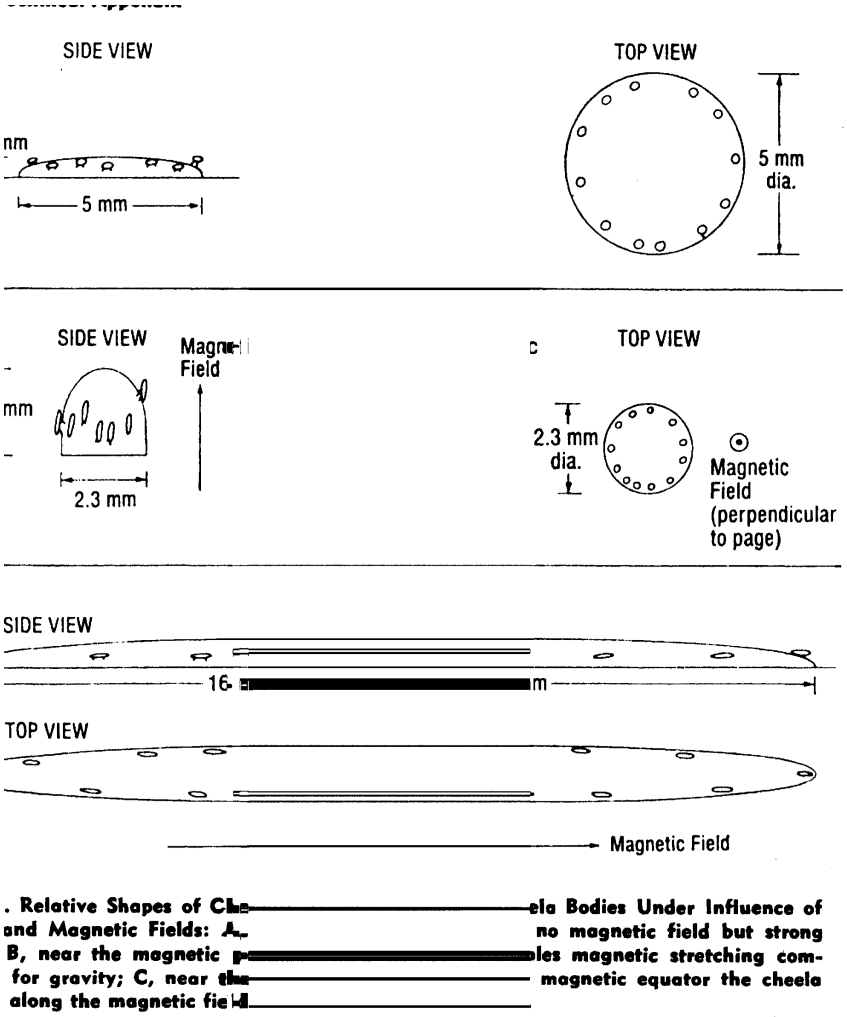

. Relative Shapes of Cheela Bodies Under Influence of and Magnetic Fields: A, no magnetic field but strong B, near the magnetic pole magnetic stretching com- for gravity; C, near the magnetic equator the cheela along the magnetic field

Figure 6. Squad Leader North-Wind with Short Sword and Dragon Tooth (Copyright 2050 by Swift-Killer, White Rock Clan)